POLITECNICO DI MILANO

Scuola di Ingengeria Industriale e dell'informazione

Dipartimento di Energetica

Corso di Laurea Magistrale in Ingegneria Meccanica

Corso di Laurea Magistrale in Ingegneria Energetica

Underwater Compressed Air Energy Storage (CAES):
system design optimization, economics and simulation

Relatore: Prof. Stefano Campanari
Co-relatori: Marco Astolfi
              Giulio Guandalini

Tesi di Laurea Magistrale di:
Marco Belloli   Matr. 876482
Adriano Hirn   Matr. 849810

Anno Accademico 2017-2018

Ringraziamenti

vicini.

Ringrazio tutti gli amici e le amiche di vecchia data e non che rendono meravigliosa la bolla in cui viviamo.

Ringrazio colui che è riuscito a ripararmi il computer.

Infine un particolare rigraziamento va a chi in questi ultimi mesi è stato al mio fianco, sopportandomi e consigliandomi.

Contents

List of Figures

List of Tables

Abstract

Human needs of energy have seen a continuous growth during years. Nowadays the renewable share is rising, reaching a grew of 17% in last year and introducing concerns about the management of the electrical grid, given the not programmable nature of that sources. Storage technologies would then play key role in managing large-scale RES power plants. This work will be focused on an innovative kind of Adiabatic Compressed Air Energy Storage (A-CAES) with a mixed onshore-offshore layout. The system is provided by a thermal energy storage (T.E.S.) able to store thermal power generated during air compression. This energy is then used to heat up the stream before expansion, avoiding any fuel consumption. The air tank is placed on the sea bed to obtain a constant pressure vessel by exploiting the hydro-static load. Turbo-machines and the T.E.S. are instead placed on-shore. A system design optimization, off design performance assessment and techno economical analysis will be conducted. Then the UW-CAES will be coupled with a deep water off shore wind farm to simulate real case applications. Particular attention will be given to a peak shaving management strategy given the need to improve energy dispatchability. The aim of the work will then be to evaluate the plant performance to understand if the adopted configuration could compete with other large scale storage systems, e.g. pumped-hydro.

Sommario

La richiesta di energia del genere umano é aumentata costantemente negli anni. Oggigiorno la produzione di potenza da fonti rinnovabili é in crescita, registrando un aumento del 17% nell'ultimo anno, introducendo problematiche nella gestione della rete elettrica data la loro natura non programmabile. Le tecnologie di accumulo potrebbero permettere la gestione su larga scala di energia da fonti rinnovabili. Questa tesi propone un innovativo tipo di A-CAES (Adiabatic Compressed Air Storage) che prevede una disposizione mista on-shore ed off-shore. Sistemi di accumulo di calore (T.E.S.) sono in grado di immagazzinare l'energia termica prodotta durante la compressione, per poi sfruttarla per riscaldare l'aria in ingresso alla turbina, evitando il consumo di combustibile fossile. Il serbatoio d'aria é posto sul fondale marino per mantenere la pressione costante sfruttando il carico idrostatico. Le turbomacchine e i sistemi di accumulo termico sono posti sulla costa. Il lavoro svolto consiste nell'ottimizzazione del design, lo studio delle condizioni di off-design, la valutazione delle performance e l'analisi economica dell'impianto. Per la simulazione operativa il sistema di accumulo é stato accoppiato ad un parco eolico offshore. Per aumentare la dispacciabilitá dell'energia prodotta dal vento, un'accurata analisi viene proposta in logica peak shaving. L'obiettivo della tesi é di stimare le caratteristiche dell'impianto per valutarne la competitivitá rispetto alle altre tecnologie di accumulo su larga scala, come i sistemi pumped-hydro.

Extended abstract

0.1 Introduction

Most industrialised country are turning their electricity production towards the use of renewable energy sources [1]. However they are characterized by non-dispatchable production, difficult to be forecast. In this scenario the technologies able to store energy would help to grid stabilization and control: batteries and high energy capacity solutions like power-to-gas, compressed air energy storage (CAES) [12] [13] and pumped−hydro storage systems represent up to now the main options. The UW-CAES vessel is different from variable pressure reservoirs [14] (e.g. the existing installations in Huntorf, Germany and McIntosh, Alabama [15]) and it is designed to be isobaric, letting water entering and exiting from the air storage. Pressure is maintained by the hydro-static pressure, exerted by the water column above the tank. The Adiabatic concept of CAES, already proposed in Adele project [16] avoids the use of fossil fuels: storing the thermal energy produced though compression and giving it back to the air when extracted from the reservoir [17]. The system conceptual layout is shown in Figure 2.3 and includes four key groups of components: turbomachinery, T.E.S.-HX (thermal energy storage - heat exchanger) apparatus, piping-air tank and turbine. The compression group is made by different parallel turbomachines composed by series of axial mixed-flow and centrifugal compression stages, partially intercooled. The power from wind farm (a) is transmitted by underwater power line (b) to an electrical motor (c) which drives the compression group. T.E.S. system is made by 3 thermal fluid hot and cold vessels: salt (e-f), oil (g-h) and water (i), and by 3 heat exchangers, which cool down air heating up thermal fluid and viceversa when the UWCAES has to produce power. Air Underwater vessel lays on the seabed; it is rigid and open at the bottom (k) [18]. Water fills the tank when air is extracted to maintain constant pressure generating a variable volume storage [1]. Due to the simple design and equilibrium condition (no stresses arises since inner and outer pressure are equal), the tank is assumed to be made of concrete. This solution seems very simple but some problems

---

[1]The use of fabric tank investigated in [19] [18] with spherical shape. This solution is characterized by a more complex technology but prevents the air to be in contact with sea water.

could arise due to the salinity of water, which is in direct contact with air. Some filters could be necessary before HX inlet [2]. An axial turbine expander connected to a generator (d) and the produced power is transmitted to the grid (l). The compression section is
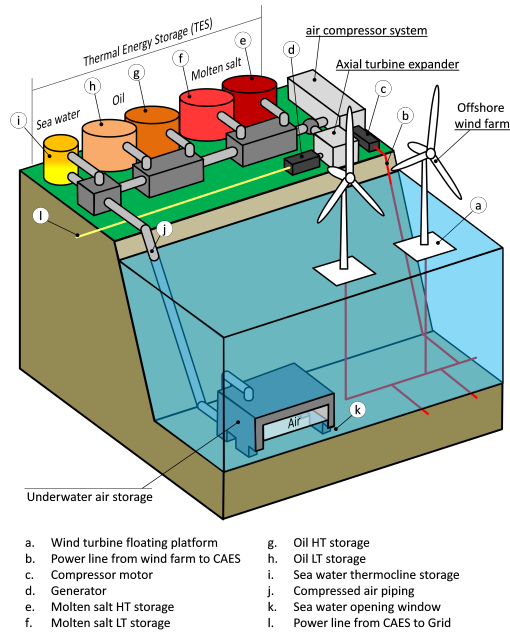
Figure 1. Conceptual view of the UW-CAES system [1]

designed to work at part-load to follow oscillating production from wind park, and according to the strategy adopted (peak shaving, arbitrage) it pumps air into the storage. Instead when there

is a lack of production from wind or costs of electricity are high, the air is extracted from the reservoir and expanded to generate power. Different deployment options can be considered: pure offshore installation, for which all the equipment are fitted on a off shore floating platform, and the air tank is located on the seabed below it, or mixed onshore-offshore installation (depicted in Figure 2.3), where a long pipeline connects the on shore plant with the UW storage. The thesis first discusses the design and off-design characterization of the overall UW-CAES system. It is then simulated a perspective case study where the UW-CAES is coupled to a wind farm, optimizing the system control strategy and round-trip efficiency. An economic analysis is made to judge the feasibility of the plant and the most profitable configuration.

0.2 Plant design

The target to be achieved is the optimization of the efficiency of all the apparatus, considering the combined action of compressors, heat exchanger, T.E.S. and turbine. To do so an estimation of round trip efficiency (RTE) considers the charging and discharging phase of the plant simultaneously as a turbo-gas: efficiency result to be $\eta_{caes} = l_{turb}/l_{comp}$. Different design option has been investigated, considering different partial intercooled solution and multi-shaft configuration. The design of compressor group relies on the use of the Baljé map for

---

[2]This solution is similar to what investigated in [20], in connection with hydraulic pump-turbine units

compressible flow machines [21] which provides efficiency as function of the specific speed ($Ns = \omega * \sqrt{\dot{V}_{in}}/\Delta h_{is}^{0.75}$) and specific diameter ($Ds = D* \Delta h_{is}^{0.75}/\sqrt{\dot{V}_{in}}$ for each stage. This map has been fitted with a smooth surface and increased by 2% efficiency points in order to update the map to state-of-the art efficiency of modern compression stages [8]. For each type of compressor stage, a different limit of pressure ratio is considered (1.4 for axial stages, 4 for radial stages; intermediate value for mixed flow compressor stages), reflecting current compressor design features. Figure 2 reports the resulting Baljé chart and the Cordier line [10] [9]. An heuristic routine for
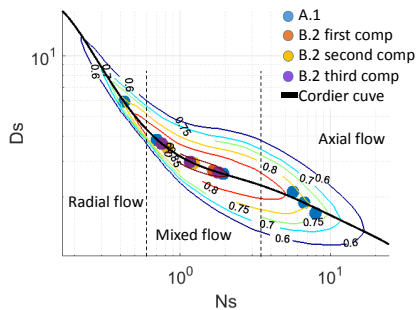
Figure 2. Baljè map of efficiency as function of specific speed and specific diameter.Markers refer to the optimized results of case B.2 and A.1 described in this section.

the estimation of compressor efficiency as function compression ratio, mass flow rate and rotational speed has been generated. Mixed and radial machine are found on the Cordier curve

(decreasing diameter) while axial stages have constant mean diameter (but lower efficiency). Results are summarized in Figure 3, where the compressor efficiency is reported against the isoentropic volumetric flow rate ratio ($Vr = \rho_{exit\,isoS}/\rho_{inlet}$) and Ns defined for the whole machine (Ns1). This curve has
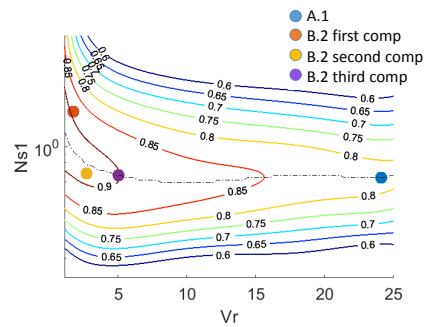
Figure 3. Maps of maximum efficiency for multistage compressors as function of overall isoentropic Volume ratio Vr and compressor specific speed Ns1. Markers refer to the optimized results of case B.2 and A.1 described in this section.

been fitted with a smooth surface, since it is characterized by discontinuities related to the discrete change in type of compressor (introducing a mean error of 1.2 %). The analysis performed changing inlet condition within the investigated range of pressure and temperature, shows variation of $\pm 0.5\%$. Optimization variables are the number of intercooler, the pressure ratio for each compressor, number of shaft and rotational speed for each of them. Referring to Figure 4, solution without intercooler

(A), with single (B) or double (C) intercooler has been tested. For each of them solution spanning from one (1) to three shaft (3) has been tried. Since the map is obtained considering continuous compression, for the solutions B and C a trade off between compressors fitted on same shaft has been found (since they are separated by intercooling), while speed of last shafts is obtained directly from the optimum of the map. The algorithm calculate air mass flow rate throw an iterative procedure in which efficiency of compressor group is guessed and then calculated. In Figure 2 and Figure 3 it is possible to see the difference between case A.1 and B.2. The first (blue dot) case is made by 3 axial stage compressor, optimized for intermediate stage, at constant mean diameter, 3 mixed flow stage and one radial stage. In stead configuration B.2 is made by only mixed flow stage: first (orange) and second (yellow) compressors have in between the intercooler and are fitted on the same shaft, optimizing the efficiency of the group. In subfigure (b) it is possible to see that they are on both side with the respect to the optimum curve,running respectively at higher and lower than their optimal speed. Instead, last is optimized on the maximum curve. The compressor outlet condition are used to calculate the charging phase (*CtS*) of the heat exchanger, considering fixed temperature difference between air and thermal fluid [3]: UA (overall heat trans-

fer coefficient*heat transfer surface), mass flow of HTF and exchanged thermal power can be calculate for each storage. The discharging phase (*HfS*) is calculated considering same air mass flow rate adopted in *CtS*, U has been rescaled to calculate turbine inlet temperature (TIT) and pressure (TIp); expansion in turbine can be truncated in case of lower turbine outlet temperature (TOT) to respect icing limit. Table 1 reports the final value of the optimization variables and the main results for each configuration. Case

Table 1. Result of plant design

Config	COT [°C]	TIT [°C]	TOT [°C]	RTE [-]	I_0 [M€]
A.1	871	409	5	0.457	45.5
A.2	810	443	5	0.528	53.2
A.3	804	446	5	0.531	53.9
B.1	625	575	16.6	0.775	76.0
B.2	625	575	16.6	0.798	77.9
B.3	625	575	16.6	0.801	78.5
C.1	625	575	16.6	0.780	76.3
C.2	625	575	16.6	0.799	78.0
C.3	625	575	16.6	0.800	78.9

without intercooler (A) benefit from the adoption of multiple shaft with an increase of 10% in RTE. This is due to the decrease in compression work, lower compression outlet temperature

---

[3]this criteria allows to prevent a non-

homogeneous utilization of the storages in real operation, with issues related to a non-simultaneous depletion and/or saturation of the T.E.S. vessels
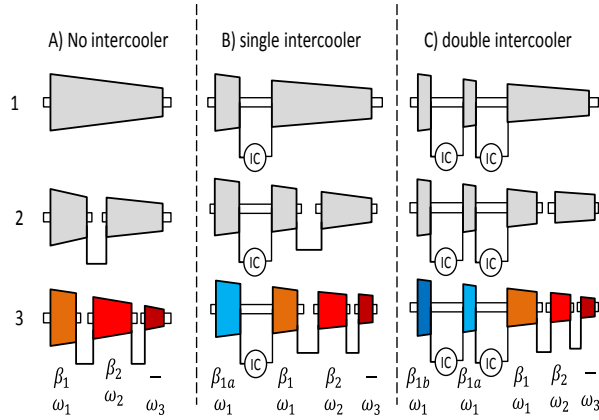
Figure 4. compressor configuration for case without intercoolers (A), case with single intercooler (B) and case (C) with three intercoolers for single, double and three shaft. Ts diagrams refers to the three shaft configuration highlighting the optimization variables

(COT), lower pinch point [4] and therefore higher TIT which means higher turbine work. Intercooled solution (B-C) enable the control of COT reaching always 625°C, guaranteeing maximum TIT. This means that the advantage in expansion is higher with the respect to the benefit of more cooled compression (lower COT). In B and C configuration the advantage of multiple shaft is reflected in only less compression work, being fixed the TIT, with small increase of efficiency (around 3%). Following the approach of [22] [11] it has been possible to roughly estimate the investment costs needed for each configuration, considering storage sized to 48h of continuous charging at nominal power, it is possible to estimate investment costs required (I_0) for any configuration. In general the main cost is related to thermal storage and it is directly related to compressor work: fixing power, lower work determine higher air flow rate which requires higher flow rate of HTF to be cooled, since T.E.S. temperatures are fixed. In the end investment cost can be related to RTE: more efficient plant are more expensive. Table 2 reports the main results of the T.E.S. system for a compressor section with a nominal power input of 75 MW. Neglecting scale effect, thanks to big size of the machine tested, it is possible to demonstrate that if rotational speed is correctly tuned, the same configuration is able to maintain same performance for different number of parallel trains or different power of the compressors. A sensibility analysis made on tank pressure highlight an advantage from thermodynamic point of view into decrease overall pressure, and strong penalization at higher depth, due to the limited expansion ratio at a maximum of

---

[4]Maximum solar salt temperature define the pinch point calculated as COT - $T_{max\ salt}$

Table 2. main results of the T.E.S. system for case B.2

Molten salt mass flow rate [kg/s]	74.5	Molten salt heat exchanger duty [MW]	35.1
Molten salt heat exchanger UA [MW/K]	1.4	Molten salt T.E.S. volume (48h at nominal power) [m³]	7124.6
Thermal oil mass flow rate [kg/s]	51.3	Thermal oil heat exchanger duty [MW]	23.0
Thermal oil heat exchanger UA [MW/K]	0.92	Thermal oil T.E.S. volume (48h at nominal power) [m³]	9889.6
Water flow rate [kg/s]	26.9	Water heat exchanger duty [MW]	5.6
Water heat exchanger UA [MW/K]	0.2	Water T.E.S. volume (48h at nominal power) [m³]	4711.1

88.5 [5]. Costs follow the opposite trend being maximum at low depth: to generate same power with lower specific work, higher amount of air is required, increasing the cost of air and T.E.S. vessels: from 40 bar the investment required is 98.3 M€ to 69.7 M€ at 140 bar [6]. The choice of 80 bar therefore seems reasonable to maintain good level of RTE, without need excessive costs. Solution with lower maximum temperature are simulated, but in the end an increase in investment and/or strong penalization on RTE has been found. The proposed model require the use of machines that are difficult to be found on the market, and has to be considered as a preliminary design for turbo-machinery. Number of stage is reasonable but technological constraints may not be verified and dedicated design stage by stage is in charge of future development of this project. Considering the state of the art of pumped hydro storage system, which achieve efficiency nearly 70% [23], and

land based CAES with RTE which span from 40-55% [24] [15] to 70% only with the most recent adiabatic-CAES projects [16], the result of 75-80% of the simulated plant is remarkable.

0.3 Plant Off-Design

The UW-CAES system coupled with a RES faces a fluctuating input electric power due to the unprogrammability of power plants based on these energy sources. In this work the analyzed storage is integrated to a wind farm. As consequence the compression section absorbs variable power inputs, depending on the wind availability. The part load managament strategy aims at maximizing the air mass flow rate, which together with the HTF is the medium used to store energy. Dimensionless performance maps are implemented starting from real compressor data sheets [25] [26] for axial and radial compressor regulated acting on VIGV closure or on the rotational speed. In Figure 5 one of the used map is reported as an example. The main issue in the off design operation is related to the compressor operability range. Indeed the peculiar conditions at which the compressors

---

[5]Calculated considering maximum solar temperature plus pinch point and minimum TOT for icing.

[6]considering 48h storage - 4 parallel compressor - 75 MW.
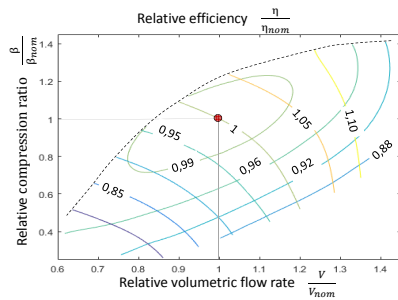
Figure 5. Dimensionless Axial compressor part-load maps, rpm control mode.

are subjected hinder their flexibility: the outlet pressure is kept nearly constant for all the power input and it is imposed by the hydro-static load since the air tank is positioned under water. In this way at partial loads the operational point moves almost horizontally on the compressor map (Figure 5). The proposed solution consists in the adoption of multiple parallel compression trains. A first optimization algorithm has been implemented to make a comparison between the compression regulation acting on the rpm or on VIGV closure angle. Single shaft configuration (B.1) has been tested resulting in a wider operational range for the case of variable speed and for an increasing number of parallel trains. Then focusing on this kind of regulation the algorithm has been adapted in order to test multiple shaft configurations. Taking as reference (B.2) two cases have been investigated: shafts connected by a gearbox or shafts with dedicated electric motors. In Figure 6 are reported the results adopting one up to four

parallel trains for shaft connected by a gearbox. With one single train the operational range is limited by the surge line at the 85% of the nominal load but already with two trains the compressor could work down to the 42% relative power. The range from 69% to 85% can not be completely exploited because two compressors would operate outside the area delimited by the surge line while a single compressor would work above the maximum load allowed by the machine. This condition in Figure 6 is represented by plateau trends. Increasing the number of trains up to four leads to a minimum load of 22% of the nominal power with a very narrow plateau range. The case of shafts with dedicated motors presented the same operational range as the gearbox case and an air flow rate increment of about the 1% at part load.

Afterwards the relation between the T.E.S. and the compressors off design behaviour is investigated. Since the COT, the outlet pressure and the outlet volume flow rate of the last compressor correspond to the input conditions of the air entering in the first unit of the thermal storage system. In Figure 7 the T-Q diagrams are reported for different load conditions of the compression section composed by four parallel trains of type (B.2). From the left (a) corresponds to the maximum overload allowed, (b) to nominal load and (c) represents 22% part load. As can be seen the thermal power exchanged by the three units varies with different ratio at off de-

(a) Relative overall mass flow rate   (b) Relative compression efficiency
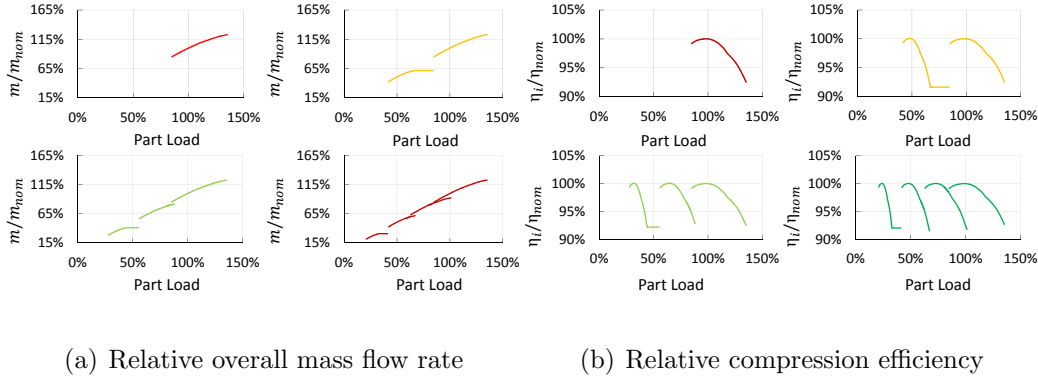
Figure 6. Part load performances of compression section (B.2) with one up to four parallel trains.

sign condition, due to the COT variation which modify sequentially the pinch points of all the HXs. The reduction in the air flow rate leads to over-sized heat exchangers. This behavior gives concern about balancing the level of stored HTF during the long term usage of the plant. To solve this issue an additional HX has been added, letting solar salts to transfer heat to the diathermic oil. The sea water aftercooler is instead provided by a bypass valve for both the *CtS* and *HfS* phases.

0.4 Case study

As introduced the UW-CAES plant could be coupled with several types of RES. Given the need of deep water location availability in the proposed case study the plant has been integrated with combinations of deep-water offshore wind farms. The UW-CAES compression section is assumed composed by four parallel trains, with

one intercooler and two shaft connected by a gearbox each (B.2). The chosen location is offshore the South West Sardinia in Italy, positioning the air tanks at about 815 m depth at which correspond an hydro-static pressure of 80 bar. Wind field measurements for the years 2015 and 2016 related to the chosen location have been provided by the Spanish harbour weather forecast company Puertos [27]. Those data sets have been used to evaluate the the wind farm annual energy production of the wind farm through the use of the SAM tool [7].

In this work the storage system is employed following two different management strategies in order to consider technical and economical aspects:

· *Peak shaving* logic aims at improving the dispatchability of the wind

---

[7]System Advisor Model, Version 2017 9.5, Release Date 2/12/2018, Author: National Renewable Energy Laboratory (NREL)
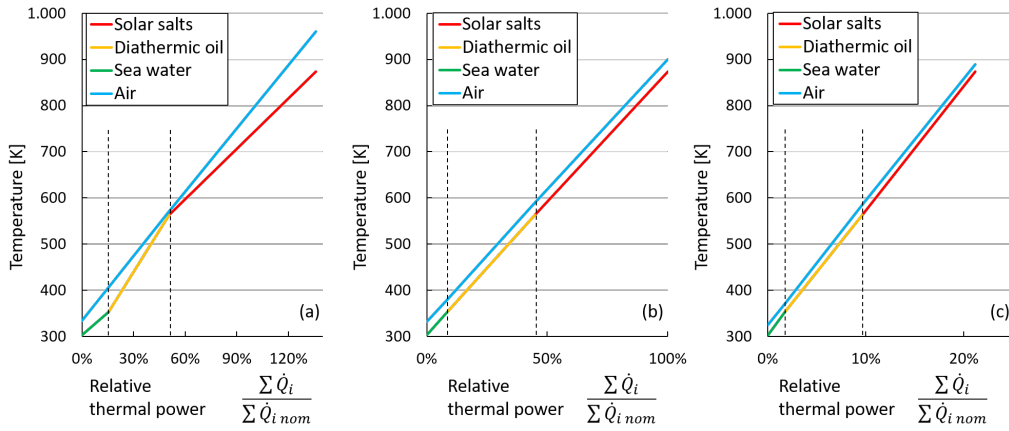
Figure 7. T.E.S. heat exchangers T-Q diagrams at different part load conditions of the compression section composed by four parallel trains of type (B.2)

energy. Fluctuations in the energy sent to the grid are mitigated by the use of a storage system. When the energy produced by the wind farm is too high part of it is stored, on the other hand when it is too low additional energy is extracted from the storage.

· *Arbitrage* logic decouples the wind availability from the price policy. The aim is to maximize the incomes of the wind park. The storage system then absorbs energy when the electricity price is low and it sells energy when it is more convenient. The dependence between prices and available energy implicitly makes the plant to operate as a grid stabilizer.

0.4.1 Peak shaving

In this case the UW-CAES is applied to a combination of wind park for a nominal power of 135 MWe. Relying on [22] the selected wind turbines are the Siemens SWT 2.3 MW. Thresholds have been defined as in Figure 8 to establish the activation strategy of

the compressor and turbine, when the power produced by the wind farm is higher than P_{up} the plant stores energy while when $P_{wind} < P_{lb}$ the UW-CAES behaves like a producer. Focusing on the effectiveness of shaving energy peaks the main indicator is the variance of the hourly energy sent to the grid, defined as:

$$\sigma_P^2 = \frac{1}{T} * \int_T \left[P_{grid}(t) - P_{ref}(t) \right]^2 dt$$

Where T is the considered time period and as reference case is kept a fully dispatchable plant($\sigma_P = 0$), with a constant flat energy output along the whole year. This analysis becomes relevant if performed comparing the cases of the wind park with and without the storage integration, to better understand which are the improvements of the UWCAES employment. As a fist attempt the plant have been simulated for different compression section sizes and different activation thresholds with the hypothesis of infinite storage capacity and $P_{ub} = P_{lb}$.
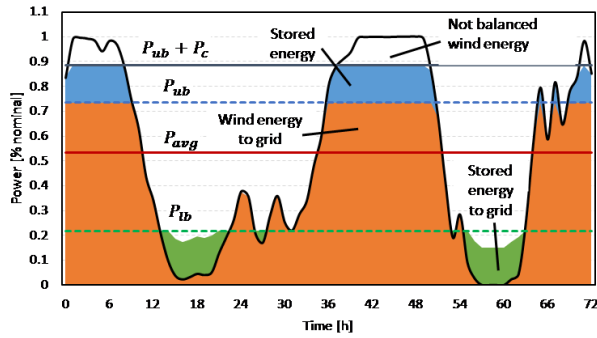
Figure 8. Example of operation strategy of the peak shaving energy storage coupled with the wind park production profile. [1]

RTE around the nominal value and standard deviation reduced of the 50% are obtained for good combinations of $P_{nom,c}$ and P_{ub} but in any case the storage volumes required resulted unfeasible. Then the storages are sized for 48 hours of charge operation. The results of representative cases are reported in Table 3. Coupling this results with an economic analysis the investment costs are defined and the net present value is evaluated for the life plant time, assumed of 30 years. As it can be seen in Figure 9 the major fraction of the investment costs is covered by the T.E.S. which counts for about the 50% of the total. It is found that the break even point is never reached, for this reason the possibility of receiving incentives is contemplated. These incentives are calculated as a extra-price for each MWh of electric energy produced by the UWCAES turbine, needed to beak even at the end of the LT and to have an IRR equal to 15%, see Table 3.

0.4.2 Arbitrage

In this case the UW-CAES is applied to a combination of wind parks for a nominal power of 68 MWe and the
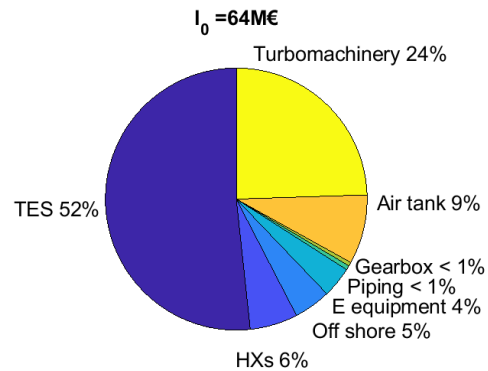
Figure 9. Investment cost sharing for case a) in table 3.

compression section of the UW-CAES is sized to manage the 100% of the wind farm capacity, choosing $P_{nom,c} = 60MW$. The storage activation strategy is defined on the basis of the electricity price profiles, provided by [28]. Two thresholds are defined as percentage increment or decrement of the mean price of the year as follow:

charging when zonal price < average price $*(1-lb)$;

discharging when zonal price > average price $*(1+ub)$.

At first the two bounds have been defined on the integral average of the hourly zonal price along the year. By this way the plant resulted in being ac-

Table 3. Technical economic results operating the plant by peak shaving logic. Case a) and b) refer to different compression section sizes, same storage capacity (48 h of nominal charge). The turbine activation threshold $lb = ub$. The reference case is the wind park without storage with energy output curtailed if above ub.

Case	ub [%]	P_c [MW]	P_T [MW]	Storage size				η_{RT} [%]	EOH_C [hours]	EOH_T [hours]	σ_P reduction [%]	Incentive ($NPV = 0$) [€/MWh]	Incentive ($IRR = 15\%$) [€/MWh]
				Air $10^3 m^3$	Salt [kton]	Oil [kton]	Water [kton]						
a)	55	60	48	139	10	7	4	78.4	1698	1674	16.8	99.31	220.2
b)	45	75	60	174	13	9	5	77.6	1643	1602	23.5	104.4	227.7

tive only few hours/year: about 1600. Then the threshold have been set on the moving mean of the EEprice, evaluated in a monthly time span. Since arbitraging aims at maximizing the economics of the plant the main parameter used to define the best threshold combination is the annual income (evaluated as income (wind park + storage) - income (wind park)). For storage capacity limited to 48 hours of nominal charge operation reference cases results are reported in Table 4. Increase in the turbine size has been shown to improve the plant performances, thanks to a faster emptying of the storage tanks.

0.5 Conclusion

This thesis presents a preliminary design and performances evaluation of an UW-CAES plant, assumed to be located off-shore South West Sardinia and coupled with deep water off shore wind farm. The design and off-design phases of the plant components have been examined and a preliminary economic analysis has been proposed. In therms of round trip efficiency and flexibility this plant results in being competitive with pumped-hydro storage system and on-land CAES. The possibility of using modular concrete air tank avoid the need of specific geological site (presence of correct orography or presence of underground geological caverns); while the presence of deep water sea or lake needed. High efficiency and wide compressors operational range are the result of sophisticated layout which include the use of parallel trains, intercooling and multiple shafts. The technology used is already mature and well known like turbomachinery (steam and turbogas derivated), heat exchanger and thermal storage. Air tank instead result to be a new storage concept, still under development. The main cost of the plant is related to the huge amount of thermal storage fluid: it covers more than half of total investment. Turbomachinery and air tank together counts for about one third of total cost. UW-CAES potentiality in grid balancing, peak shaving, black start, time shifting and many other services could be in future necessary in an electricity market with high renewable share. For this reason it could be reasonable to think that storage systems will be

Table 4. Technical economic results operating the plant by peak shaving logic. Case a) and b) refer to same compression section sizes, same storage capacity (48 h of nominal charge operation) but different turbine sizes. The reference case is the wind park without storage able to sell all the produced energy.

Case	ub [%]	lb [%]	P_c [MW]	P_T [MW]	Storage size Air $10^3 m^3$	Salt [kton]	Oil [kton]	Water [kton]	$\eta_R T$ [%]	EOH_C [hours]	EOH_T [hours]	Annual income [M€]	Incentive ($NPV = 0$) [€/MWh]	Incentive ($IRR = 15\%$) [€/MWh]
a)	20	10	60	48	139	10	7	4	78.3	1199	1020	0.88	84.99	283.9
b)	20	10	60	72	139	10	7	4	78.7	1234	813	1.02	71.2	243.6

supported in economical terms.

Chapter 1

Introduction

1.1 Energy market

Human needs of energy have seen a continuous growth during years. After the industrial revolution the use of fossil fuel became predominant, and today most of primary energy consumption derives from non renewable source [29]. The increase in energy consumption can be directly related to the increase in GDP, and this means that developing countries are going to increase their consumption during years. China for example have seen the largest growth of energy market for the 17th consecutive year. This trend is depicted in Figure 1.1. Considering the share of energy consumption in Figure 1.2 can be seen that fossil fuels play the major role. However renewable are rising, reaching a grew of 17% in last year. Inside renewable wind power is predominant providing half of total renewable power, followed by solar energy which cotribute with one third of the total. Considering the total growth of energy market, more or less half is obtained throw carbon and half with renewable sources. In the end the share of the renewables rises form 7.4 % to 8.4 % in 2017 [29]. For what concern the electricity production coal is the main energy source covering the 40 % of the total request. The natural gas provide the 23 % and hydroelectricity 15.9%. Renewables reach 8.4 %, gaining the fifth position, behind nuclear power (Figure 1.2).

Since rate of renewal of fossil fuels is much lower than their rate of consumption, they will not be always available and their use impacts on the emission of several local and global pollutants. It is important to search for alternatives, to be independent from the high fluctuation of fossil fuel price. The concentration in cities of particulate matter and nitrogen dioxide became a relevant issues which forces policy to limit the use of traditional fuels. In addition the increasing level of the CO_2 concentration in the atmosphere, seems to be related to the climate change. However there's a link between
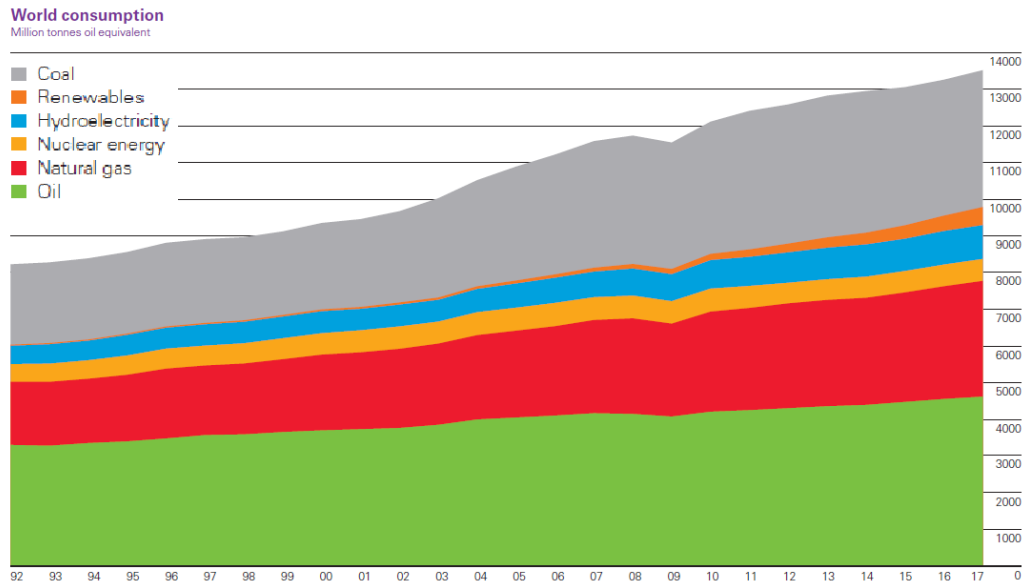
Figure 1.1. Primary energy consumption trend form 1992 to 2017 [2]
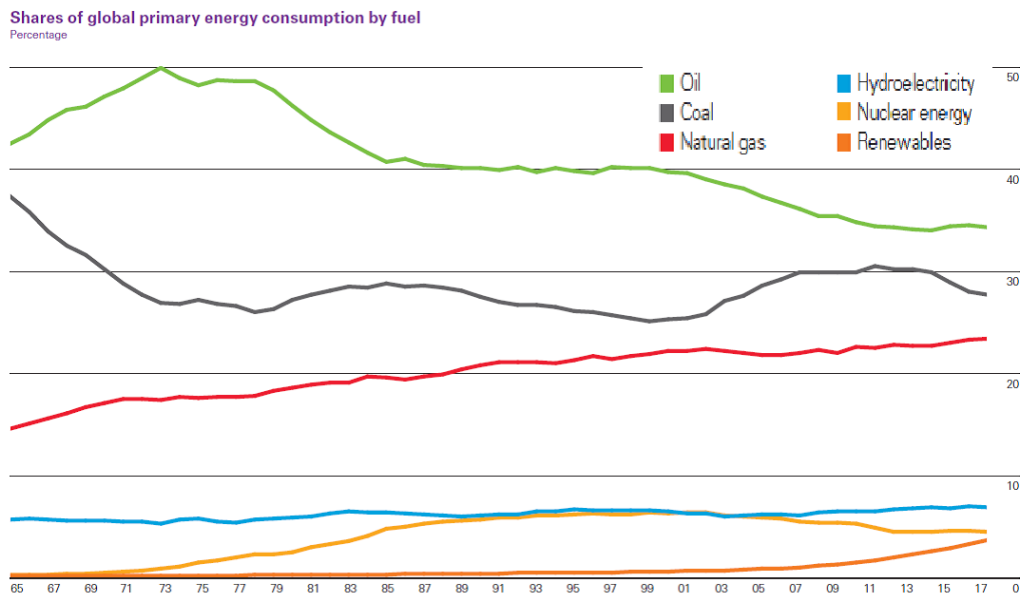
Figure 1.2. Share of the primary energy consumption from 1965 to 2017 [2]

the GDI and the energy consumption, and therefore, it is not possible to ask to developing country to stop their growth. The way in which energy consumption and pollutant emission can be reduced can be summarized in [30] :

· **Energy saving**, which can be achieved throw more attention of energy lost for bad management or insulation.

· **Improving the efficiency of power conversion**. This means that existing plant can be updated or some sophistication can be added to existing technology to improve the performance both in generation(power plants, cogeneration, trigeneration) and utilization of the resources (refrigerators, lightning, electric motors,...).

· **Improving the efficiency of the efficiency of machines and single component**. There's a continuous development, which helps in the reduction of the losses (boilers, heat exchangers, pumps,...).

· **Reduction of the environmental impact**. Same product, can be obtained throw different process, or adopting material or parameter more environmental friendly.

· **Development of renewable energy sources**

Even if it is not the only option, it is interesting to notice that renewables have seen a strong penetration, and up to now record the highest growth. In a future scenario it is reasonable to see an increase of the green sources to produce electricity, pushed by incentives [3]. In Figure 1.3 investment on different renewables are shown. Most of them are on wind and solar energy and a part from last years, a continuous growth can be appreciate.

In last years, for specific region and condition, the use of renewable becomes competitive, this means that electricity produced can be sold at the same price of the traditional plant: in Figure 1.4 different type of technology the LCOE is compared [2]. It is possible to appreciate that some renewables the technology is already mature to compete with fossil fuel costs. This means that also without incentives, technology spreads. An overview of the current renewable scenario is proposed by [4], and reported in Figure 1.5. Most of green electricity is produce throw hydroelectricity while bio-fuels are the first option for the heating systems. They represent historically the first type of non fossil alternatives. Wind and solar however start to play important role for what concern electricity production.

It is worth to highlight that renewables introduce problem into the management of the electrical grid. The non programmable nature of that sources impacts on the match between the production and consumption which must
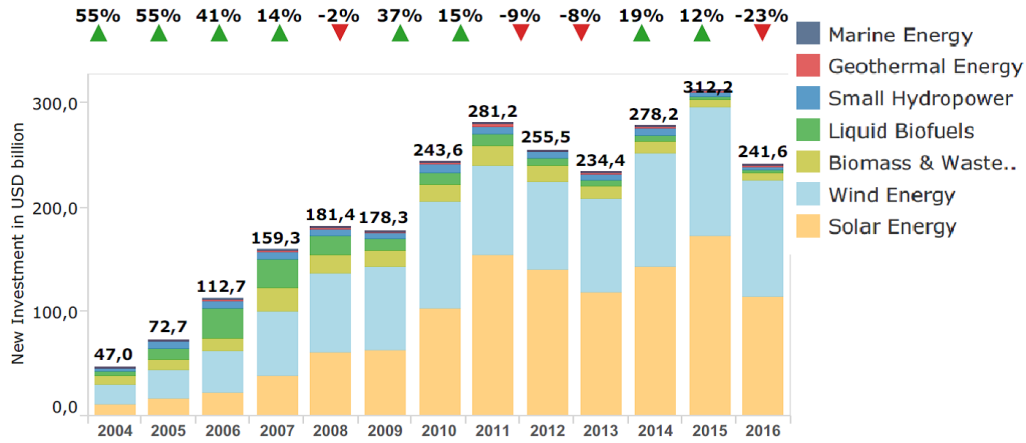
Figure 1.3. incentives trend from 2004 to 2016 for different renewable sources [3].
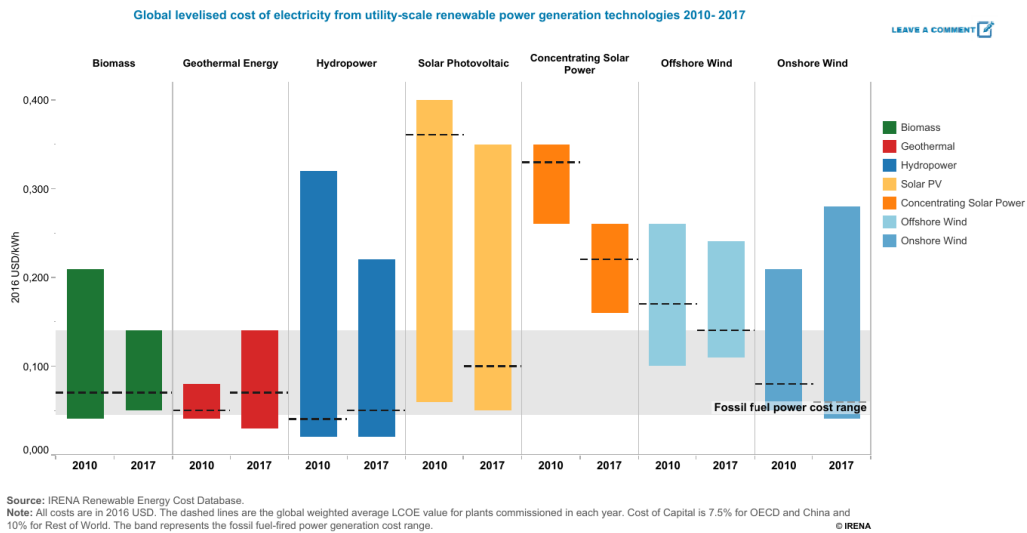
Figure 1.4. LCOE for different renewable technology, compaired with traditional fuel cost range depicted in gray [2].
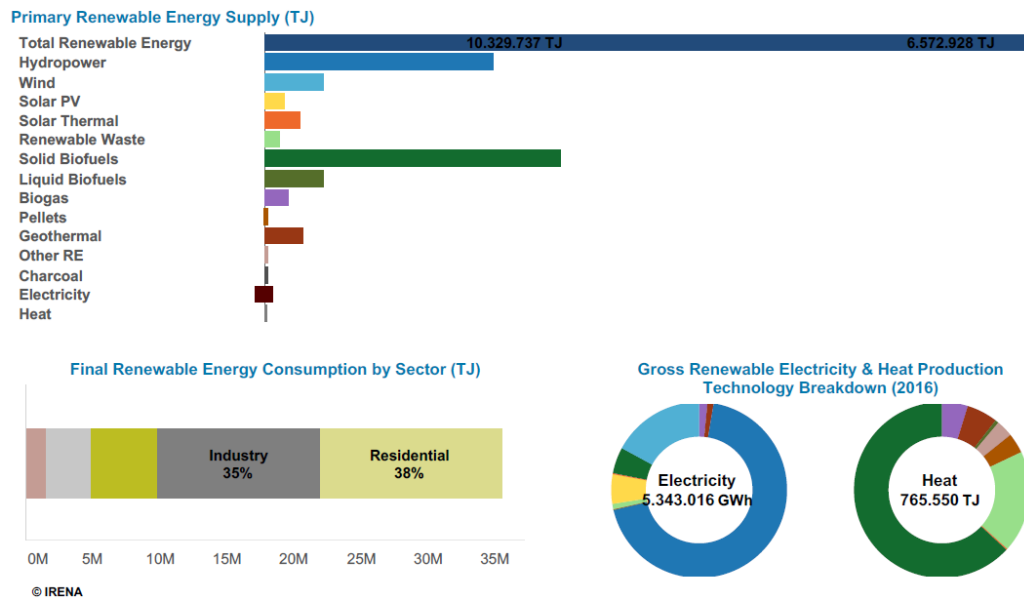
Figure 1.5. word renewable energy technology share: on the top there's the overall energy supply for different tecnology; at bottom-left side there's the use of renewable energy per sector, while at bottom-right side there's the share for renewables in electricity and heat production [4].

be always balanced. In addition typically these plant are characterized by low size and not uniformly distributed along the country. Therefore the management of the system in terms of energy production and transportation to the user require a modernization of the actual grid. In addition part of the programmable plant, those powered by fossil fuels must be devoted to the balance the random fluctuation of renewable energy. The fact is that these sources are not dispatchable and not easy to forecast. Therefore today, grid is kept stable with the use of traditional plant (powered by coal or natural gas) at part load to been able to follow energy demand. Thus exist physical limit in the penetration of renewable inside energy market To overcome these issues many strategy can be adopted:

- · grid development;

- · management of the demand;

- · improvement into the forecast model;

- · Energy storage.

1.2 Energy storage advantage

The use of energy storage seems to be very attractive for many reason:

· helps into grid balancing;

· let fossil fuel free to produce at design condition and not at part load, for grid balancing;

· reduce the need of modernization of all the electrical grid;

· possibility to increase the penetration of green energy inside electrical market;

· reduce the environmental impact;

· Time shifting: it is possible to high high production and low consumption and viceversa (wind - solar);

· peak shaving, levelling the net power to be produced, and using storage system to compensate the difference;

· loading ramp: accomplished without the ramp provided by a fossil plant;

· frequency control: the oscillation between production and consumption can cause frequency change;

· black start. It is possible to use these plants to generate a base load to been able to restart non autonomous restart plants, controlling frequency and tension of the grid, to been able to correctly restore the grid;

· mitigation of the fluctuation in the production (h,min,s);

· reduce cut off condition in which plant are stopped due to the crowded grid and limit in the power transmittable, especially in remote region. Therefore when energy can be produced but cannot be transmitted.

· protection against overload, when an element of the transmission in near its limit, power can be stored instead of being transmitted.The possibility of the use of ES (Energy Storage) both near plant than near bottle neck of the grid can be a solution.

There are several way to store energy, but the use of this systems is intrinsically inefficient because all of them are characterized by losses. Therefore if the grid is not saturated by renewable, or if the difference between demand and

production is not so high, this plant are not economically attractive. But due to their advantage of decouple production and production, becomes necessary when strong fluctuation are present inside market.

1.3 Energy storage system

The most important parameters which characterize the energy storage system are:

· **Power [kW]**, which is the maximum power which can be extracted from the storage

· **Energy storage capacity [kWh]**, which represent the maximum amount of the energy which can be extracted

· **Discharging time [h]**, which is the time needed to completely empty the storage, and it is calculated dividing the storage capacity by the nominal power.

· **Efficiency**, which is the ratio between the energy storage capacity divided by the total amount of energy needed to fill the storage.

· **Power specific cost [€/kW]**, which is the total cost of the plant divided by the nominal power.

· **Energy specific cost [€/kWh]**, which is the total cost of the plant divided by the storage capacity.

Other parameter are for example the power density [kW/kg] or energy density [kWh/kg], useful for moving devices (like cars, air planes), the variation of the performance as function of the state of the charge, reliability, availability, autodischarge losses, cost of dismission, maximum loading ramp, enviromental impact, safety. The world installed capacity in 2011 was around 125 GW of which the 98 % is made by pumped hydro system [5]. In Table 1.1 different storage technologies were presented, with the services which each storage system is able to provide. Batteries are characterized by very high reactivity in the response but they have low capacity of storage. Some other storage system are limited by ambient and geographical condition, such as pumped hydro system which require a specific morphology and presence of water. Other instead contains dangerous substances for the environment. Thanks to the high variety of the technology, each one characterized by its advantages and disadvantages, the choice of one solution depend strictly on the need of the grid.

Table 1.1. Comparison between different service that can be made by different storage system[5]:

🟢 for suitable application
🟡 for less suitable application
🔴 for not suitable application

Application	Idro	CAES	Na/S	Na/NiCl	Li/ion	Ni/Cd	Ni/MH	Pb/acid	Redox	Flywheel	SC
Time shift	🟢	🟢	🟢	🟡	🟡	🟡	🟢	🟢	🔴	🔴	🔴
Renewable integration	🟢	🟡	🟢	🟢	🟢	🟢	🟢	🟢	🟢	🟡	🔴
Primary regulation	🟢	🟡	🟢	🟢	🟢	🟢	🟢	🟢	🟢	🟡	🔴
Secondary regulation	🟢	🟡	🟢	🟢	🟢	🟢	🟢	🟢	🟢	🔴	🔴
Tertiary regulation	🟢	🟢	🟢	🟢	🟢	🟡	🟡	🟢	🟢	🔴	🔴
Black start	🟢	🟢	🟢	🟢	🟢	🟢	🟢	🟢	🟡	🔴	🔴
Tension support	🟡	🟡	🟢	🟢	🟢	🟢	🟢	🟢	🟡	🟢	🟢
Power quality	🔴	🔴	🟡	🔴	🟡	🟡	🔴	🟡	🟡	🟢	🟢

The concept of CAES systems dates back to '70s and it is gaining relevance for the coupling with big power plant around hundreds of MW. Electrochemical storage suit more for medium small application, and consist of high temperature batteries (Na/S,more economic and Na/NiCl), lithium batteries and redox/Vanadium batteries. The classic Pb/acid batteries instead are characterized by higher costs and lower life time compaired to the other solutions Those system results less economic than CAES and hydro plants

For what concern Italian energy market, many years ago incentives were spent to the conversion of the hydroelectric plant into pumped-turbined plant, to reduce the high difference in demand between day and night. Therefore this type of technology is dominant for what concern energy storage. However it is strongly dependant on the orography of the country, and there are region in which the lack of mountains or water, limit the possible site. However the penetration of renewable has balanced the difference, producing more in the day hours and less at night, making the traditional plant working in less critical condition.

1.4 Literature review- CAES

CAES concept was patented by S. Lavale in 1949 and it was under investigation since '70s with the aim of storing power produced by nuclear plants. The high cost of the crude oil lead to the first installation i 1978 of the first plant in the word in Huntorf, Germany with a nominal power of 290 MW [31]. After this first plant the decrease in oil price and the used of combined cycles decrease the economic attractiveness of this type of system. However in 1991 a new plant was open in McIntosh, Alabama with a nominal power of 110 MW [32]. After the huge increase of the renewables seen after the 2000, this type of technology regain interest due to the variability of that sources and the limit on the grid. Other projects are summarized

· Italy, Sesta (SI): in '80s with a plant of 25MW, stoped for endothermic anomalies.

· Japan, Kamisunagawa (Hokkaido): a pilot plant of 2MW in 1990

· USA, Ohio, Norton: in 2009 in which a plant of 270 MW has to be built, the biggest ever, but in 2013 the project was stopped due to the decrease of electricity price.

· USA, Iowa: the IAMU (Iowa Association of Municipal Utilities) stated in 2006, abandoned in 2011 because of the low permeability of the soil, with repect to what predicted.

- USA, Texas, Matagorda: After the opening of several wind farms and the weakness of the transmission grid. In 2013 the the construction of a 317 MW plant by Dresser-Rand e Apex Compressed Air Energy Storage [33].

- Israel: a study of a 300MW plant with porous rock always adopting the turbomachinery provided by Dresser-Rand.

- Cina: a project called "advanced large-scale compressed air energy storage system" has been proposed, with a nominal power of 20 MW.

- Germany: a project called "ADELE" has been studied, with a nominal power of 200 MW. The aim is to balance the grid in future years, where share of renewable overcome the 30 % of the overall electricity production. General electric is developing turbomachinery able to work with high pressure (100 bar) and temperature very different with respect to Turbogas or Rankine cycle. The TES is made by solid ceramic storage by Züyblin AG in collaboration with German Areospace Center (DLR) [34].

1.4.1 Classification

Exist many type of CAES system and their characteristic and configuration are:

- **D-CAES**: the traditional one in which the air is stored into a cavern (diabatic storage). It has a combustion chamber before the turbine because the heat of the compression is lost with the use of intercooler and aftercoolers, for increasing the amount of air storable.

- **steam CAES**: based on D-CAES in which part of the residual heat of the flue gasses is used for a bottom Rankine cycle, or to produce steam to be supplied in the combustion process to enhance the efficiency of the plant.

- **A-CAES**: adiabatic system in which there's no need of fuel and the heat generated during compression is stored and used to heat up air during discharging phase.

- **isoT-CAES**: which tries to reproduce isothermal transformation with the injection of water to control temperature.

- **hybrid-CAES**: which couple CAES system with a gas turbine. In this way air from the tank can be preheated with flue gasses, and the use of a fuel increases a lot the efficiency of the plant [35].

The adiabatic systems are characterized by several advantages: first of all avoid the production of CO_2 into the atmosphere, then increase the overall efficiency reachable because they don't require the consumption of a fuel, with all its exergy losses. Lower procedure of authorization of the plant is required, since no pollutant were emitted, and thus lower territorial constraints limit the use of this type of CAES. The main disadvantage of such configuration is related to the cost of the working fluid used to store the compression heat.

1.4.2 Air storage
The different technology used to store compressed air are:

- **Salts caverns**: salts is melted to obtained the correct volume using the solution mining techniques. Technology used is well known and adopt water to dissolve salt and the result is a solid cavern which assure seal also after several cycles.

- **Porous rocks**: in which a layer of impermeable rock seals a region of permeable rocks. The presence of water or natural gas make this solution more dangerous with the respect to the previous case-

- **Caverns**: adequate depth (300m to 1500m) avoid the risk of collapse. The use of old mine is the most economic option.

- **pipes or tanks**: Metal, concrete or composite material can be used to store compressed air, which are placed on the ground or some meters below. Pressure can reach also 300 bar without structural problem also considering rapid charge and discharge [36].

- **underwater tanks**: Uses the hydrostatic pressure of the water to keep constant pressure, during charge and discharge phase. An example of this configuration is made by the group Hydrostor inside lake Ontario at 80 meter depth [37] [38].

Air can be stored into constant volume condition in saline cavern, rock cavity and concrete or steel tanks. Constant pressure tank instead can be made with submerse balloons, or tanks which adopt a water column, that fills the tank during discharge to keep constant pressure. The first type of storage is intrinsically more economic, but having fluctuation into pressure penalizes the efficiency of the turbine, which see a continuous change of inlet conditions. For this reasons many of these type of plant adopt a lamination to have constant pressure at the inlet, but with a penalization of the overall efficiency. Therefore isobaric storage fix the operative condition for both compression and expansion phase. For what concern recent UW technology, a project financed by E.On, the Nottingham University (UK) and a Canadian society

Canadese Thin Red Line Aerospace have developed air tank called "Energy bag" made by layer of insulator,water, diathermic oil, and molten salts able to maintain internal temperature of 450°C [39]. Boston MIT propose a solution in which spherical air tank made of concrete are anchored to wind turbine (in an offshore configuration) and water can enters that sphere throw pumps to control pressure. [12] propose the use of multilevel storages, adopting different tank at different depth. In addition it investigate the possibility of place the plant on shore or off shore.

Chapter 2

UWCAES layout

The Underwater - Adiabatic - CAES studied in this work is made by several components:

- · air filter: to clean air from dirt and dust which can damage all air circuit;

- · compressors: used to increase the pressure to air vessel pressure;

- · intercooler: used to coll down air (and dissipate heat) to decrease compression work and control compressor outlet temperature;

- · heat exchangers: used to transfer heat between air and thermal fluid;

- · thermal energy storage (TES), used to store thermal power;

- · turbine: to extract power from air stream.

During the operation of the plant it is possible to distinguish between two different phases:

- · cooling to storage (*CtS*);

- · heat from storage (*HfS*);

When the plant have to store energy, air is compressed from ambient to storage pressure by a compressor group. The heat produced by the work provided to the fluid is stored into TES by means of series of heat exchanger which cools down the air and heat up thermal fluids (Figure 2.1). Therefore there's the simultaneus charging of air tank and hot tank of each transfer fluid used, and the consequently discharge of cold vessels. When the plant instead have to provide power, the air from the tank is discharged; then it passes throw heat exchangers where it is heated up by the thermal fluids, and reach
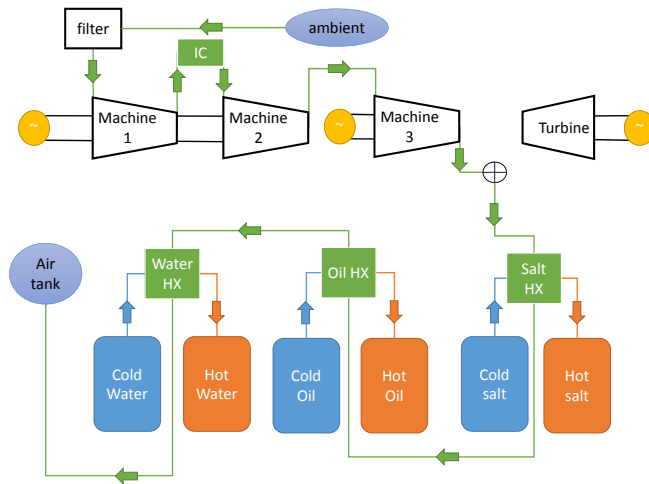
Figure 2.1. scheme of UW-CAES plant in charging phase (Cooling to Storage).
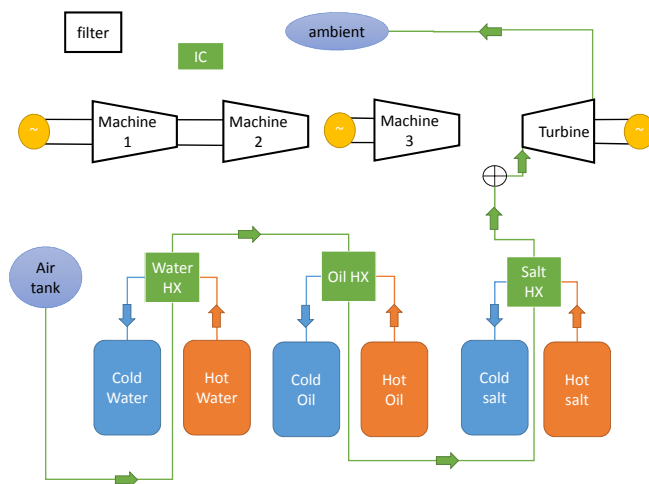
Figure 2.2. scheme of UW-CAES plant in discharging phase (Heat from Storage).

adeguate temperature to be expanded efficiently in a turbine (Figure2.2). Cold storage are filled while hot vessels are empty. Therefore this system uses well known technology of turbo machinery, and thermal energy storage. The main loss of this plant is related to the fact that due to the pinch point needed for the heat exchange process, not all the thermal energy during compression can be stored and not all the heat in thermal storage can be given to the air during expansion phase. In other words the COT(compressors outlet temperature) will be always lower than the TIT(turbine inlet temperature). The thermodynamic cycle followed by the air can be considered similar to what happen in a turbogas plant. However the layout is very different. Infact compressors and turbine never work together and thus they are fitted on different shafts. The compressors is driven by an electrical motor which absorbs power. Instead during the expansion phase the turbine will be fitted on an alternator to been able to produce power. To make the plant efficient it is mandatory to increase as much as possibile the TIT, and for this reason T.E.S or a direct combustion of natural gas is used. Exist infact phisical limit on the TOT(turbine outlet temperature) which are linked to the icing phenomena on last turbine stages. The CAES technology seems to be an alternative to the pumped hydro system, because of the possibility of storing high quantity of energy and the relative high energy density.

The concept of this layout and a possible physical diposition of the different component can be seen in Figure 2.3. It is possible to see that all the plant lays on land. This choice is related to the cost of a floating structure able to fit the big amount of thermal fluid needed to operate the plant. On land configuration has another benefit: the possibility to easily be linked with other renewables or other plant and to provide services also for them. Off shore wind farm (a) is connected to land throw high voltage cables (b). At this point a controller compair the power produced by the farm with the request of the grid to proper decide how to manage the electric power. if the controller decides that electric power from wind is too much, electricity is consumed by an electric motor (c) to feed a group of compressors. Air flows into piping and cooling to storage phase start, filling molten salt hot tank (e) thermal oil hot tank (g) and hot side of sea water T.E.S (i). Then air have to travel across piping (j) for a distance which depends on the orography of the sea and on the depth at which air tank (k) is placed. If the controller decide that electric power from the wind park is enough, the electricity goes directly to the grid, and the plant doesn't work. if the controller decide that electric power from the wind park is not enough, the electricity goes directly to the grid, and in addition air is taken from reservoir, heat from storage phase start, filling cold tank of water, oil (h) and salt (f) and discharging hot tanks. Air is expanded in a turbine, linked to the generator (d) to produce

Figure 2.3. Conceptual view of the UW-CAES system [1]
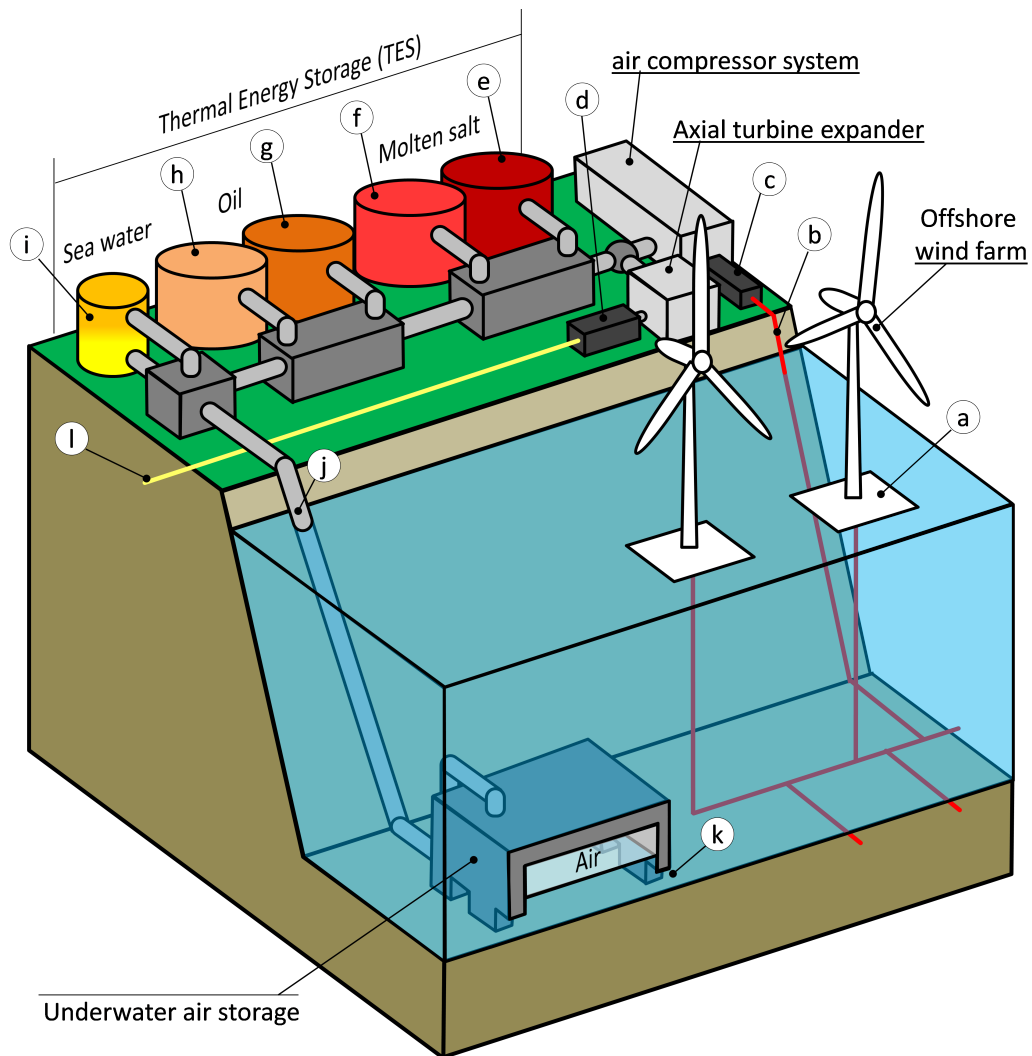
a. Wind turbine floating platform
b. Power line from wind farm to CAES
c. Compressor motor
d. Generator
e. Molten salt HT storage
f. Molten salt LT storage
g. Oil HT storage
h. Oil LT storage
i. Sea water thermocline storage
j. Compressed air piping
k. Sea water opening window
l. Power line from CAES to Grid

power which is added to the electrical power from the wind and the sum of them is sent to the grid.

2.1 Turbomachines

Turbomachinery represent crucial component of the plant. The compression ratio reached is very high, from 40bar to 140bar (depending on the depth of the case studied), and thus many compressors in series must be adopted. The possibility of using intercooled machines helps into decrease the total work required to complete the compression. However compressors have also the function of heating up the air flow, to correctly fill thermal storage tanks. Therefore a trade off between the lower work into compression obtained throw the low temperature guaranteed by intercooler adoption and the need of high temperature stream for correctly store theramal energy at high temperature must be found.

Tipically for the use of an industrial compressor the main input is the power and the compression ratio is obtained depending on the resistant curve of the plant. In this specific case instead compressors must work at constant compression ratio, independently by the input power. This particular condition require a study of the off-design map to make plant as flexible as possible. The expansion phase is made by a turbine and it is less critical than compression phase. Turbine works with constant inlet pressure and the mass flow is decided a priori, depending the management of the plant, to follow a certain production profile. In existing plant is it made by high pressure stage derived from turbogas sectors, while low pressure stages are derived from steam turbine of a Rankine cycle. In some condition it is possibile that turbine can work at part load. For this specific case the politropic efficiency is assumed to be constant. For what concern type of the plant, machine used and other general data, the work of [22] is used as starting point. Main data are the following:

· fixed pressure of the air tank 80 bar;

· power of the compression trains of 75 MW;

The main assumptions common to all investigated cases are reported in Table 2.1

For intercooler Shell and Tubes type of intercooler has been chosen, in which sea water passes inside the tubes while air flows in the shell side. The intercoolers are designed at the nominal condition of the compression train and work under the following assumptions:

· variable $\dot{m}_w$;

Table 2.1. Assumptions for performance calculation

Air molar mass	[kg/kmol]	28.96
Air specific heat, cp	[J/kgK]	1050
Air temperature in the UW-tank	[°C]	5
Ambient temperature	[°C]	20
Ambient pressure	[bar]	1.103
Mechanic electric efficiency	[-]	89.5%
Minimum IntercoolerΔT	[°C]	15
Compressor air filters pressure drop	[-]	1%
Intercooler air side pressure drop	[-]	1%
T.E.S heat exchangers air side pressure drop	[-]	1 %
Underwater compressed air piping pressure drop	[-]	2%
Minimum turbine outlet temperature	[°C]	5

- T_{in} water of 14°C;

- nominal $\Delta T_{pinchpoint}$ of 15°C;

- nominal air side $\frac{\Delta P}{P_{in}}$ of 1%;

- heat losses to and from the surroundings are neglected;

- the overall heat transfer coefficients are assumed constant, thus independent of temperature, time and position, in the heat exchangers; [22]

- the flow velocity and temperature of both fluids at the inlet of the heat exchanger on each fluid side is considered uniform over the flow cross section; [22]

- the fluid flow rate is uniformly distributed through the exchanger on each fluid side in each pass. [22]

In addition since sea water is assumed as cooling fluid, the discharge needs to meet environmental regulations, depending on the CAES location. For the studied case located in Italy the maximum T_{out} water is limited to 35°C by decreto legislativo 3 aprile 2006 n. 152 [40].

2.2   T.E.S.

The Thermal Energy Storage is the key for decoupling the compression from the expansion phase without the integration of any fuel. It is meant to store the thermal energy contained in the air stream exiting the last stage of the compression section, which otherwise would be lost. In a system without this kind of heat recovery indeed the air injected in the air tank would reach equilibrium condition with the surrounding environment, water with temperature around 5°C, dissipating its thermal energy content. The air must be cooled form high Temperature (above 600°C) down to ambient temperature. This huge change require the use of several heat tranfer fluid (HTF). The T.E.S is composed by three sequential storage units. Each unit is defined by a different thermal fluid, with a related tank and heat exchanger. Similarly to the previous work [22], the chosen thermal fluids are:

· molten salts, $60\%NaNO_3 40\%KNO_3$ [6];

· diathermic oil [7];

· sea water.

which average thermophysical properties are reported in Table 2.2.

Table 2.2. Thermal fluids properties: Temperature, specific heat, density, conductivity, viscosity and Prandtl number. [6], [7]

		Solar Salts	Diathermic Oil	Sea Water
$T_{max} - T_{min}$	$[°C]$	600 - 290	290 - 80	80 - 30
c_p	$[kJ/kgK]$	2.231	1.524	4.1794
ρ	$[kg/m^3]$	1807	896	985.7
K	$[W/(m*K)]$	0.5275	0.1071	0.6460
μ	$[Pa*s]$	0.0015	$9.7870*10^{-4}$	$5.0363*10^{-4}$
Pr	$[-]$	4.3046	19.5604	3.2609

Water is used to manage lower temeperature, below 80°C to avoiding evaporation. Diathermic oil is used for medium temperature. They are synthetic oils and due to the risk of fire and cracking phenomenon their temperature must be kept below 300°C-400°C. Melt salts are used for the

storage of the high temperature thermal energy and they are stable until 600°C. They are characterized by high solidification temperature, around 270°C limiting their range of use. It is clear that due to the constraints on the material used, the thermal energy must be stored into separate HFT and the balancing of them will define the quantity of each of fluid necessary for the purpose of the plant. Each storage is made by two tanks, one hot and the other cold. During charging phase, the HTF move from cold tank, is heated by air and is stored in hot tank. During discharging phase the motion is reversed, where the same three heat exchangers are used in reverse way for the *CtS* and *HfS* phases. The storage unit working with sea water helps in the low temperature heat recovery and it is provided with a by pass system avoiding cases during which the system could not work, being the sea water storage saturated or empty, while the oil and salt ones are still operative. Moreover an additional heat exchanger has been introduced for balancing the solar salts and diathermic oil energy levels. During yearly usage of the plant, part load is most frequent charging condition, this causes unbalances between the energy stored in the molten salts and the oil tanks, leading to a faster saturation of the first one. For this reason energy could be released by salts to the oil keeping constant the ratio between the actual energy stored and the maximum storable energy for the two units.

2.2.1 Heat exchangers

The heat exchangers are Shell and Tube type. The thermal fluids are supposed to flow in the tube side while air passes through the shell side. This last side is supposed to be finned to enhance the heat exchange process and being the air side the limiting one. The HXs have been designed on the basis of the *CtS* phase, particularly referring to the nominal design of the compression section. Hence they are sized for the air flow rate, inlet temperature and pressure resulting from the last stage of the compressors. The heat exchangers design may vary according to different compression section configurations. The following assumptions are valid:

- · Negligible heat loss to the surroundings.

- · Negligible kinetic and potential energy changes.

- · Constant properties.

- · Negligible tube wall thermal resistance and fouling factors.

- · Fully developed conditions for air and thermal fluids.

Afterwards once the compression section configuration is defined the T.E.S heat exchanger design is investigated to find the convective heat transfer

coefficients of both air and thermal fluid sides, the heat transfer surfaces and to verify that the assumption over the nominal pressure drop is respected.

2.2.2 Storage tanks

The tanks in which the thermal fluids are stored are supposed of being cylindrical structures made of concrete with a diameter and height of 20 meters. For each storage unit at least two tanks are required, one for high and the other for low temperature. Their volume is the parameter which really determines the quantity of thermal fluid containable and then the maximum amount of energy storable in the T.E.S. system. The sizing criteria is expressed as time, during which the T.E.S. is able to work at nominal condition. This means that if the sizing time is equal to 48 hours, the UWCAES system could work at nominal CtS phase for 48 hours before the thermal storage is saturated. The number required tanks is then dependent on the amount of thermal fluid required during the heat transfer phase at nominal condition and the desired sizing time. Heat losses are approximated to an hourly percentage loss of the energy content of the tanks: $\frac{Q_i - Q_{i+1}}{Q_i} = 0.01\%$. This value is estimated considering the heat flux between the external tank surface and the surrounding environment, with this parameters:

- · wall temperature, $T_{tank,wall} = 30°C$

- · ambient temperature, $T_{amb} = 20°C$

- · convective heat transfer coefficient, $h_a = 10\frac{W}{m^2 * K}$

- · external surface, $A = 1885m^2$

2.3 Underwater air tank

As explained in Chapter 1 exist many way to store air. Considering the offshore wind park at which plant will be connected and the availability of the correct orography of the sea bed, an UW-storage solution is considered. From [41] [39] it is possible to highlight that exist mainly two techniques to be adopted. The first one consist of the use of a flexible fabric structure anchored to the sea bed. The hydrostatic pressure acts on the wall of the bag and reach an equilibrium condition with the air inside. In this way air and water are kept separated. It is possible to use multiple layer configuration to keep warm the air inside the bag with the use of molten salt, oil and water. In this work it has been preferred to store cold air, and physically separate the air storage by the heat storage. Therefore the second option consist in the use of a concrete structure, with some window at the bottom. In this way air can be inflated by the top; it is in equilibrium with the surrounding

water, and when air enters, water exit from the window. In this way when the storage is empty the vessel is filled with almost water and when storage is full, only air is inside. Therefore the air is in contact with sea water and thus it reaches same pressure and same temperature. An idea of how it can be made is reported in Figure 2.3. Since the structure is in equilibrium, no particular stresses rise in the structure, and therefore no constraints are imposed on its shape. A simple parallelogram with some aperture at the bottom could be the less expensive shape. The thickness of the concrete needed depends only on balancing of the vessel, to avoid its floating. Since air (at 80 bar) have lower density with the respect to water, it generate a net force which tend to rise the tank. By increasing the weight of the concrete it is possible to balance this effect to simplify the anchoring system. To manage different level of energy storable the idea is to use modular structure of 1000 m^3 linked by piping system to reduce the cost.

2.4   Pipeline

An off-shore pipeline connects the underwater air tank to the turbo machines and the thermal energy storage. Its length is directly dependent on the plant layout, on the desired depth of the air tank, then on the desired air pressure and on how steep the sea bed is. In this work the plant is considered with on-ground layout meaning that the machines and the thermal fluids tanks are located at the shore, while only the wind farm and the air storage are positioned off-shore. Considering the orography of the seabed in Sardinia, where the off shore plant is located, the target pressure of 80 bar is reached at almost 40 km far from the land, at a depth of 815 m [42]. Typical subsea flowlines for nonsour sevice are made of carbon steels with grades from B to grade $X70$ or higher, of the API standards (Pag 177 [43]). The UWCAES pipeline has to carry just pressurized air so the tubes are assumed being made of carbon steel API $X65$ which characteristics are reported in the Table 2.3. The sizing procedure is based on the assumption of a reasonable pressure drop value accepted along the pipeline. Fixing $\frac{\Delta p}{p_{in}} = 2\%$, for a given air flow rate is possible to calculate the corresponding inner tube diameter required. The Darcy Weisbach equation is used together with the Colebrook White equation, solved with an iterative method [46]:

$$\begin{cases} \Delta p = \lambda * \rho * \frac{v^2}{2} * \frac{L}{D} \\ \frac{1}{\sqrt{\lambda}} = -2 * \log \frac{\epsilon/D}{3.7} + \frac{2.51}{Re*\sqrt{\lambda}} \end{cases} \tag{2.1}$$

Where λ is the friction factor, ρ is the fluid density, v is the fluid average velocity, L and D are length and diameter of the pipeline respectively, $\frac{\epsilon}{D}$ is the relative pipe roughness and Re is the Reynolds number. In Figure 2.4

Table 2.3. Material characteristics

API $X65$			
Specified minimum yeld stress	$[MPa]$	448	[44]
Young modulus	$[MPa]$	207000	[45]
Poisson Ratio	$[-]$	0.3	[45]
Roughness	$[\mu m]$	25	[45]
Steel Density	$[\frac{kg}{m^3}]$	7850	[45]

the relation between inner tube diameter, air flow rate and required pressure at the air tank is represented. The diameter decreases with the increment of the desired pressure since higher pressure means higher tolerated pressure drop, then higher fluid velocity and smaller inner diameter. Once the inner
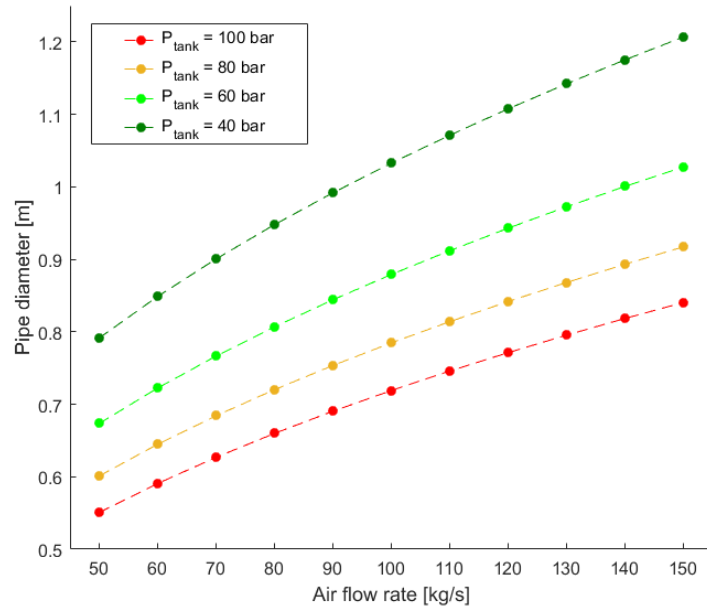
Figure 2.4. Pipeline inner diameter as function of air flow rate and air pressure.

diameter is set the required wall thickness can be investigated. In literature the DNVGL$-$ST$-$F101 [44] is described as the most appropriate design

guideline for deep offshore pipelines [47]. As reported in [Table 5−7 pag.93 DNVGL-ST-F101 [44]] the wall thickness design of a pipeline is stated by pressure containment, external pressure collapse and buckling propagation limits. However for the specific case of deep water installations it could be assumed that collapse under external hydro-static pressure replaces internal pressure as the dominating load case for the pipeline design [48]. This load condition is representative of the most stressing case during which the internal pressure is null and the external one is at its maximum value. The collapse pressure can be expressed as function of the elastic capacity p_{el}, the plastic capacity p_p and ovality o_o, equation.

$$\begin{cases} (p_c - p_{el}) * (p_c^2 - p_p^2) = p_c * p_{el} * p_p * o_o * \frac{D}{w} \\ p_{el} = \frac{2*E*\left(\frac{w}{D}\right)^3}{1-v^2} \\ p_p = f_y * \alpha_{fab} * \frac{2*w}{D} \end{cases} \tag{2.2}$$

Where D is the tube diameter, w is the wall thickness, E is the Young modulus, v is the Poisson coefficient, f_y and α_{fab} are the characteristic material strength and fabrication factor and their value is reported in [44].

The wall thickness, diameter ratio is plotted as function of the underwater air tank depth in Figure 2.5, for a given air flow rate equal to 100 kg/s. As can be seen the wall thickness over diameter ratio is increasing with depth as expected while the wall thickness net value is slightly deceasing since the tube diameter is smaller for deeper air tanks.
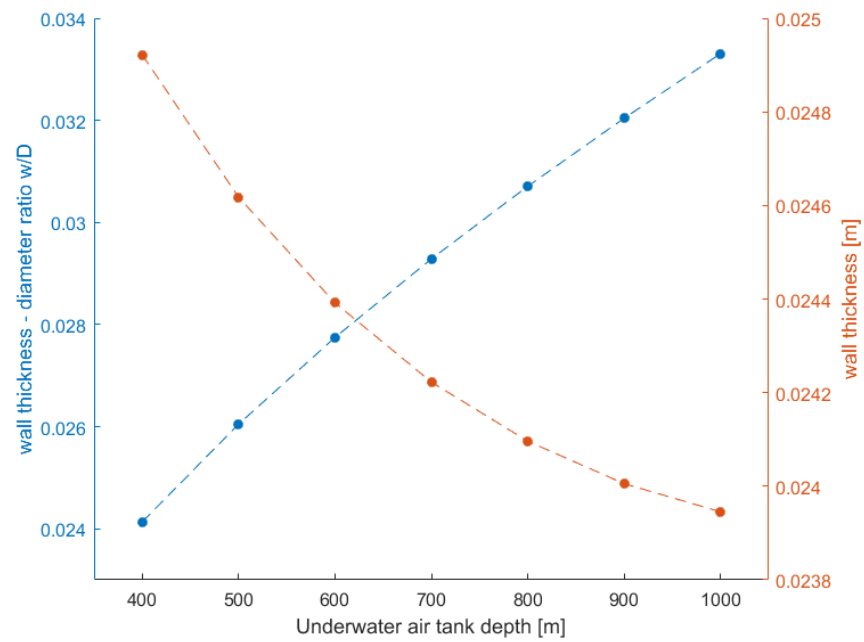
Figure 2.5. Pipeline wall thickness as function of the underwater air tank depth.

Chapter 3

Plant design

3.1 Introduction

During the design procedure, some specific terms will be used in order to be more clear since there are several component which can be defined as compressors. The term *train* will be used to define the group of compressors in series which provide the overall pressure ratio, from atmospheric pressure to air tank pressure. The train is made by several blocks of compression called *machines* each of them composed by several stages to produce a partial compression. According to the industrial limit of such machines, reported in Table 3.1, each machine is divided in many *stages*. To clarify the notation

Table 3.1. Main characteristic of compressor type: limit[8], maximum efficiency and operative area on Cordier diagram [9] [10].

Type of machine	maximum β_{stage}	maximum $\eta_{Cordier}$	range
axial	1.4	0.8476	$Ns \geq 2.5$
mixed flow	2.2	0.8756	$2.5 > Ns > 0.6$
radial	4	0.8297	$Ns \leq 0.6$

an example is reported in Figure 3.1, in which a configuration with two train in parallel is shown. The stages belonging to the same machine are characterized by the same compression ratio. Trains in parallel are equal in terms of dimension, number of machines and intercoolers, an thus they are characterized by the same performances.

(a) whole compressors subdivision   (b) machine subdivision
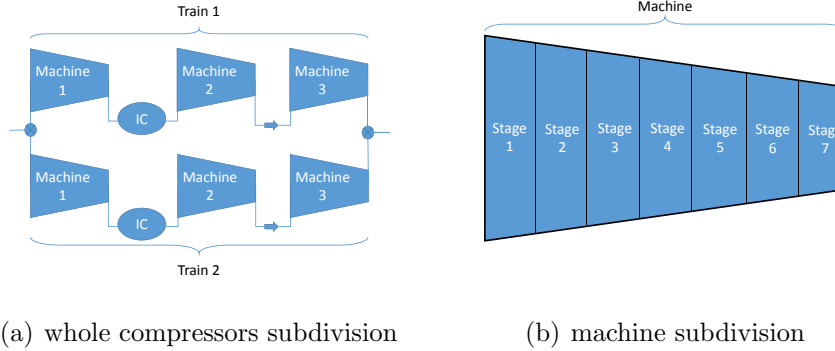
Figure 3.1. example of configuration for the explanation of the terminology: Trains refers to series of compressor which generate beta require. Machine are each compressors, made by different stages.

The approach to the compression design rely on the use of the Baljé diagram for compressible machines to find the efficiency of each single stage of compression phase. This diagram has been digitized from [49] [50] [21]. It refers to Ns and Ds defined as:

· specific speed:

$$Ns = \omega * \frac{\sqrt{\dot{V}_{nom}}}{dh_{is}^{0.75}} \tag{3.1}$$

· specific diameter:

$$Ds = D * \frac{dh_{is}^{0.25}}{\sqrt{\dot{V}_{nom}}} \tag{3.2}$$

where ω is the rotational speed in rad/s, $\dot{V}_{nom}$ is the volumetric flow rate at the inlet of the stage in m^3/s, dh_{is} is the ideal work (at constant entropy) made by the stage in J/kg and D is the mean diameter of the stage in m. Results are depicted in Figure 3.2. This diagram is referred to quite old machines (1981) and does not consider the compressors performance development during years. In Table 3.1 the type of machines and the maximum efficiency are reported. The optimum compressor design lays on the Cordier curve and its maximum efficiency is 0.876, while today industrial compressors can achieve efficiencies of 0.92. To adapt the old curve to modern compressors what is done is to consider a corrected version of this diagram in which all values are shifted to reach commercial performances. This is a huge assumption and lot of effort has been put to check consistency of the design, comparing the result of our code with nowadays available machines. In the same way also Cordier curve has been digitized and re-scaled, form [9] [10], as can be seen in Figure 3.3.

(a) 2D representation   (b) 3D representation
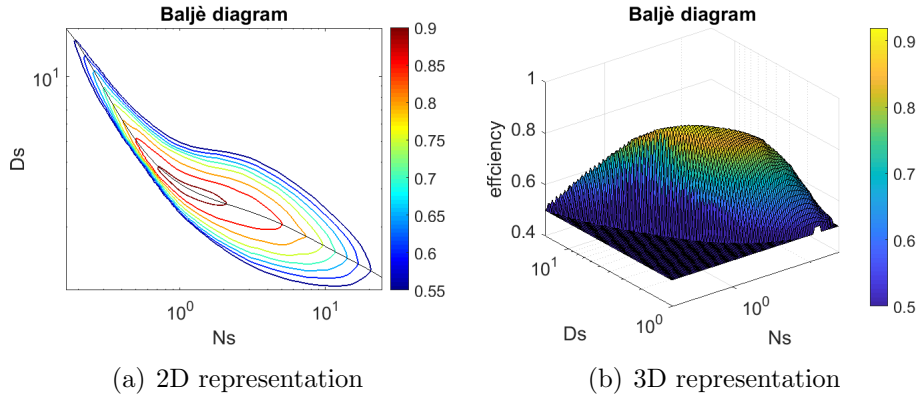
Figure 3.2. Baljé digitalization

This procedure is the same followed by [22], in which the authors scaled Baljé

(a) Ns - efficiency interpolation   (b) Ns - Ds interpolation
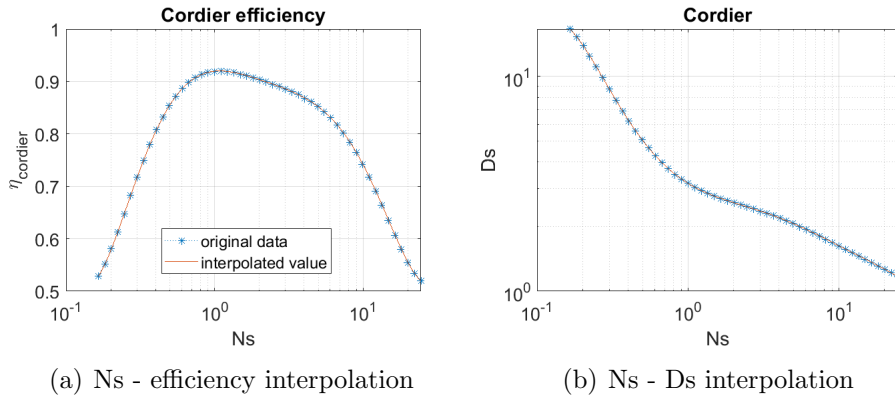
Figure 3.3. Cordier curve digitalization

diagram considering the development of compressors during years. The fact that different types of machines have seen different growth is not considered, and the hypothesis that the diagram is simply shifted and not stretched is taken. The aim of the design procedure is to maximize the overall round trip efficiency (RTE), calculated with the Equation (3.3).

$$\eta_{caes} = \frac{l_{turbine}}{l_{compressor}} \tag{3.3}$$

In the design phase η_{caes} is evaluated considering same flow rate and same operational time for charge and discharge phases. Therefore before studying

different compression designs also the entire T.E.S apparatus has to be defined for a correct simulation. The thermal energy storage as already reported in Chapter 2 is composed of three different stages, heat transfer to Solar Salts, to diathermic oil, and to sea water. During the operation of the CAES plant two different phases can be individuated: see Figure 2.1:

- · Cooling to Storage *CtS*, see Figure 2.1;

- · Heating from Storage *HfS*, see Figure 2.2.

Heat transfer process is designed according to *CtS* phase, while the *HfS* phase is calculated, since heat exchangers are the same and temperatures of the HTF are fixed.

3.2   Methodology

3.2.1   Compressor
The first problem to be solved is that Baljé diagram refers to single stages and not to machines. Therefore before its employment, there is the need of defining a strategy to subdivide each compressors into stages: the first idea is to consider machine as a single stage. Then this machine is iteratively subdivided into stages until the constraints on the compression ratio are satisfied.

However when the compression is split, the ideal work drops and therefore the value of Ns change a lot: this means that compressors change type, from radial to mix or from mix to axial. This technique however forces to have radial machines when possible, because once the limit on the compression ratio is respected, the machine is not split anymore. The next step is to start the design considering all mixed stages and then to group axial and radial machines.

It has been interesting to judge the effects of the subdivision into stages alone, without the influence of the solver [1]. To do that the simpler configuration with no intercooling and just one shaft is tested. Spanning different rotational speed; the target is to obtain a curve of efficiency as function of the rotational speed similarly to what happens in a single machine. The result is the depicted in Figure 3.4. RTE is very discontinuous and it is affected by jumps. This trend is related to the discontinuous type of stage. When the design move from all mixed flow compressor to axial compressor, it is reasonable to have some fluctuation. Discontinuities rise where there's a change

---

[1]the solver is **fmincon**,which is a Nonlinear programming solver implemented in **Matlab**
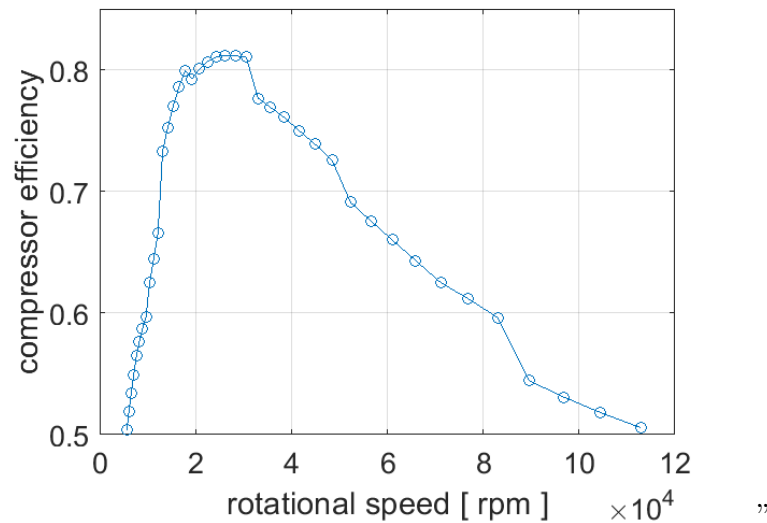
Figure 3.4. Trend of the efficiency as function of the rotational speed for single shaft not intercooled solution, 80 bar of tank pressure and 75 MW power.

into the type of the machine: the main cause can be related to the fact that efficiency is a continue function of Ns, while the limit on compression ratio is a step function. During sensitivity analysis mixed compressors, characterized by higher β, are more efficient. Moving to axial compressors, what originally was mixed has to be splitted along several stages, characterized by decreasing efficiency. In addition the compression ratio made is lower and this means that even if the efficiency is high, it is related to small compression: the sum of small efficient compression result into more inefficient overall compression. To try to move to smoother behaviour, helpful when running optimization, a smooth change of β is tried. This solution seems also more intuitive, and modify the mixed flow compressor as a transition from axial to radial compressors. The limit on beta will be determined using a function and not a discrete value, reported in Figure 3.5. Before and after the region of mixed flow compressors the different limited curves result to be perfectly superimposed. This new limit oblige to modify the algorithm: at each iteration limit changes and this causes strong movement on Cordier diagram. Each machine can be composed by different type of compressors (axial, mix or radial); inside a machine the stage belonging to the same compressor type is characterized by same compression ratio. Therefore considering the case without intercooler, starting from one single machine, at the end three machine were generated in any rotational speed tested: the first is axial, the second is mixed and the last is radial. Unfortunately this way of decompose the machine lead to lower efficient compression train for many reason:
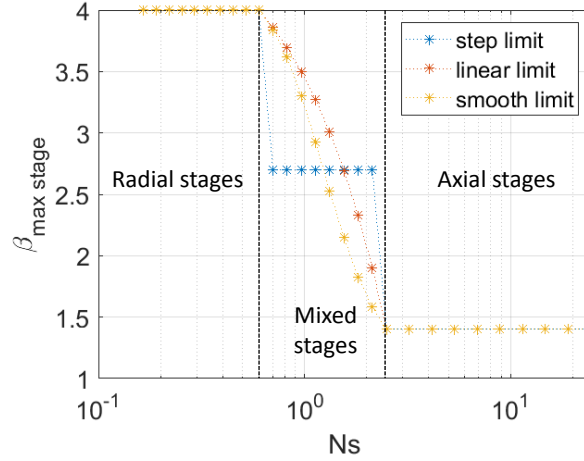
Figure 3.5. different limit on beta analysed, as function of Ns: step limit define a unique maximum compression ratio for mixed flow compressor; liner limit define a linear decrease form radial to axial, while smooth limit define a cure which interpolate smoothly from radial to axial in mixed-flow region.

· mixed flow compressors since have to have the same compression ratio, are limited by the first one: this is the only one near the limit, while the others are very far. Thus all of them provide a β near to that made by axial machine.

· Due to the low limit, machine are split and ideal work continue to reduce, moving most of the point on axial machines. This means that in the end there is the mix flow region (characterized by the higher efficiency) which results almost empty, and most of the machine are radial or axial, with an overall lower efficiency.

Running the case with smooth limit what is obtained is axial machine made by 6 stages, 1 mixed flow stage and 2 radial stages. Efficiency as function of the rotational speed is not yet satisfying since is still discontinuous: this occurs because in the end the discontinuity is still present and it is related to the fact that Cordier curve is not filled properly.

Independently by the logic used and the sophistication implemented, in the end of the work the efficiency curve remains always affected by several fluctuation. In the case of single shaft in which the number of variable to be optimized is equal to the number of intercoolers adopted, the algorithm returns result more or less independently by the initial vector. The optimization variable is the compression ratio done before the intercooler and the analysis on the rotational speed is made manually, and not by the solver, running the

code adopting several speed. Spanning all the range and manually consider the best option, the problem of local or global minimum is avoided. Unfortunately when a multiple shaft case have to be analyzed this technique cannot be used. The efficiency and the rotational speed of the machine which precede affect the results of the following. Since compressors are not hydraulic machines, the inlet temperature is fundamental to evaluate the work and the efficiency. Considering an ideal gas indeed:

$$l_{comp} = c_p * T_{in} * (\beta^{\frac{\gamma-1}{\gamma}} - 1) \tag{3.4}$$

Therefore the analysis must be done evaluating lot of different combination of rotational speed of different shaft. This can be in theory done with the solver but the already fluctuating solution do not assure to reach correct result [2] Trying it the solvers always stops near initial guessed value, making these analysis useless. The idea to overcome the problem is to generate a map of compressors design, which can be smoothed, helping the solver to do the job. This can be done considering the design of a huge series of compressors characterized by different compression ratio and mass flow rate. In this way when the program have to design a machine it simply enters the function with initial data and function gives back the result of design. A curve of efficiency as function of volumetric flow rate, compression ratio and rotational speed however is seen to be strongly dependent on the initial condition. Different temperature, lead to different mass flow rate and the results are no more unique. Moving to some characteristic parameters used for the design of a turbo-machine these three parameter are defined, all of them referred to the whole compression and no more linked to the stage:

· specific speed:

$$Ns1 = \frac{\omega * \sqrt{\dot{V}_{nom}}}{dh_{is}^{0.75}} \tag{3.5}$$

· isoentropic volume ratio:

$$Vr_{is} = \frac{\rho_{exit\,isoS}}{\rho_{inlet}} \tag{3.6}$$

· size parameter:

$$SP = \frac{\sqrt{\dot{V}_{nom}}}{dh_{is}^{0.25}} \tag{3.7}$$

---

[2]**fmincon** is a gradient-based method designed to work on problems where the objective and constraint functions are both continuous and have continuous first derivatives.

where $\dot{V}_{nom}$ in m^3/s is the volumetric flow rate, dh_{is} is the ideal work in J/kg, obtained considering the same outlet pressure, but constant entropy. ω is the rotational speed in rad/s; $\rho_{exit\,isoS}$ is the density at outlet pressure considering isoentropic transformation. With this parameter is possible to calculate all what is needed: from Equation 3.6 it is possible to find the ideal work of the overall machine and overall compression ratio, knowing inlet condition. From Equation 3.7 it is possible to calculate the volumetric flow rate, and knowing inlet condition also the mass flow rate. Finally form Equation 3.5 it is possible to obtain the rotational speed.

All compressors are guessed as mixed machines (the type characterized by the highest efficiency), and number of stages necessary to produce the overall compression ratio is calculated. Single stage quantity Ns using Equation 3.5 is found and a function which interpolate the Cordier curve is used to obtain stage efficiency:

$$\eta_{stage} = f_{Cordier}(Ns) \qquad (3.8)$$

Then a check has been made to verify that the Ns related to each stage is consistent with the type of the machine. For example, a mixed machine must be made by all mixed flow stages. If not, the stages out of the initial machine are splitted (in case of axial machines) or grouped (in case of radial machine) to have the correct maximum pressure ratio. New check is made, since ideal work is connected to the compression ratio. In the end number of stage, and the type of machine can be found, and overall performance of compression train can be evaluated.

The code has been run for very high number of possible combination of these three parameter and several interesting results have been observed. SP inflence the mass flow rate and the dimension of the machine, but, relaying on Baljé diagram, which do not consider scale effect, in our design do not affect the efficiency. Therefore it is possible to move to a simplier 3D curve in which the efficiency can be simply found from Ns and Vr_{is}. The result can be seen in Figure 3.6. This graphs result to be very general, since it is able to represent many cases, form one single stage compressor (for low Vr_{is}) to complex machine, made by axial, mixed flow and radial compressors in series, needed to generate huge compression ratio. In addition this trains has been designed for several rotational speed, until they fit inside Baljé diagram. It is possible to recognize that exist a maximum for each single volume ratio: it is possible to define optimum Ns function to calculate rotational speed of maximum performance for that train. In this analysis all machine are characterized by the same shaft. It is possible to see that increasing Vr_{is} the overall efficiency decreases. This is due to the fact that i need more stages to provide the overall compression ratio and therefore they move on Cordier line. The optimum speed is found to optimize the train, penalizing

(a) 2D representation

(b) 3D representation
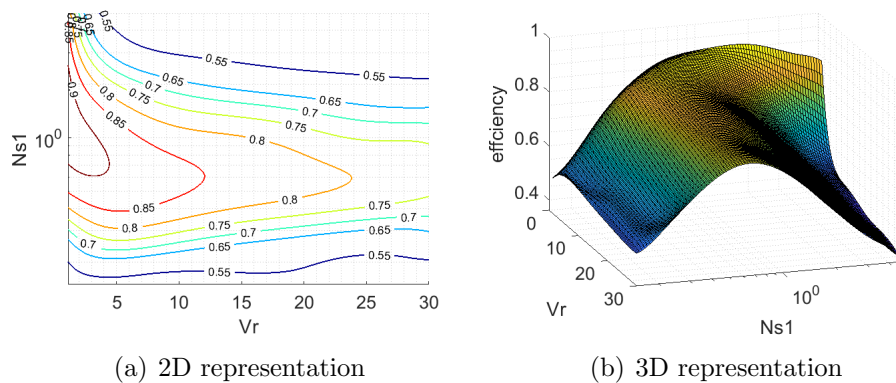
Figure 3.6. Compressor curve for the design of the compressor: for a couple of Ns1 and Volume ratio is able to provide efficiency of the whole train of compression.

the first and last stages. This map enable the simply design of the compression train: however to be general it must be verified for a various range of initial condition. Inlet temperature has been changed from 20°C to 600°C, with a maximum difference of 0.5% in whole map. The same has been done for pressure, changing inlet condition from 1 bar to 20 bar, recording almost the same difference. With this simple analysis the independence on inlet condition is verified and the map results applicable for our scope. The solver is *fmincon*, implemented in *Matlab*[3], which is a local minimum solver. To avoid the solver to stop near local minimum, interpolation has been made on the design map to have smooth curve (Figure 3.7). This step introduces an error defined as $(\eta_{orginal} - \eta_{interpolated})/\eta_{orginal}$ and it has a mean error of 1.2 %. The interpolation function is optimized to be more precise on the top of the curve, where compressors will be placed, and less accurate on the side. The analysed case with the information of the variable to be optimized are reported in Table 3.2. The optimization is made on the rotational speed, the compression ratio made by the same shaft and the compression ratio after which an intercooler is placed. The layout of different cases is presented in Figure 3.8. The idea is to try to split compression ratio in more uniform way along different shafts. Therefore since the intercooled part of compression is very low, the result is that on the first shaft fit all intercooling phase, and on the others not intercooled part.

For what concern the use of the map, with the first shaft it is necessary to optimize the rotational speed, to try to find the best trade off between separate part of compression. Since there's an intercooler in the middle, the

---

[3]Matlab, version R2018a, Mathworks

(a) original
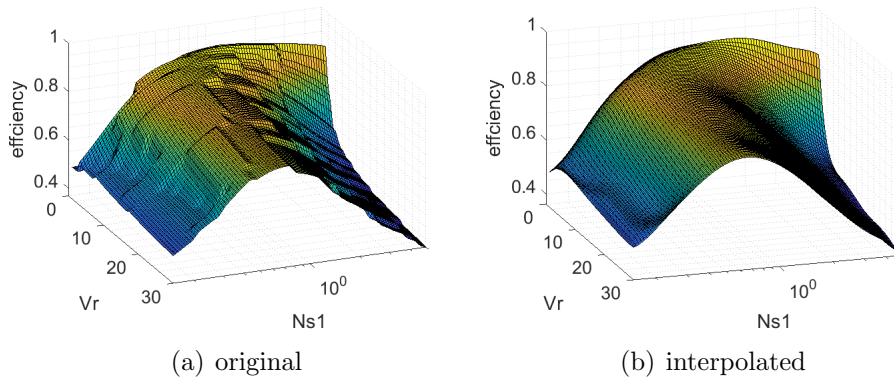
(b) interpolated

Figure 3.7. Compressor curve for the design of the compressor: comparison between original and interpolated curve.

Table 3.2. Case tested: ω is the rotational speed, followed by the number of the shaft; β is the compression ratio: the number is related the overall compression ratio made by the shaft, while the letter represent the compression made before the intercooler

IC	shaft	name of the configuration	variable to be optimized
0	1	A.1	ω_1
0	2	A.2	$\omega_1, \beta_1, \omega_2$
0	3	A.3	$\omega_1, \beta_1, \omega_2, \beta_2, \omega_3$
1	1	B.1	ω_1, β_{1a}
1	2	B.2	$\omega_1, \beta_{1a}, \beta_1, \omega_2$
1	3	B.3	$\omega_1, \beta_{1a}, \beta_1, \omega_2, \beta_2, \omega_3$
2	1	C.1	$\omega_1, \beta_{1a}, \beta_{1b}$
2	2	C.2	$\omega_1, , \beta_{1a}, \beta_{1b}\beta_1, \omega_2$
2	3	C.3	$\omega_1, \beta_{1a}, \beta_{1b}, \beta_1, \omega_2, \beta_2, \omega_3$
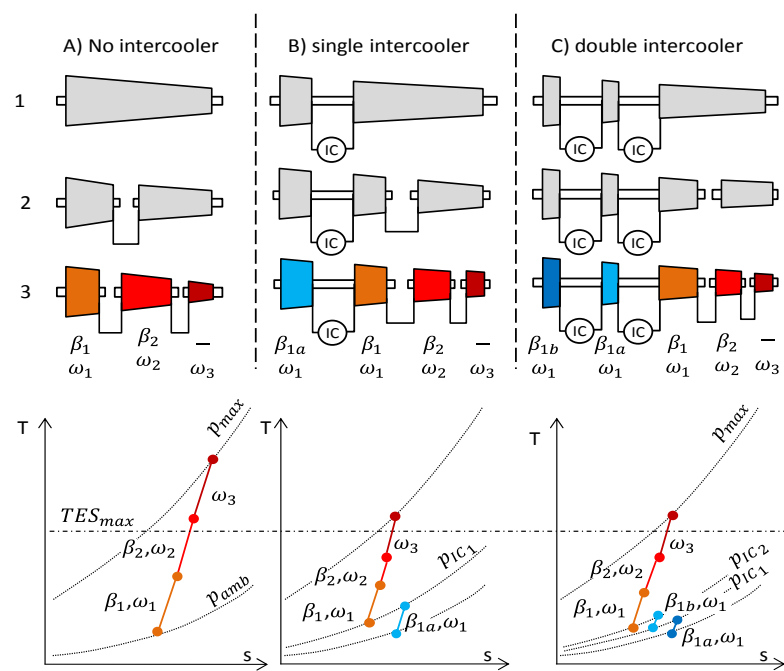
Figure 3.8. Compressor configuration for case without intercoolers (A), case with single intercooler (B) and case (C) with three intercoolers for single (1), double(2) and three shaft (3). Ts diagrams refers to the three shaft configuration highlighting the optimization variables. [1]

map cannot be used for the whole shaft, because it is obtained for continuous compression. The intercooler changes inlet condition and therefore must be treated separately. Instead stages which lays on second or third shaft are all in series, and for them it is possible to adopt the map: to each Vr_{is} is related an optimum Ns, and rotational speed is found directly from the optimum curve, without need of any optimization. This is the strong potentiality of the map, which enable an easy management of multiple shaft configuration. To clarify how the algorithm works, the example of the case with one intercooler and two shaft is considered. In Scheme 3.9 the logical passages made are shown. The solver tries many combination of input data (blue octagon), calculate
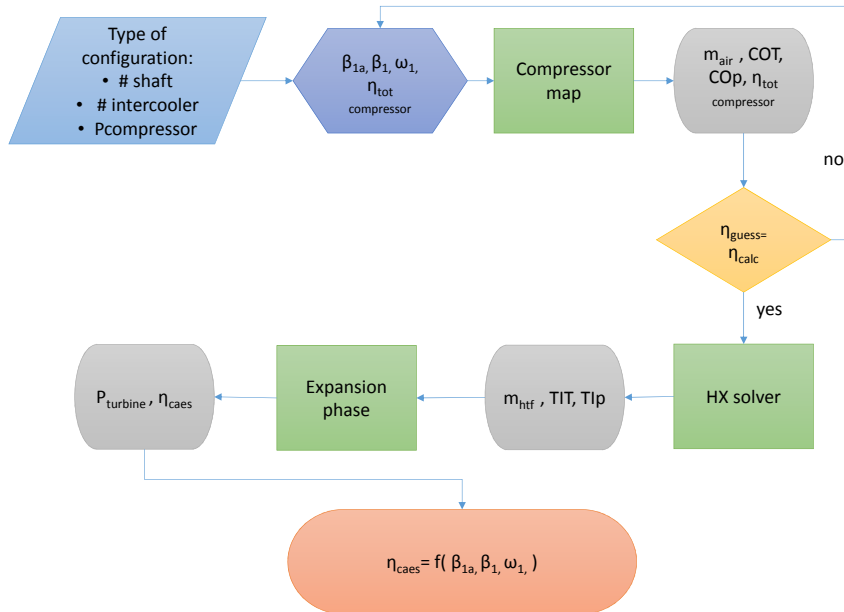
Figure 3.9. Algorithm for the design. Green blocks represent function, in gray the output of green function. In blue there is the part managed by the solver.

compression part, finding air flow rate, exit temperature and compression efficiency. As can be appreciate, the algorithm is iterative and requires to guess efficiency and recalculate it. This is necessary because in our scope the power of the compressor is fixed, and therefore the efficiency of the

compression phase determine the mass flow rate:

$$\dot{m} = \frac{P_{nom} * \eta_{tot\,compression} * \eta_{organic-electric}}{dh_{is}} \qquad (3.9)$$

Therefore volumetric flow rate and $Ns1$ depend on the result, and thus require a recursive algorithm which iteration after iteration reduces the error. Then it is possible to calculate charging (CtS) and discharging phase (HfS) of the air vessel to move from compression outlet thermodynamic propriety to turbine inlet condition. Expansion is then calculated to finally found RTE (Equation 3.3). Trying many combination of input variable it is possible to find the combination which respect the constraints and optimize the efficiency.

3.2.2 T.E.S

To switch from compression to expansion phase the design of heat storage and transfer phase must be analyzed. Maximum and minimum temperatures of oil and solar salts have been defined in Chapter 2. Knowing the compressor outlet temperature it is possible to calculate the pinch point at the inlet of the solar salts HX:

· if (COT - $T_{max\,salt}$) is below 25°C: the maximum salt temperature is calculated maintaining the pinch point at 25°C, the minimum allowed, to reduce the required area.

· if (COT - $T_{max\,salt}$) is above 25°C: the maximum salt temperature is limited to 600°C as explained in Chapter 2 and therefore the adopted pinch point will be higher than 25°C.

In Figure 3.10 two cases corresponding to different values of COT are compared to better understand the impacts of the changing pinch point. As can be seen the temperature difference between air and heat transfer fluid is kept constant along all the 3 heat exchangers. Thermal powers, air temperatures and thermal fluid flow rates are computed by solving the thermal balances across the three HXs, considering negligible the heat losses:

$$\begin{cases} \dot{Q}_{hx} = \dot{m}_{air} * cp_{air} * \Delta T_{air} \\ \dot{Q}_{hx} = \dot{m}_{HTF} * cp_{HTF} * \Delta T_{HTF} \\ \dot{Q}_{hx} = UA * \Delta T_{mln} \end{cases} \qquad (3.10)$$

where $\dot{Q}_{hx}$ is the thermal power exchanged, ΔT_{air} stands for the difference between inlet air temperature and the outlet one, UA is the overall heat transfer coefficient multiplied by the exchange surface and ΔT_{mln} is expressed as:

$$\Delta T_{mln} = \frac{(T_{air,in} - T_{HTF,in}) - (T_{air,out} - T_{HTF,out})}{log\left(\frac{(T_{air,in}-T_{HTF,in})}{(T_{air,out}-T_{HTF,out})}\right)} \qquad (3.11)$$
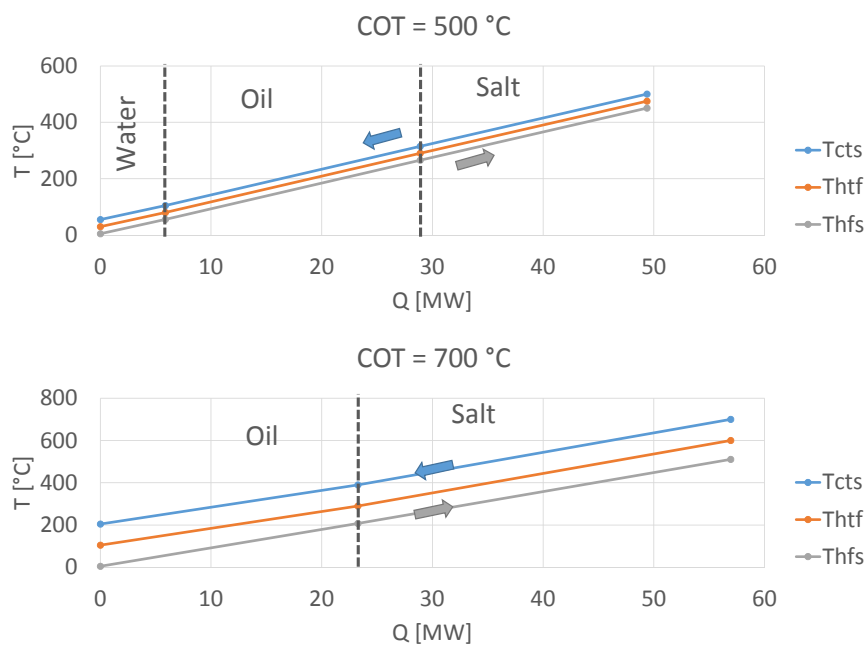
Figure 3.10. T−s diagram of the heat transfer process for the case of COT = 500°C, resulting in a pinch point of 25°C and COT = 700°C, resulting in a pinch point of 100°C. Water HX is not present in bottom graph since minimum thermal fluid temperature is 105°C. T_{tank} = 5°C, maximum heat transfer fluid temperature = 600°C

The air tank is considered to be at thermal equilibrium with the surrounding water, at 5°C and then the minimum temperature of the water exiting by the heat exchanger during *CtS* phase is found by adding ΔT_{pp} to T_{tank}. During *HfS* phase the HX are crossed by the air flow in a reverse way: starting from the the under water tank air enters in the sea water/air HX, in the oil/air HX and lastly in the solar salt/air unit. The air temperatures at inlet and outlet of each heat exchanger are found through the equation 3.10. Where the thermal fluids temperatures are known and the air mass flow rate is determined by the turbine dimension factor (TDF) introduced in the previous work [22] and formulated as:

$$TDF = \frac{\dot{m}_{turbine}}{\dot{m}_{compressor}} = \frac{\dot{m}_{HfS,nom}}{\dot{m}_{CtS,nom}} \tag{3.12}$$

The algorithm is synthetized in Figure 3.11: The used solver [4] calculates
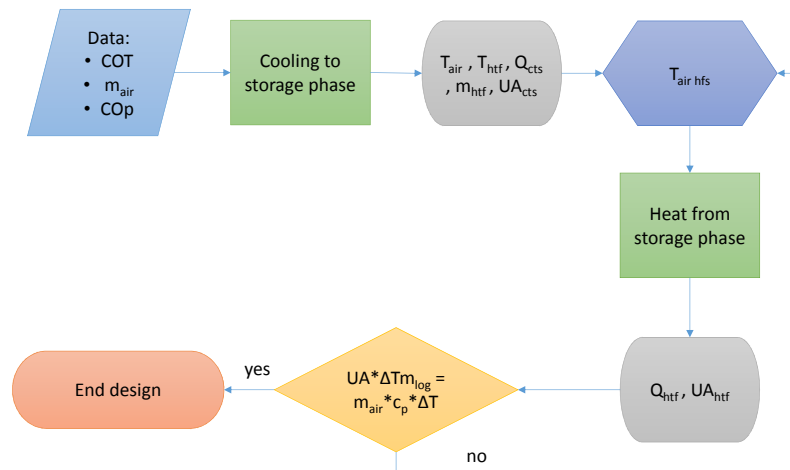
Figure 3.11. Algorithm for the design of heat exchangers. Green blocks represent functions, in gray the output of green functions. In blue there is the part managed by the solver.

the *CtS* phase and then guesses air temperatures for *HfS* phase, until the thermal balances (Equation 3.10) are verified also for discharging phase. The global heat transfer coefficient U variation are considered starting from the Dittus Boelter equation and the Nusselt number expression:

$$\begin{cases} Nu = 0.023 * Re^{4/5} * Pr^n \\ Nu = \frac{h*D}{K} \end{cases} \tag{3.13}$$

With Nu Nusselt number, Re Reynolds number, Pr Prandtl number; T_s is the tubes surface temperature, and T_m is the bulk temperature while n is 0.3 if $T_s < T_m$ (hot fluid is in the shell, in our case during *CtS* phase) or 0.4 otherwise (hot fluid is inside tubes, in our case during *HfS* phase). Valid for fully developed turbulent flow and $Re_D \geq 10000$, $0.6 \leq Pr \leq 160$ and $L/D \geq 10$. The approximation of evaluating the average Nu number over the entire tubes length is taken and properties are calculated at the mean bulk temperatures, $T_{mean} = \frac{T_{m,in} - T_{m,out}}{2}$ [52]. Then the overall heat transfer coefficient is estimated by Equation 3.14, assuming negligible the tube wall thermal resistance and the fouling factors:

$$\frac{1}{U} = \frac{1}{h_{air}} + \frac{1}{h_{HTF}} \tag{3.14}$$

The convective heat transfer coefficients variation can be estimated working on 3.13:

$$Nu = 0.023 * Re^{4/5} * Pr^n; \tag{3.15}$$

Since:

$$Nu \propto h; \quad Re = \frac{\rho * v * D}{\mu}; \quad \rho * A * v = \dot{m};$$

the Reynold number can be rewritten as:

$$Re = \frac{\dot{m} * D}{A * \mu}; \tag{3.16}$$

And considering the same heat exchanger simply working at different conditions, A and D are constant:

$$\frac{Re_{HfS}}{Re_{CtS}} = \frac{\dot{m}_{Hfs}}{\dot{m}_{CtS}} * \frac{\mu_{CtS}}{\mu_{HfS}};$$

---

[4]The solver is **fsolve**, implemented in **Matlab**. The function to be solved must be continuous. It is a nonlinear system solver, a variant of the Powell dogleg method described in [51].

Introducing TDF (Equation 3.12), the equation can be rewritten as:

$$\frac{h_{HfS}}{h_{CtS}} \propto \left(TDF * \frac{\mu_{CtS}}{\mu_{HfS}}\right)^{4/5} * \frac{(Pr_{HfS})^{0.4}}{(Pr_{CtS})^{0.3}} \qquad (3.17)$$

However to have a good estimation of h at least a preliminary design of HX is required. To simplify calculations in this analysis, the hypothesis to scale directly the U coefficient on the basis of the air side properties variation is taken:

$$U_{HfS} = U_{CtS} * \left(TDF * \frac{\mu_{CtS}}{\mu_{HfS}}\right)^{0.8} * \frac{(Pr_{HfS})^{0.4}}{(Pr_{CtS})^{0.3}} \qquad (3.18)$$

This strong approximation is considered since the air side would be the limiting one, affecting majorly the U variations. Once the design of compressors is fixed and also the thermodynamic condition have been fixed, a preliminary design of the HXs is possible, evaluating the convective heat transfer coefficients of both air and HTF sides, see Chapter 4. An iterative procedure is necessary to be able to calculate all the thermodynamic proprieties which are necessary for the Equation 3.18.

3.3 Axial compressor design: Fixed mean diameter vs Variable diameter

In [22] authors show two methodology for the design of axial compressors: fixed diameter and variable diameter. At the end of the analysis they demonstrate that the use of fixed diameter is less efficient. However since many choices are different in this work, like the type of the machine or the limit on compression ratio, it is interesting to see which is the weight of such reduction. In addition the variation in diameter is not free and exist physical limit in manufacturing a machine with huge change of diameter. Therefore an analysis is made considering also the possibility of adopting fixed diameter. Axial compressor rotational speed is optimized for intermediate stage, which lays on Cordier curve, while the others are found, fixing the diameter:

$$Ds = D * \frac{dh_{is}^{0.25}}{\sqrt{\dot{V}_{in}}} \qquad (3.19)$$

Efficiency is found by asking to the function which interpolate Baljé diagram with Ns and Ds:

$$\eta_{stage} = f_{Balje}(Ns, Ds) \qquad (3.20)$$

As can be seen in Figure 3.12, the choice of fixed diameter is responsible of changing the position of just axial machine. Since their compression ratio is

(a) fixed diameter   (b) variable diameter (Cordier)
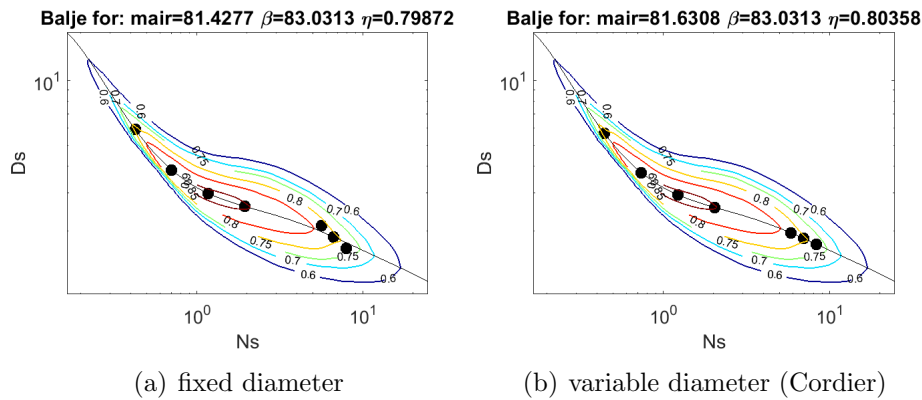
Figure 3.12. Comparison fixed diameter and variable diameter - case A.1. The black dot rappresent each single stage. The black line represent the cordier curve. In the title of the graphs is possible to see which are the condition (mass flow rate (mair) and compression ratio (β)) and the overall compressor efficiency (η

low and there are few stages, in the end the difference in compression efficiency is very low. Therefore the easier manufacturing of constant mean diameter compressors and very low penalization, suggest to adopt this methodology for the design of the compressors. It is clear that this have more impact where there are lot of stages on the same shaft. Considering the case with multiple shaft and multiple intercooling, all stages are placed in mixed region, and therefore the result is exactly the same.

3.4   T.E.S. design

Before entering into a detailed analysis of the compressors configuration it is fundamental to discuss the T.E.S. design, to better understand the obtained results. Considering a simplified case with the same air flow rate during charge and discharge phases, the turbine inlet condition and the total thermal power exchanged between air and HTF of the whole T.E.S. system are reported in Figure 3.13. From subfigure (a) it is possible to see the choice made on pinch point, which is kept equal to 25 °C when the compressor outlet temperature (COT) is below 625°C while for higher COT values it has to be varied, respecting the limit on maximum salt temperature, as explained in Subsection 3.2.2. In subfigure (b) it is possible to see that when pinch point is:

· between 25°C and 75°C: means that the minimum HTF temperature is in the range of water T.E.S., and therefore all 3 thermal fluid are employed;
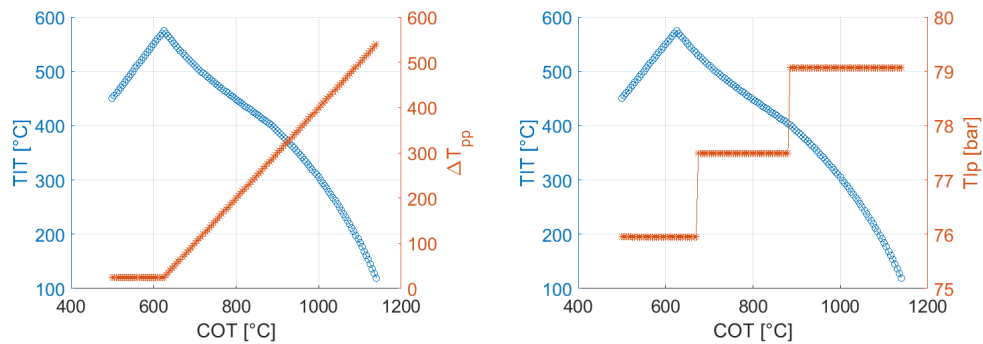
(a) Pinch point variation as function of COT and thermal power exchanged during *HfS* phase in the whole heat recovery section against COT variations.

(b) variation of Turbine Inlet Temperature (TIT) and Turbine Inlet pressure (TIp) as function of COT.

Figure 3.13. Trend of several main quantities for heat transfer process. Analysis made considering same mass flow rate.

- · between 75°C and 285°C: means that the minimum HTF temperature will be above 80°C: sea water unit can not be used and only thermal oil and solar salt T.E.S. are employed;

- · higher than 290°C: means that minimum HTF temperature is in the range of solar salt T.E.S. and nor water neither oil are employed.

Reducing the number of HXs the pressure losses induced by the whole recovery section result in being lower, as consequence higher turbine inlet pressure (TIp) can be achieved for higher COT. The change in the relationship between COT and TIT (that can be seen in subfigure (b)). The maximum TIT is achieved for the value of COT at which corresponds also the maximum thermal power exchanged. Indeed an increase of the COT implies higher ΔT_{pp} and as consequence: an higher outlet HTF temperature from the last HX during *CtS* phase is found, being it calculated as $T_{tank} + \Delta T_{pp}$. The temperature drop between the maximum salt temperature and the TIT increases together with the ΔT_{pp}. The non linear trend is due to U scaling effects dependent on the change of viscosity value between *CtS* and *HfS* phases (Equation 3.18).

3.5 Analysis of the layout of the plant: #intercoolers # shaft

As anticipated different design were presenting adopting different shafts and different number of intercoolers. Table 3.3 reports the optimal value of the

Table 3.3. Design tested:

β_{1i} is the compression ratio before the intercooler i on shaft 1 (the only which have intercooled stages);

· η_{1i} is the efficiency of the machine before the intercooler i;

· η_i is the efficiency of the machine fitted on the shaft i. For the first is defined as the efficiency of the machine after the intercooler;

· RPMi is the rotational speed of shaft i;

· β_{exp} is the pressure ratio between inlet and outlet of the turbine;

· RTE stands for Round Trip Efficiency, and it is the CAES efficiency.

Config	β_{1a} [-]	β_{1b} [-]	η_{1a} [-]	η_{1b} [-]	η_1 [-]	η_2 [-]	η_3 [-]	RPM1 [rpm]	RPM2 [rpm]	RPM3 [rpm]	COT [°C]	TIT [°C]	TOT [°C]	β_{exp} [-]	RTE [-]
A.1					0.799			18200			871	409	5	36.9	0.457
A.2					0.893	0.895		9111	31598		810	443	5	44.7	0.528
A.3					0.908	0.908	0.908	6480	14989	34459	804	446	5	45.6	0.531
B.1	2.38		0.795		0.851			16195			625	575	16.6	75.1	0.775
B.2	2.23		0.899		0.904	0.893		6676	27475		625	575	16.6	75.1	0.798
B.3	2.19		0.903		0.920	0.909	0.908	6522	13402	30838	625	575	16.6	75.1	0.801
C.1	1.59	1.57	0.784	0.821	0.839			14023			625	575	16.6	75.1	0.780
C.2	1.51	1.51	0.899	0.907	0.910	0.886		6102	24729		625	575	16.6	75.1	0.799
C.3	1.50	1.48	0.901	0.908	0.917	0.908	0.908	5719	13388	30937	625	575	16.6	75.1	0.800

optimization variables and the main results for each configuration. The cases without intercooler (cases A) have very low efficiecy: this is due to very high COT and therefore very high $\Delta\mathrm{T}_{pinchpoint}$. This lead to have very low TIT and less expansion work. Due to the limit on turbine outlet temperature (TOT) set at 5°C expansion must be truncated, as can be seen looking at β_{exp}. Value below 75.1 means that turbine is discharging at a pressure which is higher than ambient condition, causing a strong decay of the RTE. Multiple shaft configuration (moving from A.1 to A.2 and A.3) benefit on efficiency are achieved thanks to:

· higher compressors efficiency;

· resulting lower COT which guarantees higher TIT and therefore higher work of the turbine;

· possibility to expand more the gasses, and delay the truncation of the expansion phase;

The increase of number of shaft in the end is responsible for an increase of 10% of RTE. Moving to inter-cooled solution (case B and C) the optimum solution always reach the maximum temperature of the T.E.S. plus the minimum ΔT. The compression work increases as the COT temperature increase; however a

higher temperature guarantees higher work of the expansion. In the end it is possible to verify that the RTE is strongly dependant on the TIT, and the optimum solution tends to maximize it. The benefit in the power extractible is higher than the higher work required by the compression. The value of RTE rise, justifying the use of at least one intercooler in the design of compression train. Both in case B and C the use of multiple shaft is less evident than the case A, and efficiency see an increase of just 3%. Cooled solution gain lower benefit on RTE by the adoption of multiple shaft configuration because only the compression phase is changed: COT is kept to optimum value thanks to the use of the intercooler. Increasing compressor effiency decrease the compression ratio done before the intercooler: same TIT is obtained. Therefore the expansion of the case B and C is done between same temperature and pressure levels, recording same expansion work.

Since the advantage of multiple intercooling is very low, due to the low compression ratio done before them, this solution become less actractive compaired to the other, also because of the higher complexity required. For the cases A.1 (no IC and one shaft) the location of each stage is reported on the Baljé diagram and the efficiency of each machine is shown on performance map in Figure 3.14. The compressor consists of three axial stages with the

(a) Baljé   (b) compressor map
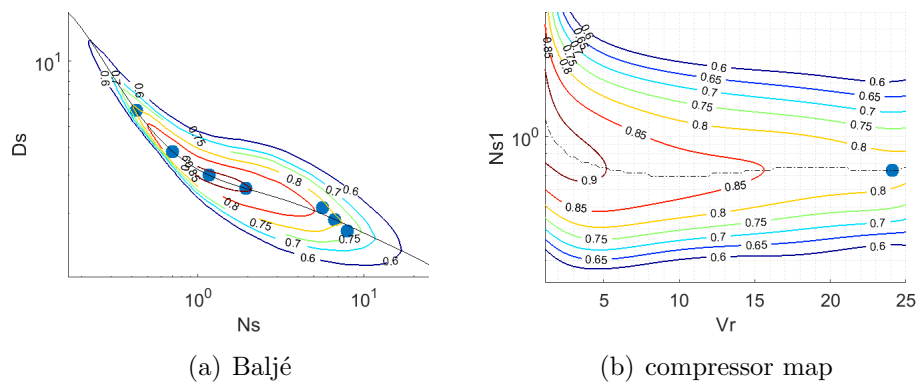
Figure 3.14. Case A.1: placement on Baljé diagram and on compressor map

same diameter optimized for the intermediate stage, four mixed flow stages and one radial stage; rotational speed is optimized to hit the maximum efficiency. It is worth to recognize the difference with the respect the case A.3 depicted in Figure 3.15. The effect of having multiple shafts lead to have the possibility to place more stage in the optimum region. In Balé chart stages are almost super imposed, and the same can be seen in compressor

(a) Baljé (b) compressor map
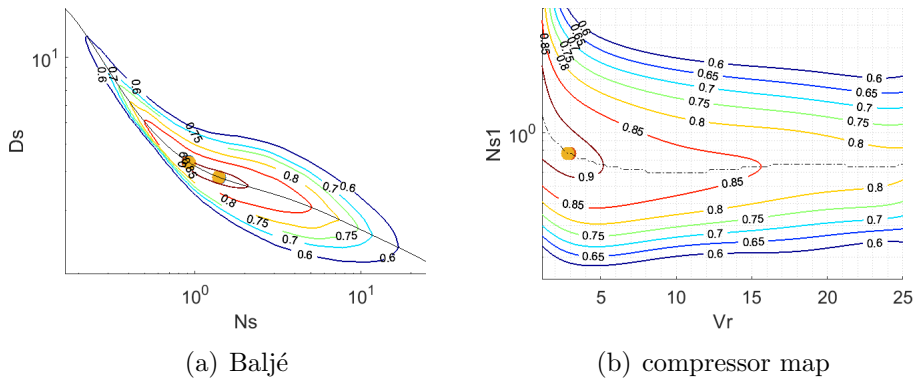
Figure 3.15. Case A.3: placement on Baljé diagram and on compressor map: three different machines are almost superimposed in both graphs.

map. The compression efficiency in this way result higher. On the other hand, case B.2 (Figure 3.16) uses three compressors: the first two have two mixed flow stages each, mounted on the same shaft, while the third runs on an independent shaft and has three mixed flow stages. Optimal rotational speed of the first shaft is selected as trade-off between the requirements of the first and the second compressors as highlighted in Figure 3.16 (where first and second compressor run respectively at higher and lower speed than their own optimal value). Table 3.4 reports the main results of the T.E.S.

(a) Baljé (b) compressor map
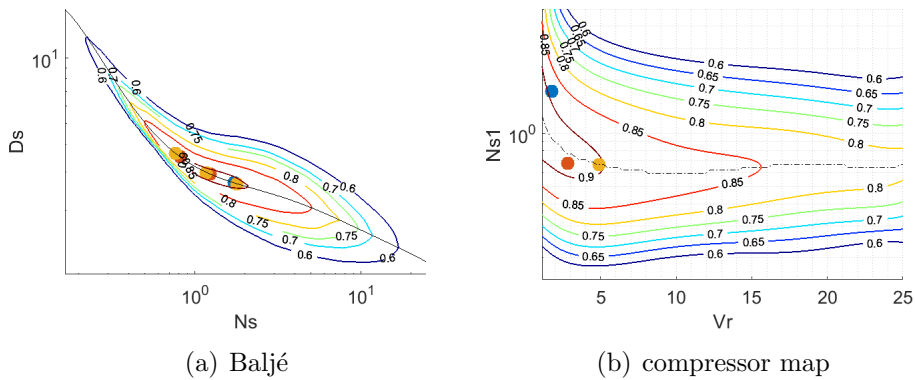
Figure 3.16. Case B.2: placement on Baljé diagram and on compressor map: in blue first compressor (which provide β_{1a}) in red second compressors, mounted on same shaft (providing β_1) and in yellow the third shaft mounted on the second shaft

system for a compressor section with a nominal power input of 75 MW, 1 intercooler, 2 shafts (B.2). Considering the T.E.S. structure described in

Table 3.4. main results of the T.E.S. system for case B.2

Air mass flow rate	[kg/s]	103.18
Molten salt mass flow rate	[kg/s]	74.5
Molten salt heat exchanger duty	[MW]	35.095
Molten salt heat exchanger UA	[MW/K]	1.404
Molten salt T.E.S. volume (48h at nominal power)	[m^3]	7124.6
Molten salt T.E.S. # hot tanks	[-]	2
Thermal oil mass flow rate	[kg/s]	51.3
Thermal oil heat exchanger duty	[MW]	23.041
Thermal oil heat exchanger UA	[MW/K]	0.922
Thermal oil T.E.S. volume (48h at nominal power)	[m^3]	9889.6
Thermal oil T.E.S. # hot tanks	[-]	2
Water flow rate	[kg/s]	26.9
Water heat exchanger duty	[MW]	5.6
Water heat exchanger UA	[MW/K]	0.225
Water T.E.S. volume (48h at nominal power)	[m^3]	4711.1
Water T.E.S.# hot tanks	[-]	1

Chapter 2, in which T.E.S. are cylindrical tank 20m height with a diameter of 20m, the power loss of $0.1885MW$ is obtained which correspond to an amount of $0.1885MWh$ of energy lost each hour form each hot tank. For the same compression train configuration the number of required thermal storage tanks is plotted as function of the sizing time of the T.E.S. in Figure 3.17.
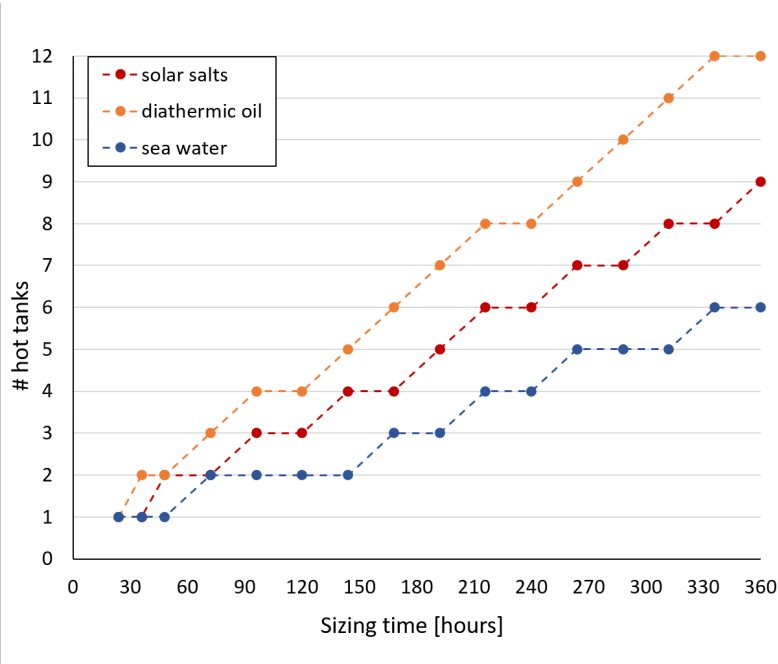
Figure 3.17. Required number of thermal fluids hot tanks as function of the T.E.S. size.

3.6 Analysis of number of compression parallel trains

This analysis is foundamental for the off Design. Since the real problem of the CAES proposed by previous work [22] was the low flexibility of the plant, in off design condition, when different volumetric flow rate are required. To make plant more profitable and able to work also when wind power is low, the idea of using parallel compressors seems to be the more promising. Compressors works at constant compression ratio and the electrical power affect the volumetric flow rate. At full load all trains work in parallel, and decreasing the power input train go in off design and there is small region after reaching stall. Turning off progressively train, volumetric flow rate in the other compressors rise, and prevent stall. For this analysis it is supposed to use identical train, made by machine characterized by compression ratio optimized in Section 3.5. Before going on it is better to study which is the effect of splitting the air flow rate along different trains. Keeping fixed rotational speed, stages moves on Balé and thus also efficiencies change. This condition forces to reoptimize the design each time that number of parallel compressor change. Instead considering the case in which rotational speed can be changed, it is possible to try to keep same working point (on Balé)

of one single train configuration, modifying ω to compensate the decrease in $\dot{V}_{nom}$:

$$\omega = \frac{Ns * dh_{is}^{0.75}}{\sqrt{\dot{V}_{single\,train}}} \tag{3.21}$$

where Ns is the same of single train configuration,dh_{is} is the same being compression ratio fixed, while $\dot{V}_{nom}$ depend on the number of parallel trains and it is equal to:

$$\dot{V}_{single\,train} = \frac{\dot{V}_{tot}}{N_{parallel\,trains}} \tag{3.22}$$

Then moving on Cordier line for the design, the same couple of Ns and Ds point is obtained and therefore same efficiency of each single stage. The diameter change depending on the parallelization and decrease, since volumetric flow rate is splitted.

$$D = \frac{Ds * \sqrt{\dot{V}_{single\,train}}}{dh_{is}^{0.25}} = \Downarrow \tag{3.23}$$

Finally peripheral speed in m/s is defined as:

$$U = \omega * \frac{D}{2} \tag{3.24}$$

substituting Equation 3.23 and Equation 3.21 in Equation 3.24, U results to be:

$$U = \frac{Ns * Ds * \sqrt{dh_{is}}}{2} = const \tag{3.25}$$

It is interesting to see that it is independent by the volumetric flow rate. This means that the decrease in diameter is compensate by the increase of rotational speed. By this design procedure it is possible to work on same point, for different configuration, which means work in similarity and therefore same efficiency of the machine.

It is important to remind that this analysis is made comparing the possibility of using parallel trains always in design condition. The conclusion is that not only it is feasible, but performance are not penalised by the use of smaller machine. This is true following the approach adopted for the design. In this work losses related to the scale of the machine are neglected, therefore the losses generated by tip clearance losses [5], the weight of the boundary

---

[5]Considering fixed the clearance depending on the manufacturing process of the compressor stage, the lower is the dimension and the higher will be the percentage of the flow which is able to escape from tip clearance, without being processed by the blades.

layer with the respect to mean dimension of the machine [6] and Reynolds effect inside compressor channel [7]. All of them strongly depend on the size of the machine. This more precise analysis will be made in future work related to this project.

Results of the analysis are reported in Figure 3.18. The relationship between diameter and rotational speed is verified by the model. In the same way no dependency of the RTE efficiency is recorded.
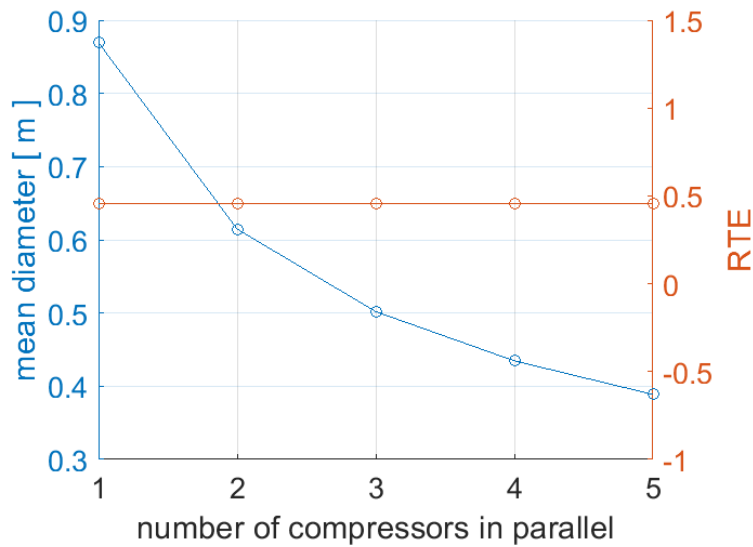
Figure 3.18. Trend of mean diameter calculated over the whole machine and RTE as function of number of parallel compressors for case A.1

Same efficiency of the compressor, same compression ratio and therefore same efficiency of the overall plant, are obtained, satisfying all the constraints. The choice of the best configuration therefore do not depend on the design condition, but it has to be found as a trade off between the gain in flexibility in off-design condition and the cost of the machines, see Chapter 6.

---

[6]Roughness depends on the machining process and not on dimension. Since wetted surface losses depends on relative roughness (ϵ/D), scaling up the problem, the friction factor decreases.

[7]In small machine the percentage of the channel interested by the boundary layer is higher with the respect to a bigger machine.

3.7 Analysis of different tank depth

The depth and therefore the pressure at which air is stored has great impact on cost, as can be discussed in Chapter 6. It is interesting to investigate performance of the plant going at higher depth: the possibility of increasing pressure of the tank enable the storage of higher amount of energy (fixing the volume of the air tank). Therefore an analysis is made to predict which is the implication on thermodynamic point of view of that choice. This analysis is made calculating the CAES efficiency considering:

· configuration B.2;

· 1 train configuration (no parallel trains);

Since the beginning of the test, problems arise since expansion is increasing (higher $\beta_{turbine}$), while maximum temperature is fixed. Therefore for high pressure ratio is not possible to avoid freezing phenomena on the last stage of turbine blade. After certain depth, even in design condition there's the need of adopting lower efficient turbine or stop expansion and laminate until ambient pressure. Maximum temperature of salts limit the TIT, while the icing phenomenon limit the TOT. Considering the polytropic efficiency of the turbine:

$$\frac{TIT}{TOT} = (\beta_{exp})^{\theta * \eta_{polytropic}} \tag{3.26}$$

Considering TIT equal to max temperature salt minus $\Delta T_{pinch\,point}$, the TOT limited by icing, maximum expansion is found equal to 88.4. The corresponding tank pressure, considering heat exchanger and piping losses is 94 bar. This represent the limit over which from a thermodynamic point of view there is no reason to go deeper with the air storage. This is true considering the available technology of molten salts, which do not overcome 600°C. Higher Temperature media will allow to increase first of all overall efficiency and also to go deeper without losing expansion. Result of the analysis are reported in Table 3.5. It is interesting to see that RTE decreses with the increase of depth. The compressor efficiency maintains good levels: this happen because the increase of pressure (form 40 bar to 140 bar) is all in charge of the compressors before the intercooler. In this way all compressors beyond it felt the same inlet temperature and thus provide similar work. This effect can be seen from the super imposition of the different T−s diagram for the case analysed, in Figure 3.19. First machine compression starts from ambient temperature, than according to hypothesis made, intercooling is always able to decrease temperature down to 29°C. After that there's the compression made by the machine fitted on the same shaft and then the one made by the third machine on its own shaft. To achieve the target of 625°C

Table 3.5. Analysis of the air vessel pressure on the performance of the plant: Optimization variable are reported (β_{1a} and rotational speed (RPM)), efficiency of each machine, temperature at the outlet of compression train (COT), inlet of turbine (TIT) and outlet of the turbine. β_{exp} is calculated as turbine inlet pressure (TIp) over turbine outlet pressure TOp.

Tank pressure	β_{1a}	η_{1a}	η_1	η_2	RPM1	RPM2	COT	TIT	TOT	β_{exp}	RTE
[bar]	[-]	[-]	[-]	[-]	[rpm]	[rpm]	[°C]	[°C]	[°C]	[-]	[-]
40	1.21	0.840	0.910	0.908	6616	19204	597	547	59	37.5	0.797
60	1.63	0.896	0.905	0.905	7218	23644	625	575	38	56.3	0.811
80	2.23	0.899	0.904	0.893	6676	27475	625	575	17	75.1	0.798
100	2.75	0.897	0.908	0.899	8046	29514	625	575	5	88.45	0.784
120	3.46	0.913	0.872	0.897	6052	32022	625	575	5	88.45	0.756
140	3.92	0.907	0.907	0.890	7918	32658	625	575	5	88.45	0.739
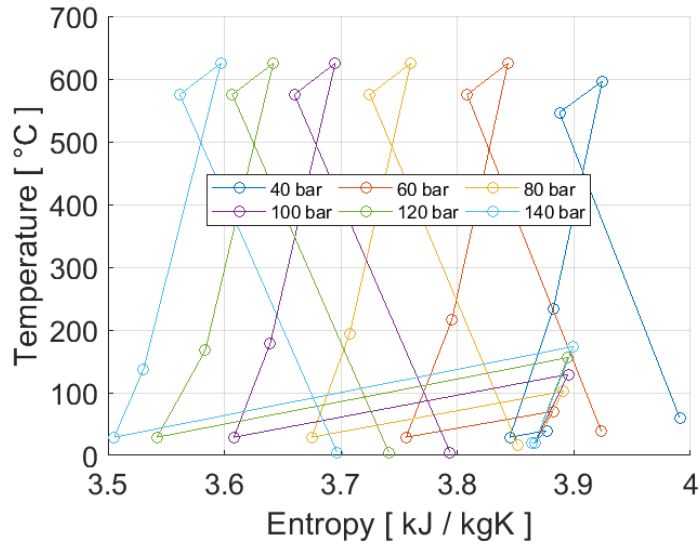
Figure 3.19. Comparison between the T-s diagram for different tank pressure, for a 75 MW plant, configuration B.2. The point represent the outlet and inlet condition of the different machines. On the top it is possible to recognize the temperature loss between *CtS* and *HfS* phase.

the compression ratio required after the intercooler can be calculated from the two temperature difference:

$$\frac{COT}{CIT} = (\beta_{comp})^{\theta/\eta_{polytropic}} \qquad (3.27)$$

where CIT stand for Compressor Inlet Temperature. It remains constant for all the configuration: intercooler have to work more as the pressure increase. Limitation of the expansion can be seen after 100 bar and the expansion ratio is equal to what forecast considering just temperature levels. Except for the case at 40 bar in which heat produced during compression is not enough to reach maximum temperature, for the other cases, efficiency is decreasing as the pressure of the storage increase. After 94.2 bar it can be seen that minimum temperature at the exit of turbine is reached, and turbine discharging pressure is higher than atmospheric. This fact penalise a lot the efficiency which drops down. Performance of low pressure system can be improved removing the intercooler. Vice versa deeper configuration can be improved from compression side by increasing the number of intercooler, however the limit on maximum and minimum temperature cannot be overcame, and thus, these configurations result in any case penalized.

Configuration with one intercooler have limitation of at least one axial stage compressor before intercooling. For 40 bar case, the COT is low also for not intercooled plant: adopting configuration A.1 the outlet temperature is near 630°C. An estimation of the pressure level which assure to reach target COT of 625°C without intercooler can be derived from Equation 3.27: considering same polytropic efficiency for the case at 80 bar, optimum air pressure vessel is 36.4 bar for A.1 case, 42.4 bar for A.2 and 43 bar for A.3 case. For the case below 45 bar the not intercooled solution are favoured, and tuning correctly the tank pressure it is possible to reach high efficiency. Out of optimum depth these solutions are less efficient, as can be seen in Figure 3.20 where RTE is reportes as function of the tank pressure for the case A.2. At lower depth, with respect to the optimal one, the heat produced by compression is not enough to reach maximum allowed temperature. This result into lower TIT and thus less RTE. Instead at higher depth, the COT overcome maximum value, and pinch point have to increase. As already mentioned, compression work increase but TIT decreases and allowed expansion decreases, causing a strong penalization on the efficiency.

3.8   Analysis of different plant power

Another analysis made is on the power of the compressor used. This choice has great effect not only on cost but also on the dimension of thermal storage.
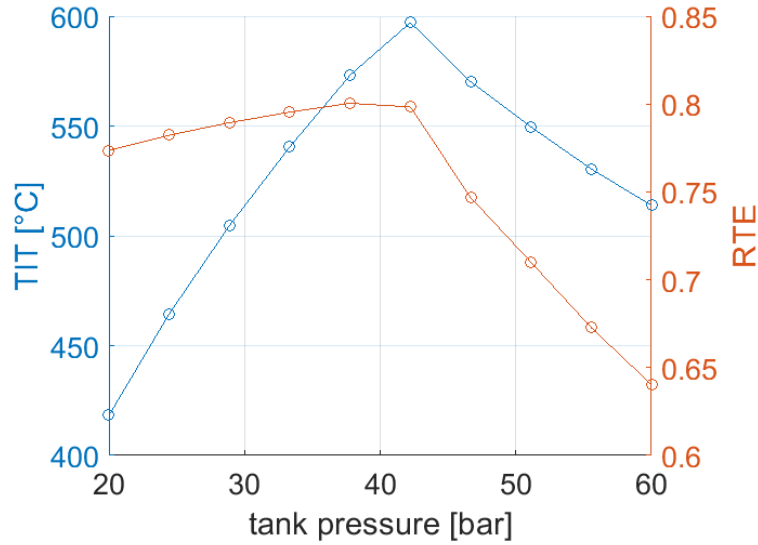
Figure 3.20. variation in RTE and TIT for different tank pressure for the case A.2

The analysis is made spanning the power of the plant from 15 MW to 150 MW. The best way to proceed, as for Section 3.6, is the study of the possibility of working using similar compressors at different power level. Size of the plant impact on the air which flows inside the pipes as aready seen in Equation 3.9 Considering the density and the number of parallel trains, it is possible to calculate which is the volumetric flow rate for each train:

$$V_{single\,train} = \frac{\dot{m}_{air}}{\rho * N_{parallel\,trains}} = \frac{P_{nom} * \eta_{organic\,electric} * \eta_{tot\,compression}}{dh_{is} * \rho * N_{parallel\,trains}} \quad (3.28)$$

If it is possible to work in similarity keeping fixed Ns, ω should change following Equation 3.21. In this way $\eta_{tot\,compression}$ is kept constant and it is possible to recalculate rotational speed:

$$\omega = \frac{Ns * dh_{is}^{1.25} * \sqrt{\rho * N_{parallel\,trains}}}{\sqrt{P_{nom} * \eta_{organic\,electric} * \eta_{tot\,compression}}} \quad (3.29)$$

In the end being same Ns, same Ds will be obtained and therefore same peripheral speed, as explained in Equation 3.25. Result are shown in Figure 3.21. In all case proved, same RTE has been obtained based on the approach proposed, which do not consider size effect of the machine. This result shows that the dimension of the plant do not impose severe condition from compressor point of view, and same design can be simply scaled to manage higher flow rate. Therefore no problem rise for little plant and no advantage from thermodynamic point of view can be achieved with the scale of the
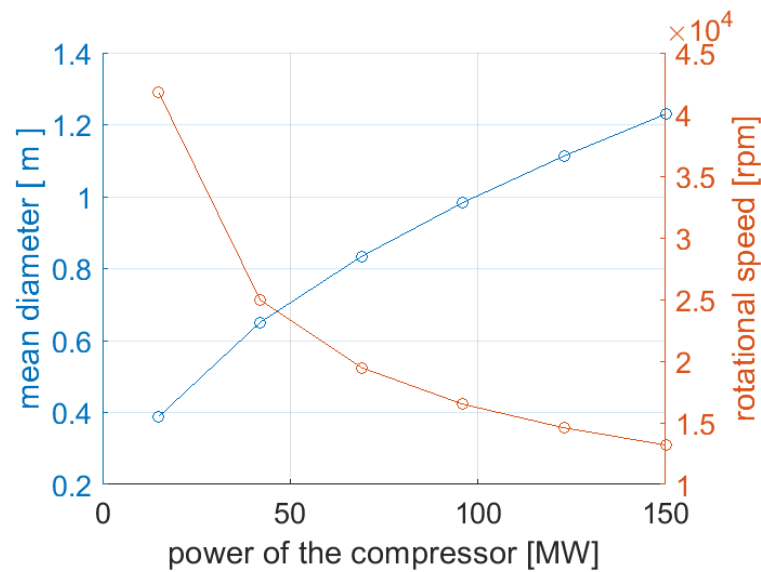
Figure 3.21. Trend of mean diameter and rotational speed for case A.1

plant. The increase in dimension due to bigger plant can be easily managed increasing the number of trains in parallel.

3.9   Peripheral speed problems

In the end of the work an accurate review highlight that the value of peripheral speed is not consistent with the general limit that typically are adopted. Searching for the cause of this difference it is found that problem is related to the approach adopted. Infact considering a design according to Corder curve, the couple Ns and Ds is fixed. But this quantity will affect the peripheral speed, as seen in Equation 3.25. Therefore starting from a limit on peripheral speed is possible to find a compression ratio which allow to stay on Cordier curve:

$$dh_{is} = \left(\frac{2 * U_{limit}}{Ns * Ds} \right)^2 \tag{3.30}$$

Considering inlet condition to the stage it is possible to calculate maximum pressure ratio:

$$\beta_{limit\,stage} = \frac{p\left(h_{in} + dh_{is}, s_{in}\right)}{p_{in}} \tag{3.31}$$

The result (shown in Figure 3.22) highlight that the compression ratio changes continuosly along the Ns and in particular assume very low value, below 1.01 for axial compressors. This limit in addition changes with inlet condition. As mentioned in Section 3.2 the use of continuos changing limit force to
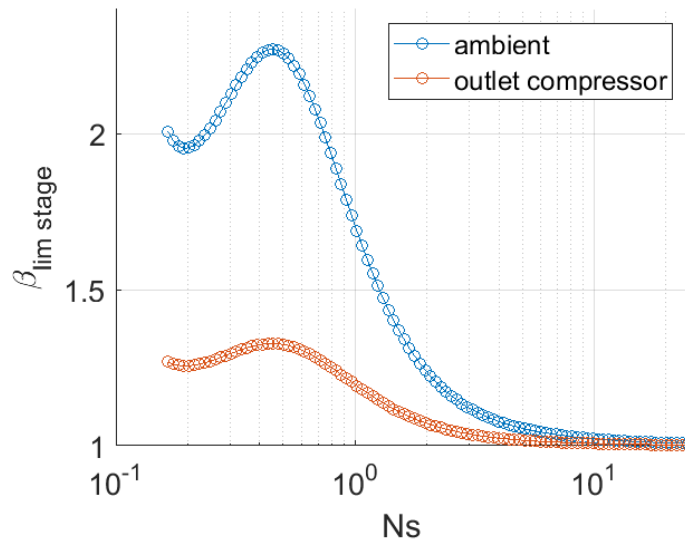
Figure 3.22. Maximum compression ratio allowed to stay on Cordier curve with maximum peripheral speed equal to 400 m/s. Two line represent the effect of the change in inlet condition form 1 bar 20°C (blue line) to 80 bar and 625°C (orange line).

continuously split compressors, leading to have just axial and radial machine. In addition, axial stages will be limited to very low work per stage, and in the end the number of stage requires rises, reaching also 50 stages, which are not comparable to commercial machine. Therefore the correct use of this diagram, adopting correct limit on U lead to have machines that in practise do not exist.

The methodology adopted is able to provide information about number of stages and compressor efficiency. These results enable the study of a huge quantity of cases, and provide useful data to start the analysis of all the other component of the plant. However the final compressor design will be accurately studied in future work, and the precise design, stage by stage can be performed ones that machine characteristic like compression ratio, mass flow rate and type of machine have been found. This methodology therefore helps into fix those variable for future investigation on compression train.

3.10   Conclusion

For a preliminary analysis of an UWCAES system the methodology proposed provide interesting results.

The influence of the action of the intercooling is carefully investigated

highlighting its fundamental role for obtaining high value of RTE. Comparing result it is possible to recognize an increase of more than 50% for the case with 1 intercooler with the respect to the case without it. This advantage is related to the optimal use of T.E.S. to been able to correctly store and transfer heat at high temperature. Fixing the limit on maximum temperature at 600 °C, more efficient solution is found for COT equal to maximum molten salt temperature plus minimum pinch point allowed. The advantage of a hotter expansion wins against the higher work required by the compression less cooled.

The possibility of using several shaft, on which compressor stages are fitted on, has been investigated. The analysis shows that it is possible to increase performance of more than 2% moving from one shaft to two shaft. For higher number the increase is less than 1% while the layout of the plant result to be more complex.

In the end the most probable configuration, able to reach good level of efficiency and maintaining a simple design, is the B.2 characterized by two shafts and one intercooler. The RTE recorded is near 0.8, a competitive value compared to pumped hydro technology. For this case it has been reported the T.E.S. and HX design result, which provide all the data necessary to a future detailed design of each element.

On land plants, described in Chapter 1 are characterized by efficiency in the range of 40% - 55% [24] [15] while the newest project of adiabatic-CAES plant reaches RTE around 70 % [16]. RTE estimation of the UW-CAES spans from 75 to 80% in case of intercooled solution. These values compared to pumped-hydro storage (the competitive technology which operate with an efficiency of 70% [23]) and compared to existing plants are promising for future development of the project.

Independently by the preliminary value obtained, analysis were made to assess the influence of layout decision: the possibility of using parallel compressors has been studied and result shows that neglecting the dimensional effect, number of parallel trains do not affect overall performance. In the same way also the power of the plant result to not influence final RTE of the plant. Instead the pressure at which air is compressed strongly affect thermodynamic aspects of problem: low pressure cases result to be more efficient, while high pressure plant are characterized in general by lower efficiency. The main reason is related to the increase in compression work required to reach high pressure, and a loss in expansion. Temperature gap is fixed, and depend on maximum heat transfer fluid temperature (in the case studied 600°C) and minimum allowed turbine outlet temperature (in the case studied 5°C). Therefore with current thermal fluid technology after 94 bar of the UW air tank expansion must be truncated to avoid icing phenomenon on the turbine

blades.

However some concern on the possibility of realization of the turbomachinery chosen rises: type of stages selected are difficult to be found on the market and some technological and practical constrained may not be satisfied. A more refined compression design is left for future work regarding this project.

Chapter 4

Plant off-Design

4.1 Introduction

Predicting the behavior of the plant at Off-Design conditions becomes a fundamental step strictly correlated to the design phase. Since the CAES system is supposed to be coupled with a wind farm the input electric power depends on the wind fluctuations and then is rarely equal to the nominal one, for which the machines have been designed. Therefore the compression block would be needed to work for a wide range of power inputs to better exploit the available wind power along the year. Moreover if the CAES system is operated following a *peak shaving* logic a wider range of power inputs accepted by the compression section, for a given design power, means a flatterer electrical output sent to the grid and less dissipated energy, see Chapter 6 So that the performance parameters that really matter in this section are the operational range and the air flow rate manageable by the compressor; this last is the real useful effect of the plant.

4.1.1 Compressors

It is important to underline the peculiar conditions at which the compression section has to work: constant final pressure and power input imposed. The first constraint is determined by the hydro-static load, since the air tank is positioned under water and implies a constant compression ratio, despite pressure drops variations. The second one instead derives from the need of operating the plant with the available power coming from a RES, in this case from wind, avoiding power dissipation. These two constraints hinder the part load management of the compression block leading to limited operational ranges.

The off-design performances prediction is conducted on the basis of dimensionless maps implemented by real compressors data sheets:

· MAN AG/AGM series representative of axial compressors [26].

· AtlasCopco GT series representative of radial compression stages [25].

Each map has been digitized by using $Scanit^1$ and $MatLab^2$, determining functions able to give as ouput the efficiency value, VIGV closure (Variable Inlet Guide Vanes) or Rotational speed, receiving as input the relative volume flow rate, V_r and relative compression ratio β_r, see Figure 4.1. V_r and β_r are defined as $V_{actual}/V_{nominal}$ and $\beta_{actual}/\beta_{nominal}$. From the previous work
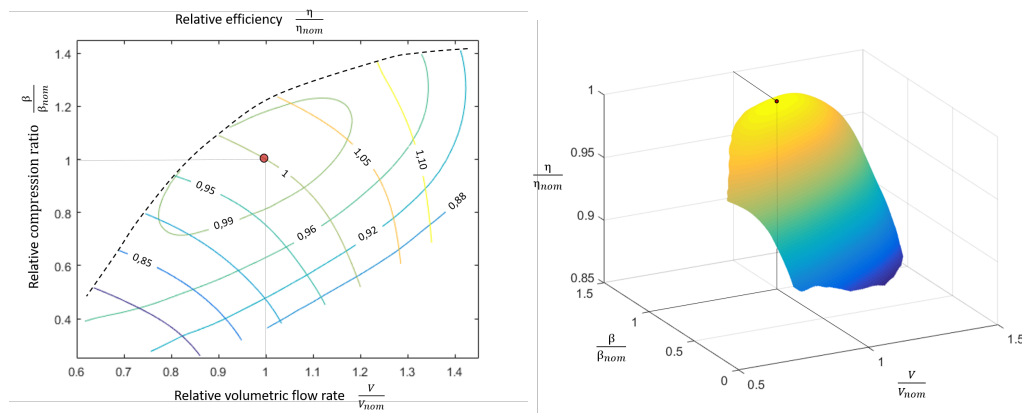
Figure 4.1. Digitized performance map for an axial compressor with variable rotational speed.

conclusions a compression section configuration composed by multiple parallel compression trains has been suggested [22]. The main concept is to enhance the part load flexibility introducing the possibility of cutting-off one of the parallel trains when the operational condition of the compressor gets close to the surge limit. So that the air flow rate flowing in the active machines is increased and the system can work for wider power input ranges. Hence as a first step a preliminary analysis is performed in order to test the effectiveness of this solution and to compare two different management strategies, regulation on rpm or on VIGV. Then an algorithm has been implemented in *MatLab* environment, able to simulate the whole train performances given the configuration of the compression train coming from the design phase and a certain power input. Referring to notation presented in Figure 3.8 the design configuration B.1, with one intercooler and single shaft, is tested for one up to

---

[1]**Scanit**, version 2.07, amsterCHEM
[2]**Matlab**, version R2018a, Mathworks

four parallel trains with both the regulation strategies, rotational speed and VIGV closure variation. Afterwards the algorithm has been reviewed in order to test multiple shaft trains, focusing on the rotational speed control, which results in being the most effective management strategy. The configuration B.2 with one intercooler and two shaft is considered with:

· multiple shafts connected with gearboxes and single electric motor,

· multiple independent shafts with dedicated electric motors.

4.1.2 T.E.S.

The T.E.S. heat exchangers are designed at nominal condition of the *CtS* phase, with the aim of balancing the thermal powers exchanged durign *CtS* and *HfS* phase. This is done in order to reduce unbalances between the energy stored by the three different tanks during the yearly usage of the plant.

During charging phase, off-design condition indicates that the wind power available to the compressors is lower, or higher than the nominal value, as consequence the air flow rate and the conditions at the outlet of the compression section vary and they correspond to the flow passing through the first air/Solar Salts heat exchanger and the T, p at inlet of it. This implies that also thermal power exchanged by air and thermal fluid is different form the nominal case.

The discharging phase instead is expected to work mostly at nominal conditions, since the air flow extracted from the underwater tank can be arbitrary chosen and air enters the first heat exchanger, air/sea water, at constant temperature, equal to the $T_{tank} = 5°C$. Having constant flow rate and temperatures means also constant pressure at the turbine inlet. Therefore the turbine is managed to work at nominal condition for most of the time, and only when required it works at part load conditions. For example when the plant is operated following a peak shaving logic and the electric output given by the contribution of wind power and turbine output overcomes the power the grid expects to receive, see Chapter 5.

The heat transfer fluids temperatures are required to be constant, also during part load conditions in order to avoid thermal unbalances in the hot or cold tanks. This fact implies also constancy of their thermophysical properties, reported in Table, 2.2 which are evaluated at the average between their maximum and minimum temperature and pressure.

The mass flow rates of the HTF instead are not constant, they could be regulated through a variable speed pump. At off-design condition indeed if the exchanged thermal power lowers and ΔT_{HTF} is constant, as well as the specific heat transfer coefficients, the $\dot{m}_{HTF}$ needs to vary, being valid:

$$\dot{Q}_{hx} = \dot{m}_{HTF} * cp_{HTF} * \Delta T_{HTF} \qquad (4.1)$$

4.2 Preliminary analysis on parallel trains configuration

As already introduced the first solution adopted to improve the off design performances, in terms of acceptable power input range and maximum air flow rate consists on a multiple parallel trains configuration of the compression block. A compression section designed in this way leads to the possibility of taking off one of trains when the air flow rate is required to decrease more than how is allowed by the operational area delimited by surge and chocking effects. Each train could be composed by one or more compressors, which can be: *Axial, Mixed flow* or *radial* and the parallel trains are assumed to be equal between each other. Maintaining the same compression ratio and same nominal power of the whole compression section, having more parallel trains implies smaller machines. Compressors are assumed to follow the similitude theory and the scale effects are neglected, as already reported in the Chapter 3. Therefore is important to keep in mind that each time a different number of parallel trains is considered, the whole compression block is implicitly redesigned and what is changing are the rotational speed, the machine diameters and the nominal air flow rate of each machine.

Before performing any simulation with the *MatLab* model, a preliminary analysis over a single axial machine has been conducted in order to initially estimate how the increasing number of parallel trains could affect performances. The axial maps [26] are used in order to find the V_r limits given a fixed compression ratio equal to the nominal one. These limits are imposed by surge and chocking effects. Then the volumetric flow rate is varied evaluating the operative ranges for one up to five parallel trains, with rpm and VIGV regulation. By this way no information about efficiency or pressure drops are considered and moreover the examined trains are composed by just one axial compressor. Anyway as first approach this analysis helps in understanding the minimum number of parallel trains required to reach an acceptable operational range and to compare the flexibility of the compressor obtained for the two types of regulation: variable rotational speed or variable inlet guide vanes. The obtained results are reported in Table 4.1, where n_{trains} stands for the number of parallel equal compressors and $V_r = \dot{V}/\dot{V}_{nom}$ is the ratio of the volumetric flow rate at the inlet of the compressor and its nominal value. In the results when more ranges of $\dot{V}/\dot{V}_{nom}$ are reported for one case it means that the compression train is not able to work at the corresponding power input and there is a gap during which the compressors work at the maximum overload condition, while the exceeding power is dissipated. This behavior can be better visualized looking at the Figure 4.2; where $\dot{m}/\dot{m}_{nom}$ is plotted against the V_r variation. An increasing number of parallel trains as expected

Table 4.1. Operational ranges in terms of allowed relative volume flow rate obtained from a preliminary analysis on different number of parallel trains composed by one axial compressor and different control strategies.

Control method	n_{trains}	$\dot{V}/\dot{V}_{nom}$
rpm	1	[1.4 - 0.825]
	2	[1.4 - 0.825, 0.6875 - 0.400]
	3	[1.4 - 0.5375 , 0.4625 - 0.2625]
	4	[1.4 - 0.4000 , 0.3375 - 0.2000]
	5	[1.4 - 0.3250 , 0.2750 - 0.1625]
VIGV	1	[1.1 - 0.885]
	2	[1.1 - 0.885 , 0.545 - 0.440]
	3	[1.1 - 0.885 , 0.730 - 0.585 , 0.365 - 0.290]
	4	[1.1 - 0.885 , 0.820 - 0.660 , 0.550 - 0.440, 0.275 - 0.220]
	5	[1.1 - 0.705 , 0.660 - 0.530 , 0.440 - 0.350, 0.220 - 0.175]
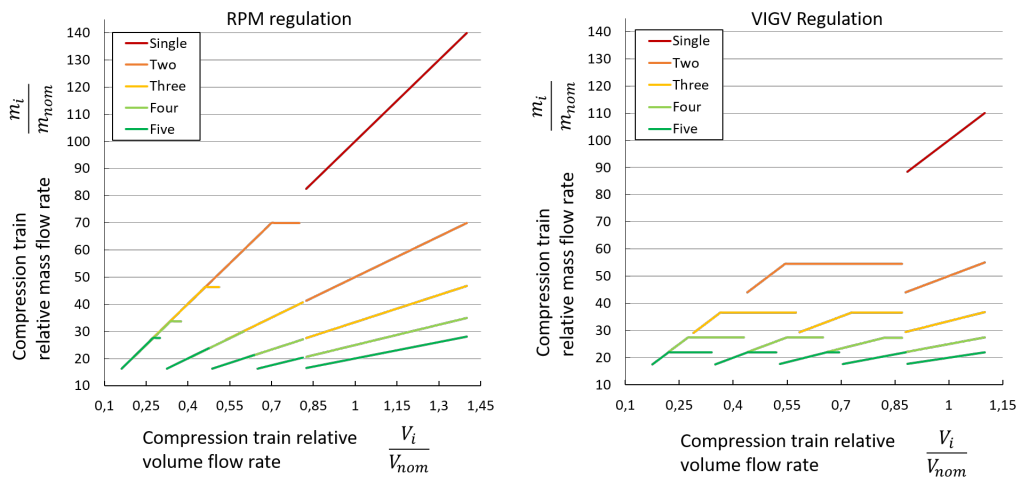
Figure 4.2. Axial compressor preliminary analysis varying the number of parallel trains from one up to five and different control strategies.

results in wider operational ranges. The choice of the more convenient n_{trains} needs to be taken on the basis of the plant application and of an economic analysis, since it will be the result of the trade off between what is gained due to the wider power input range and the costs of the machines, see Chapter 6. Finally form this simple analysis the regulation acting on the rotational speed appears to be definitely more performing. But a more accurate analysis needs to be conducted in order to fully understand the part load behavior of the machines and to find the best management strategy.

4.3   Methodology

A deeper analysis has been conducted through a dedicated *MatLab* model. The algorithm is based on the real compressor performances maps found in literature:

- · MAN AG/AGM series for axial compressors. [26]

- · AtlasCopco GT series for radial compressors. [25]

The first one is referred to a whole axial compressor, while the second one represents a single compression stage, see Figure 4.3. Mixed-flow compressors off design performances are assumed to be similar to axial machines and for them the MAN AG/AGM map has been used. The maps are reported in an adimensional form, giving the opportunity to fit them in a proper way into the analyzed case. The compressors have been designed maximizing the efficiency, moving along the Cordier line and by this way the design point, used as the reference one, corresponds to the highest efficiency point, see Figure 4.3. For this reason the map have been scaled, making the reference point to match the design one. The input parameters coming from the design phase are:

- · nominal power absorbed by the whole compression section,

- · number and type of compressor in series,

- · number of intercoolers,

- · nominal efficiency and compression ratio of each machine,

- · nominal rotational speed,

- · nominal pressure drops.

(a) Axial, rpm

(b) Axial, VIGV

(c) Radial, rpm
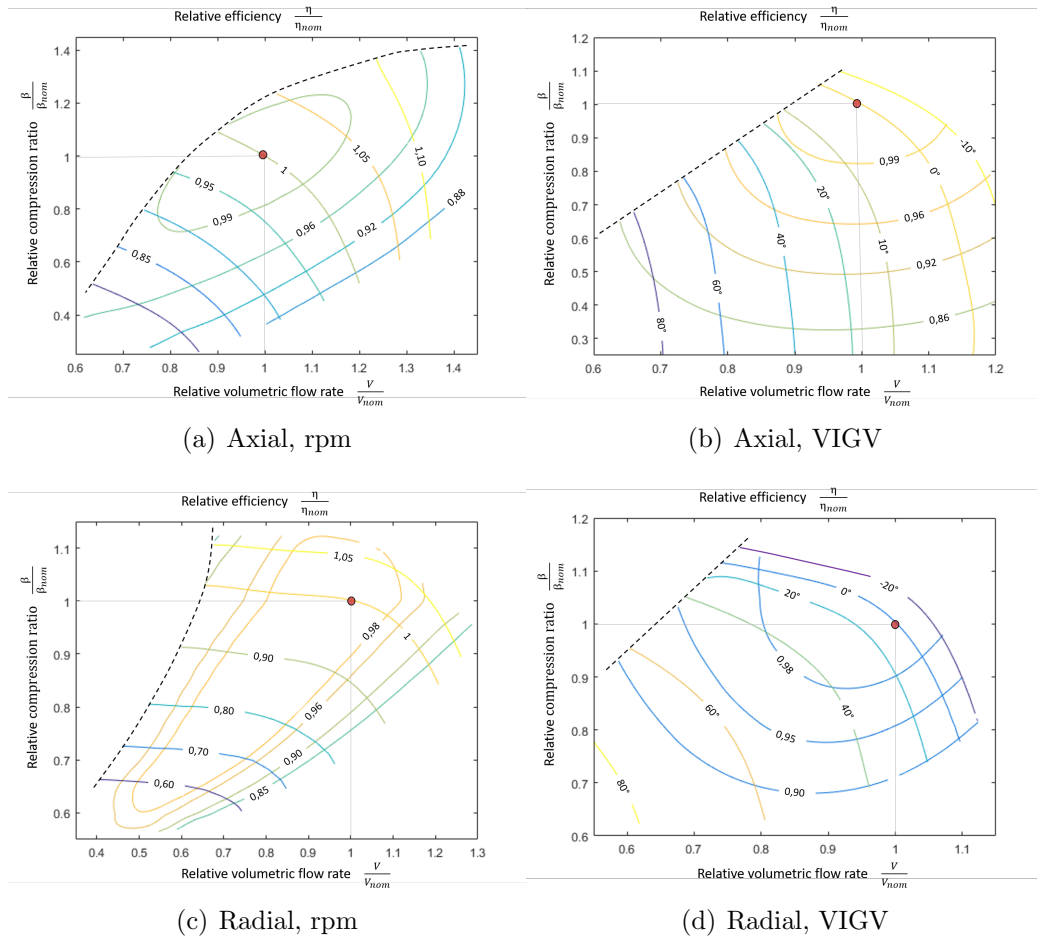
(d) Radial, VIGV

Figure 4.3. Off-design performances maps of axial and radial compressors for part load management based on variable rotational speed or on VIGV. The highlighted points correspond to the design operational point, assumed as nominal.

Then the performances maps have been digitized through the use of *Scanit* and *MatLab*, turning them into 3-dimensional curves and generating interpolation functions; which relate $V_r = \dot{V}_{od}/\dot{V}_{ref}$, $\beta_r = \beta_{od}/\beta_{ref}$, relative efficiency: $\eta_r = \eta_{od}/\eta_{ref}$ and relative rotational speed: $N = rpm_{od}/rpm_{ref}$. These functions are needed to be at least of class C^1, since the algorithm works as an optimization problem and is solved by gradient-based method, that is designed to work on problems where the objective and constraint functions are both continuous and have continuous first derivatives[53]. The algorithm structure is schematized in Figure 4.4 and it is able to perform simulations for:

· series of axial and radial compressors,

· parallel multiple trains,

· regulation method acting on the rpm or VIGV,

· eventual presence of one or more intercoolers.
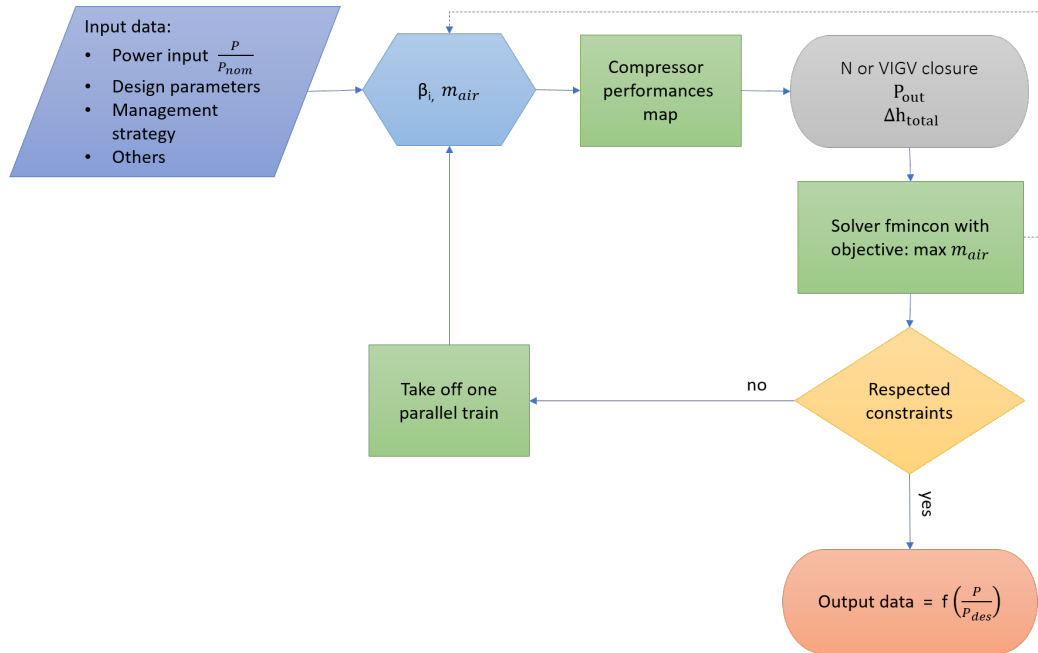
Figure 4.4. Compression section off-design algorithm: general version suitable for both rpm and VIGV control method.

The model, as already reported receives as input the compression trains, intercoolers and pipeline characteristics coming from the Design phase, together

with the plant configuration, the actual electric power absorbed, expressed as fraction of the nominal one: $P_{absorbed}/P_{nom}$ and the chosen control method. All the input data are listed in the Table: 4.2, where n_{series} is the number of compressor positioned in series in a train, n_{ic} is the number of intercoolers, n_{trains} indicates the number of parallel compression trains. This optimization

Table 4.2. List of input data to Off-Design algorithm.

Input data		
Air tank depth	*regulation method*	*compressor type*
P_{nom}	$P_{fraction}$	$\Delta p_{piping,nom}$
n_{ic}	n_{series}	n_{trains}
T_{amb}	p_{amb}	$\Delta p_{filter,nom}$
$\Delta p_{ic,nom}$	T_{water}	$\Delta T_{pp,ic,nom}$
$\dot{m}_{air,nom}$	$\beta_{C,nom}$	$\eta_{C,nom}$

algorithm aims to maximize the air flow rate, which is the real useful effect of the plant and it implicitly allows to reach the higher efficiency points since the enthalpy variation is inversely proportional to the efficiency and air flow, having compression ratios almost constant and the power input imposed.

$$P_{in} \propto \dot{m}_{air} * \frac{\Delta h_{is}}{\eta} \quad \rightarrow \quad P_{in} = const. \quad \dot{m}_{air} \uparrow \quad \eta \uparrow \qquad (4.2)$$

The variables handled by the solver *fmincon* are the $\dot{m}_{air}$ and the compression ratio β_i with $i = 1 : n_{series}$. From the performance maps for each combination of air flow rate and compression ratio, the efficiency and rotational speed, or VIGV closure degree are determined. All the thermodynamic points are calculated with *Coolprop* [54] and the total enthalpy variation can be computed. The solver is required to meet the following constraints on the power absorbed by the compressor and on the outlet pressure:

· $P_{in} * \eta_{mec,el} = \dot{m}_{air} * \Delta h * n_{trains}$

· $\frac{P_{tank}}{P_{inlet}} = \prod_i \beta_i$ with $i = 1 : n_{series}$

If convergence is reached the optimization is repeated for a different power input and the results corresponding to each absorbed power are saved. Otherwise one of the parallel trains is taken off, obtaining an increase in the air

flow inside the working compressors, moving the operational point in the performances map away from the surge line. The model finds the values of:

· $\dot{m}_{air}$

· β_i with $i = 1 : n_{series}$

· η_{total}, η_i with $i = 1 : n_{series}$

· COT and p_{outlet}

The intercooler behavior at off design condition and the pressure drops variations are described in the following subsections.

4.3.1 Intercoolers

Intercoolers are key components of the plant since they are carefully positioned and designed in order to have a compression train with a COT that allows to reach the higher round trip efficiency, see Chapter 3. A value of COT equal to 625°C gives the possibility to better exploit the Solar Salts temperature variation, allowed by their physical properties. Indeed the T_{max} of Solar Salts is 600°C. Moreover a compression with intercooler allows to reach the desired pressure requiring a smaller specific work than a case without intercooling. Considering an imposed nominal power lower specific work means higher air flow, which is the parameter wanted to be maximized.

At off-design condition the unknowns $T_{out,air}$ and $\dot{m}_{water}$ are found solving the following energy balance:

$$\begin{cases} \dot{Q}_{ic} = \dot{m}_{air} * cp_{air} * \Delta T_{air} \\ \dot{Q}_{ic} = \dot{m}_{water} * c_{L\,water} * \Delta T_{water} \\ \dot{Q}_{ic} = UA * \Delta T_{mln} \end{cases} \tag{4.3}$$

Where $\dot{Q}_{ic}$ is the exchanged power, cp_{air} and $c_{L\,w}$ are the specific heat of air and water respectively, U is the overall heat transfer coefficient. Having an imposed T_{out} at the water side implies variation of the water mass flow rates and the T_{out} of air to respect the energy balances at different T_{in} and $\dot{m}_{air}$ at the air side. U variations during off design condition are estimated by the Dittus Boelter correlation [52] (Equation 3.13). It can be approximated to:

$$\frac{U_{od}}{U_{nom}} = \left(\frac{\dot{V}_{od}}{\dot{V}_{nom}} \right)^{4/5} \tag{4.4}$$

valid under the same assumptions of Equation 3.13. This simplification has been taken considering that the air side is the limiting one during the heat

transfer process, that the Prandtl number variations are negligible and the volumetric flow rate proportional to the Reynolds number elevated at 0.8.

The pressure drop variation instead is estimated by the Darcy Weisbach Equation:

$$\Delta p = \lambda * \rho * \frac{v^2}{2} * \frac{L}{D} \tag{4.5}$$

Where Δp is the actual pressure drop,λ is the friction factor ,ρ is the density of the flowing fluid, v is the average flow velocity, L/D is the ratio between the length of the pipe and the hydraulic diameter. Since the HX is the same, constant λ is considered to been able to approximate Darcy Weisbach equation (Equaiton 4.3.1) to:

$$\frac{\Delta p_{od}}{\Delta p_{nom}} = \left(\frac{\dot{V}_{od}}{\dot{V}_{nom}} \right)^2 \tag{4.6}$$

4.3.2 T.E.S.
The thermal energy storage is composed by the three heat exchangers:

- · air/solar salts;

- · air/diathermic oil;

- · air/sea water.

Each of them is assumed to have a nominal percentage pressure loss equal to 1%, corresponding to the volumetric flow rate obtained for a compression section absorbing the power at which has been designed. During part load condition the air flow varies together with the T_{in} of the first heat exchanger (COT). Consequently the pressure drops are not constant and they are estimated on the basis of the Darcy Weisbach equation, Equation 4.3.1 approximated to Equation 4.6. A reduction or increase in the pressure drop needs to be compensated by a variation in the total compression ratio of the compression section, obtaining a constant pressure in the air tank also at part load conditions.

At this point a more detailed design of the heat exchangers is computed finding the convective heat transfer coefficients corresponding to the air and thermal fluids sides. The air flow rate, the inlet temperature and pressure are the ones resulting from the design point of the compression section. Then the assumption of designing the HXs properly for each compression section configuration is made. As first guess the tubes diameter is assumed equal to 0.20 mm [55] and thermal fluid velocities are assumed of some m/s. To find the proper characteristics of the HXs the hypothesis over the pressure drops

is considered and then diameters and velocities are varied in order to respect
the equations:

$$\begin{cases} \Delta p = \lambda * \rho * \frac{v^2}{2} * \frac{L}{D} \\ \frac{\Delta p}{p_{in}} = 1\% \end{cases} \tag{4.7}$$

For compression configuration B.2 in nominal condition, the resulting HXs
design is reported in Table 4.3. When the compressors absorb a power value

Table 4.3. main results of the HX design for case B.2

Molten salt global heat transfer coefficient U	[W/m²K]	992
Molten salt heat transfer coefficient h	[W/m²K]	3994
Air heat transfer coefficient in molten salt HX h_{air}	[W/m²K]	1320
Thermal oil global heat transfer coefficient U	[W/m²K]	692
Thermal oil global heat transfer coefficient h	[W/m²K]	1563
Air heat transfer coefficient in thermal oil HX h_{air}	[W/m²K]	1240
Water global heat transfer coefficient U	[W/m²K]	437
Water global heat transfer h	[W/m²K]	1398
Air heat transfer coefficient in water HX h_{air}	[W/m²K]	452

different from the nominal one then the temperature, pressure and air flow
rate entering in the first heat exchanger vary. This new conditions imply
a change of the flow velocities inside the heat exchangers and of the fluids
properties, so that the thermal balance needs to be solved again (Equations
3.10) taking into account these two effects. The overall heat transfer coefficient
in off design condition can be scaled using same procedure used for the design
of T.E.S. apparatus in Chapter 3. Starting from Dittus Boelter equation
(Equation 3.13), with the same demonstration it is possible to reformulate
Equation 3.17 with respect the case of design and offdesign:

$$\frac{h_{od}}{h_{nom}} \propto \left(\frac{\dot{m}_{od}}{\dot{m}_{nom}} * \frac{\mu_{nom}}{\mu_{od}} \right)^{4/5} * \frac{(Pr_{od})^{0.3}}{(Pr_{nom})^{0.3}} \tag{4.8}$$

In this way it is possible to estimate the convective heat transfer coefficient
for both air side and HTF side, for each HX. Global heat transfer coefficient
is found by Equation 3.14 [52]. The T.E.S. behavior during the *HfS* phase is

determined following the same approach used for the off design management of the *CtS* phase. Using the nominal quantities of the the *CtS* phase as reference, new values of the overall heat transfer coefficients are found and the energy balances in Equation 3.10 are solved. The air temperatures at the outlet of heat exchangers, the thermal powers and the corresponding thermal fluids flow rates are found. Starting from the Dittus Boelter correlation in this case, the Equation 3.17 results in being expressed as:

$$\frac{Nu_{HfS}}{Nu_{CtS}} \propto \frac{h_{HfS}}{h_{CtS}} \propto \left(TDF * \frac{\mu_{CtS}}{\mu_{HfS}} \right)^{4/5} * \frac{(Pr_{HfS})^{0.4}}{(Pr_{CtS})^{0.3}} \tag{4.9}$$

The turbine polytropic efficiency is assumed to be constant and equal to the nominal value of 89%.

4.3.3 Pipeline pressure drop

The pipeline, designed to obtain a percentage pressure drop equal to 2%, see Chapter 2, faces a lower or greater volumetric flow during partial or over load conditions of the compression block. This effect is taken into account by the Darcy Weisbach equation (Equation 4.3.1). In this case the friction factor λ is computed by solving the Colebrook White equation with an iterative method [3]

$$\frac{1}{\sqrt{\lambda}} = -2 * \log \frac{\epsilon/D}{3.7} + \frac{2.51}{Re * \sqrt{\lambda}} \tag{4.10}$$

Where ϵ/D is the relative pipe roughness and Re is the Reynolds number. Valid for $Re \geq 4000$. As for T.E.S. pressure drop a reduction or increase in the pipeline pressure drop needs to be compensated by a variation in the total compression ratio of the compression train.

4.3.4 Inlet filter pressure drop

The same procedure is applied to compute the pressure drop variation of the filter, located at the inlet of the first compressor. The nominal $\Delta p/p_{in}$ is equal to 1% and its variation at part load is quantified by Equation 4.6

4.4 Single-shaft compression train part load operation

As introduced the compression sections with train configuration B.1 has been confronted for one to four parallel trains. The A.1 configuration is

---

[3]Method: Quartic iterations, Reference: http://arxiv.org/abs/0810.5564, Author: D. Clamond, 2008-09-16

less interesting since it allows to reach lower round trip efficiencies while the configuration C.1 results in a low performance increment with respect to the B.1 and faces higher cost and layout complications related to a second intercooler. The assumed initial data are the same tabled in Chapter 2 and the compressors nominal data are ones coming from Table 3.3. The results are reported in Figure 4.5. In general all the single train configurations present a very limited power input variability. This fact is due to the peculiar conditions at which the machines have to work: constant pressure in the underwater air tank imposed by the hydro-static load. The adopted solution of parallel trains helps in solving this issue. Just with two parallel trains the power input could decrease down to the 42% relative power. Referring to Figure 4.5 the flat trend of the operational curves represents conditions for which N trains would operate outside the area delimited by the surge line while $N-1$ trains would be above the allowed machine overload. Then the corresponding power input can not be completely exploited and compressors are let to operate at the maximum overload, dissipating the power in excess. Increasing the adopted parallel trains allows to narrow these plateau regions and to wide the operative ranges. More in detail for case B.1, the performances reported
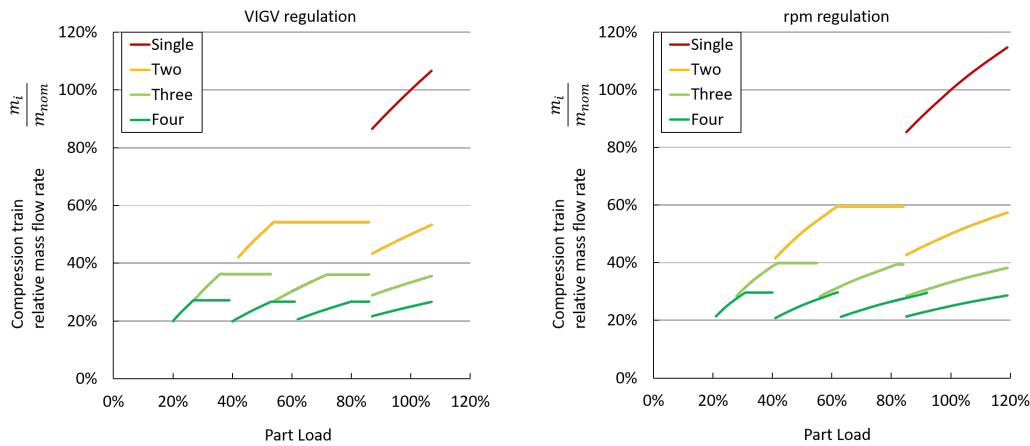
Figure 4.5. Compression train relative mass flow rate plotted for different relative power input, for one up to four parallel trains and for different control strategies.

in Table 4.5 are achieved. Similarly to what resulted from the preliminary analysis the most effective part load management strategy appears to be the rotational speed control. The only issue regarding this kind of regulation is related to stresses on the mechanical components. The machines have to change the rotational speed each time a train is excluded. Related to this fact

Table 4.4. Relative power ranges referred to compression train configuration B.1 at part load conditions considering one up to four parallel trains and different control strategies.

Management strategy	# parallel trains	P/P_{nom}	$P_{plateau}$
rpm	1	$[119\% - 85\%]$	$[-]$
	2	$[119\% - 42\%]$	$[85\% - 62\%]$
	3	$[119\% - 28\%]$	$[85\% - 81\% \; ; \; 56\% - 42\%]$
	4	$[119\% - 21\%]$	$[42\% - 31\%]$
VIGV	1	$[107\% - 87\%]$	$[-]$
	2	$[107\% - 42\%]$	$[87\% - 54\%]$
	3	$[107\% - 27\%]$	$[87\% - 72\% \; ; \; 54\% - 36\%]$
	4	$[107\% - 20\%]$	$[87\% - 80\% \; ; \; 62\% - 53\% \; ; \; 40\% - 27\%]$

it can be observed that the case with four parallel trains presents overlapped operational curves while switching from four to three trains. Therefore during a real case management it can be avoided to frequently change the number of working trains if the power input is fluctuating in that switching range.

4.4.1 Control based on rotational speed and compression ratio

Both the preliminary analysis and the simulations performed by the *MatLab* model evince that the more effective management strategy at partial load conditions consists on acting on the rotational speed of the machines. Moreover from the compressors design cases multiple shafts configurations results in having more performing machines, see Table 3.3. For these reasons the algorithm is re-thought focusing on this kind of control method in order to test multi-shaft machines, to have a more stable model and to reduce the variables number that the optimization function has to handle. The main structure remains the same as the first algorithm and the objective is still maximizing the air flow rate, the real useful effect of the plant, see Figure 4.6. But two options are taken into account:

· control on rpm and multiple shaft connected by gearbox,

· control on rpm and multiple shaft with dedicated electric motors.

In the first case the compression ratio and the rotational speed of the first machine are considered as the optimization variables. Once they are set, the efficiency of the first compressor and the air mass flow rate are determined.
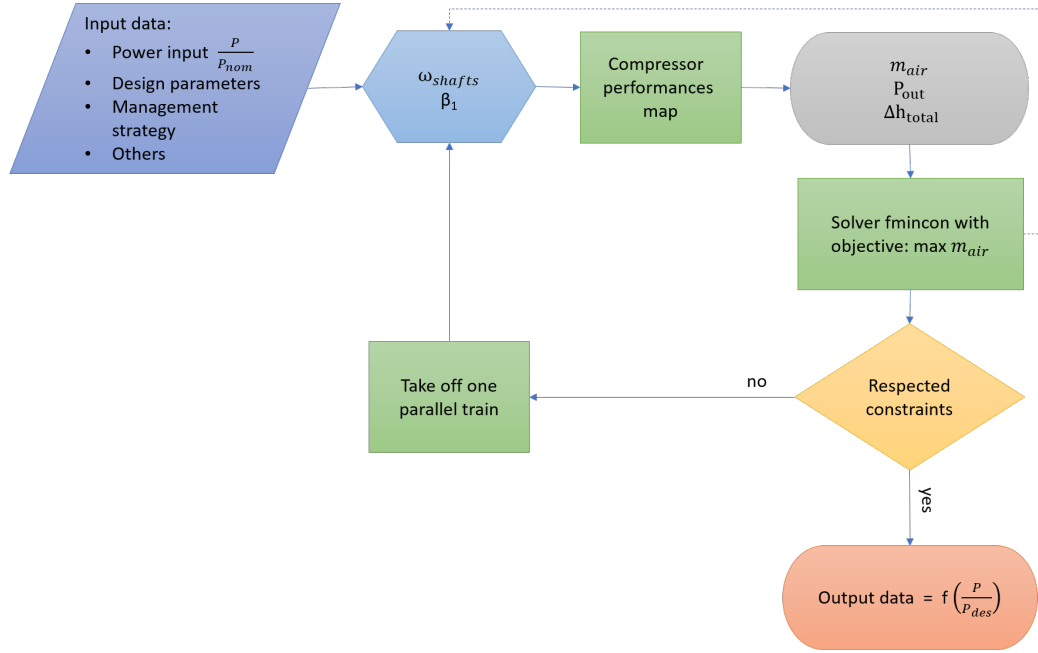
Figure 4.6. Compression section off design algorithm: rpm version which enable the simulation of multishaft configurations with gearbox or moved by different electric motors.

The rpm of the following shafts can be easily found from the speed of the first shaft multiplied by the gear ratio. Then from the performances maps for a given value of $\dot{m}_{air}$ and rpm the unique corresponding compression ratio and efficiency are interpolated for all the n_{series} machines.

The case with multiple shafts and different electric motors instead is simulated optimizing the compression ratio of the first compressor and the rotational speed of the different shafts.

The constraints at which the variables are subject remains unvaried:

· $P_{in} * \eta_{mec,el} = \dot{m}_{air} * \Delta h * n_{trains}$

· $\frac{P_{tank}}{P_{inlet}} = \prod_i \beta_i$ with $i = 1 : n_{series}$

Also in this case the usage of multiple parallel trains is considered and the trains follows the same assumptions reported in Chapter 3

4.5   Multiple-shaft compression train part load operation

The configuration B.2 with one intercooler and two shaft is studied with:

· shafts connected with gearboxes and single electric motor,

· independent shafts with dedicated electric motors.

All the assumed input parameters are reported in Table 2.1 and the nominal characteristics of the compression train are in Table 3.3.

For both cases the operational range and the power fraction corresponding to the maximum over load of the compressors are the same and reported in Table 4.5. The case with independent shafts simply leads to an air mass flow

Table 4.5. Relative power ranges referred to compression train configuration B.2 at part load conditions considering one up to four parallel trains.

# parallel trains	P/P_{nom}	$P_{plateau}$
1	$135\% - 85\%$	$-$
2	$135\% - 42\%$	$85\% - 67\%$
3	$135\% - 28\%$	$56\% - 44\%$
4	$135\% - 22\%$	$42\% - 33\%$

rate increase of around 1% at part load, facing a high number of adopted electric motors (e.g. 8 motors are required by the four trains configuration).

In Figure 4.8 the compression train relative mass flow rate, the total relative mass flow rate and the relative efficiencies are plotted against the relative power input, for the case B.2 with gearbox. For the configurations with three or four parallel trains the operational curves present overlapped stretches. This effect is interesting for the part load management. As an example a possible management strategy can be visualized looking at Figure 4.8, where the relative rotational speed is plotted against the relative power. The power input is high enough to have the compression section working with four parallel trains then power is decreasing till (d) but the working trains can be still four till (a) this leads to the option of following a sudden power increase without switches. Remembering that power is supposed to come from RES source, and in this case from wind, it could fluctuate in a small time span. The same behavior can be identified in the opposite direction with power which increases, from three (c) to four trains (d). Other interesting parameters consist on the compressor outlet temperature and pressure which together with the air mass flow rate, influence the T.E.S. performances. Looking at the Figure 4.9 it can be seen how the outlet pressure is decreasing due to
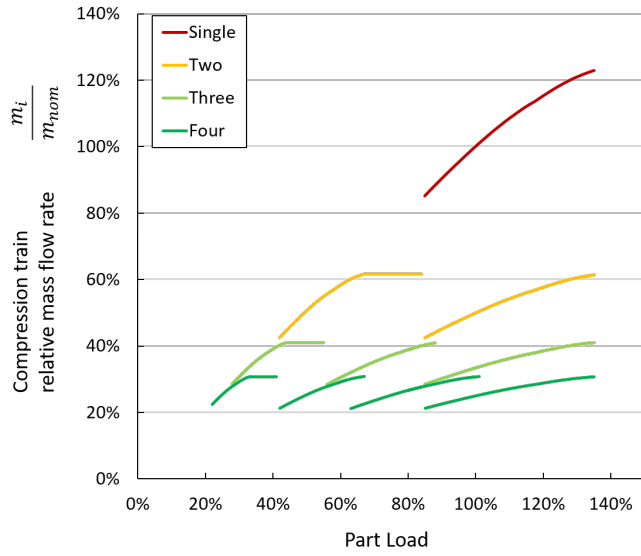
(a) Compression train relative mass flow rate against relative power.
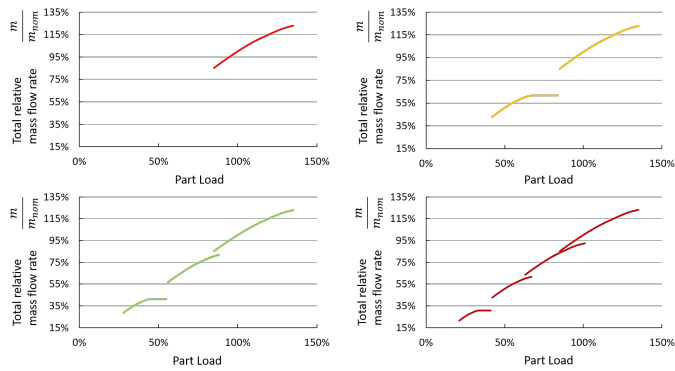
(b) Total relative mass flow rate against relative power.
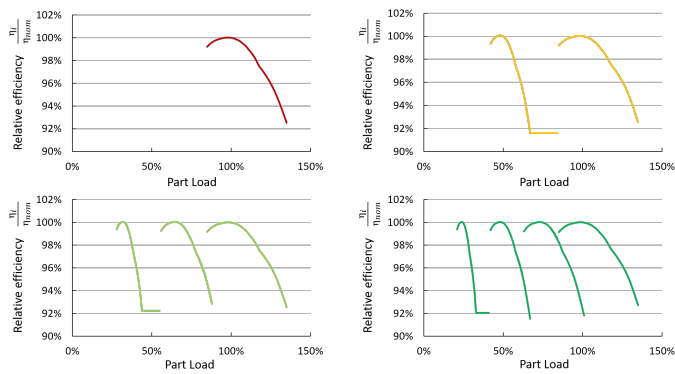
(c) Relative efficiency against relative power.

Figure 4.7. Results referred to compression train configuration B.2 at part load conditions considering one up to four parallel trains and shaft connected by a gearbox.
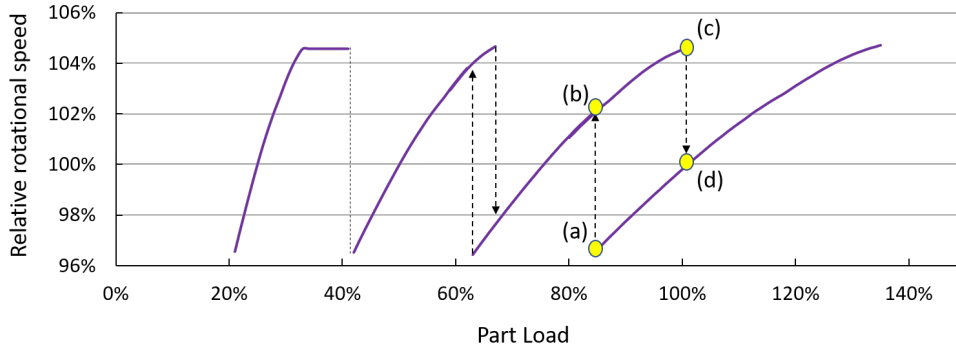
Figure 4.8. Relative rotational speed at part load of a compression section composed by four parallel compression trains of type B.2 with shafts connected by gearbox. The points (a)-(b), (c)-(d) represent a possible speed regulation strategy in case of decreasing or increasing power respectively.

the pressure drops reductions at part load, while the temperature trend is affected by both the compression efficiency and the outlet pressure. If a constant iso-entropic enthalpy drop is considered the COT variation would be inversely proportional to the the efficiency trend. Albeit in this case the outlet pressure reduction implies a compression ratio modification and the Δh_{is} results in not being constant at part load conditions. For this reason the COT minimum is slightly shifted with respect to the efficiency maximum point.

$$COT \propto \Delta h \propto \frac{\Delta h_{is}}{\eta}$$

4.6   Charge phase: Cooling to Storage

In Figure 4.10 the part load behavior of the T.E.S. system is represented in terms of relative thermal power exchanged by the whole recovery section and by each single heat exchanger during the *CtS* phase. These values are referred to a compression train configuration B.2 with 4 parallel trains and shafts connected by gearbox. The almost linear trend of the total relative thermal power is explicable considering that the total thermal power exchanged could be calculated as: $\dot{Q}_{total} = \dot{m}_{air} * c_p * (COT - T_{out,HX3})$. Once computed the off-design behavior of the three heat exchangers it resulted that $T_{out,HX3}$ vary of $\pm 5°C$ during part load conditions; m_{air} and COT can be expressed as
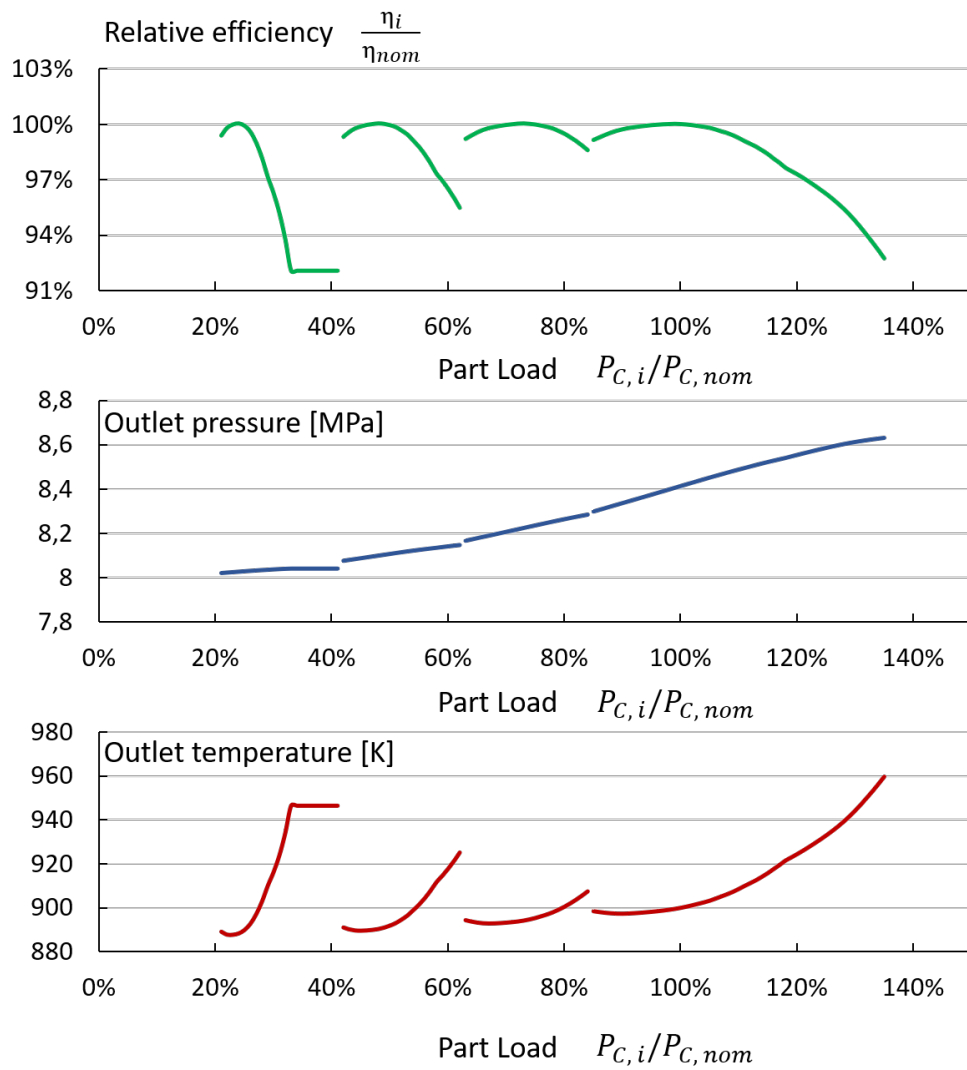
Figure 4.9. Relative efficiency, outlet pressure and outlet temperature against relative power input of a compression section composed by four parallel trains of type B.2 with shafts connected by gearbox.
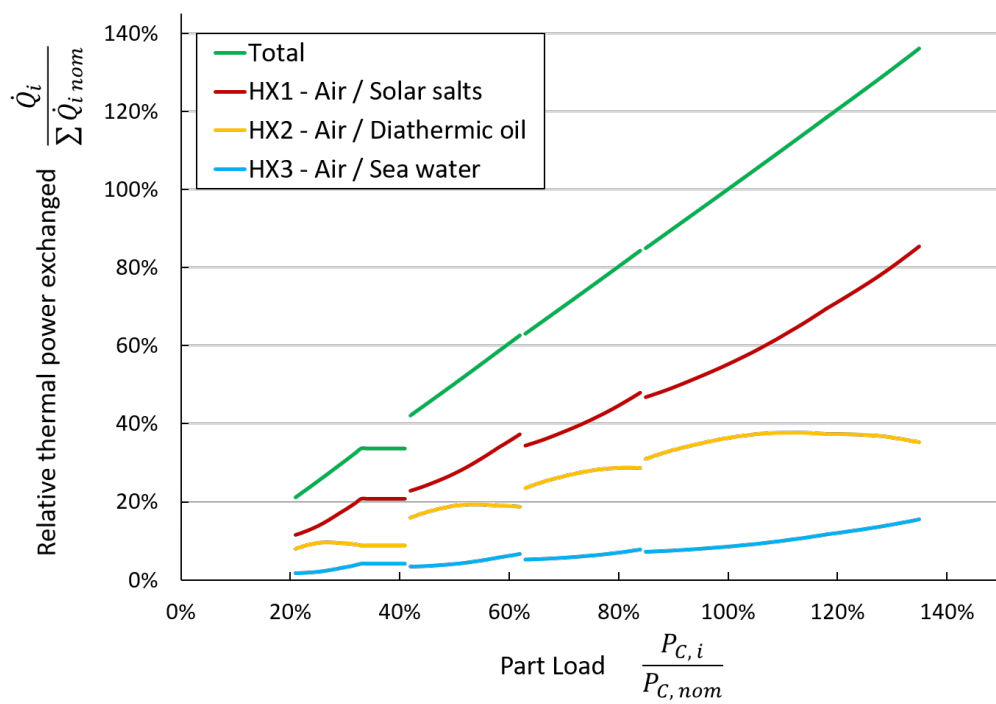
Figure 4.10. Total relative thermal power and relative thermal power exchanged by each T.E.S. unit against relative power absorbed by the compression section. The compression block is composed by four parallel trains of type B.2 with shafts connected by gearbox

function of the compressor efficiency and compression ratio as follow:

$$\begin{cases} m_{air} \propto \frac{P_{compression}}{\Delta h} \propto \frac{P_{compression}}{f(\eta,\beta)} \\ COT \propto \Delta h \propto f(\eta,\beta) \end{cases}$$

Considering the almost constant outlet temperature of last HX it is possible to obtain:

$$\dot{Q}_{total} \propto \dot{m}_{air} * COT \propto P_{compression}$$

Then a linear decrease in the power input to the compressor coincides with a nearly linear thermal power recovered by the whole T.E.S. system.

Fluctuations of the relative thermal power exchanged in the three different HXs are due to the different values of COT, Figure 4.9. Having sequential units a variations at the inlet of the first affect all the other in cascade, modifying the pinch point of each unit. To better understand this behavior the T-Q diagram of some representative cases can observed in Figure 4.11:

a) P/P$_{nom}$ = 135% at which correspond the maximum COT of 960 K and the maximum air flow rate of 126.8 kg/s.

b) P/P$_{nom}$ =100% at which correspond the nominal COT of 898.15 K and the nominal air flow rate of 103 kg/s.

c) P/P$_{nom}$ = 22% at which correspond a COT of 889 K and the minimum air flow rate of 22 kg/s.

In case a) with respect to b):

$$COT \uparrow, \quad mair \uparrow$$

then $UA_{HX1} \uparrow$ and $dT_{mln} \uparrow$ having $\dot{Q}_{HX1} \uparrow$ but $T_{out,HX1} = T_{in,HX2} \downarrow$

then $UA_{HX2} \uparrow$ and $dT_{mln} \uparrow$ having $\dot{Q}_{HX2} \uparrow$ and $T_{out,HX2} = T_{in,HX3} \uparrow$

then $UA_{HX3} \uparrow$ and $dT_{mln} \uparrow$ having $\dot{Q}_{HX3} \uparrow$ and $T_{out,HX3} \uparrow$

The case c) instead presents a COT which is close to the nominal value implying a behavior similar to b) only with lower ΔT_{mln} and much lower Q_{HX} due to the m_{air} consistent reduction.

At part load of the *CtS* then the thermal powers stored in the thermal tanks are not anymore balanced, leading to unequal percentage filling of the storage units. During a yearly usage of the UWCAES plant this aspect could lead to plant shutdowns having for example the solar salts storage saturated and the hot oil tank empty. To solve this issue an additional heat exchanger is introduced in which the solar salts and diathermic oil could exchange thermal energy. Regarding the sea water unit it could be easily by-passed in case of saturation or emptying.
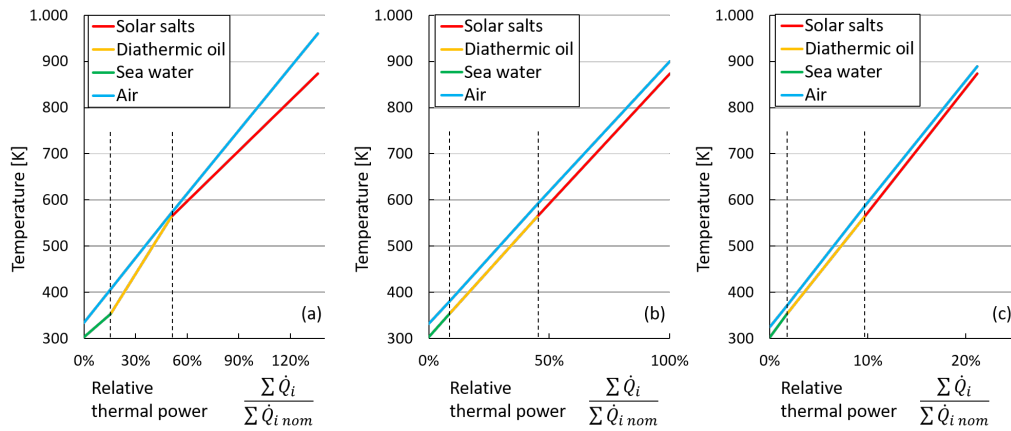
Figure 4.11. T.E.S. heat exchangers T-Q diagrams at different part load conditions of the compression section composed by four parallel trains of type B.2. (a),(b),(c) are referred to relative power absorbed by the compression section of 135% , 100%, 22% respectively.

4.7   Discharge phase: Heating from Storage

The nominal condition of this phase is dependent on the turbine sizing. The turbine is designed to process an air flow which is expressed as function of the air mass flow elaborated by the compression block at its design point, by the TDF (Equation 3.12. Then having a TDF equal to one means that the air mass flow rate sent and extracted by the underwater tank are the same. The design power of the turbine instead results in being lower than the nominal power of the compression section with a dependency proportional to the η_{RT}. The TDF assignment is an arbitrary choice and depends on the plant application and on the economic advantage of having a bigger or smaller turbine, see Chapter 6. During the design phase a TDF equal to one has been considered.

The obtained total thermal energy recovered by the T.E.S. and the turbine electric power output are plotted against different TDF values in Figure 4.12. It can be seen that the two curves are about linear for TDF variations but they are not parallel as would be expected for a constant turbine efficiency. The reason lies on the pressure drop and TIT modification, affecting the inlet conditions of the turbine and then the enthalpy drop. In Figure 4.13 the inlet turbine pressure and TIT are plotted as function of the TDF.

Moreover depending on the chosen management strategy of the plant the turbine could be required to work at part load conditions. For example it could be the case for which the CAES is employed to flatter the electric power input to the grid along the year following a peak shaving logic, see Chapter
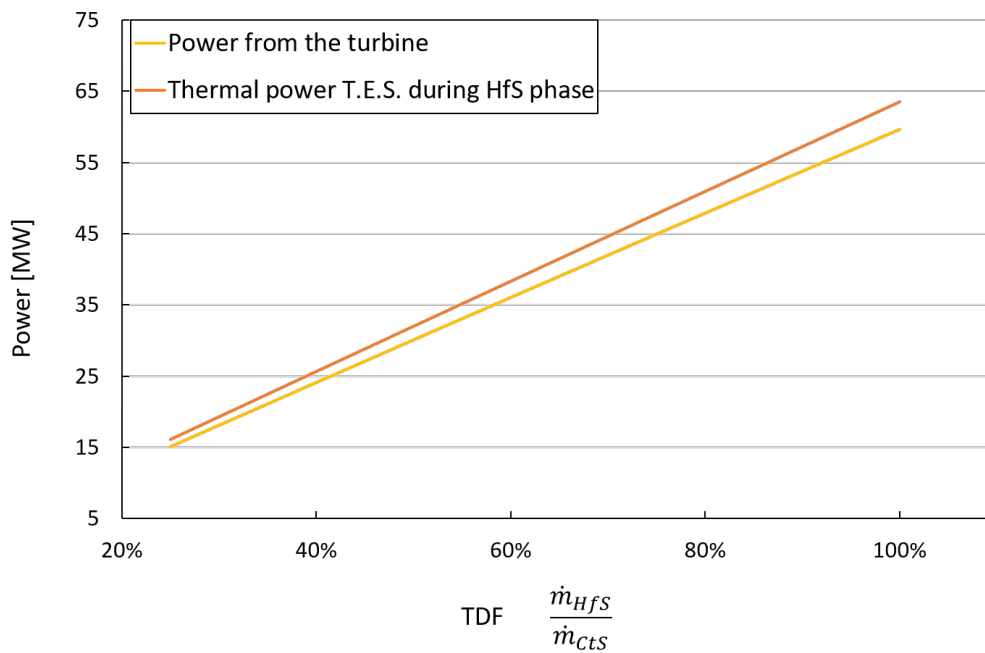
Figure 4.12. Thermal power form the T.E.S. to air and electric power produced by the turbine against TDF. Considering a compression section composed by four parallel trains of type B.2 and shafts connected by gearbox.
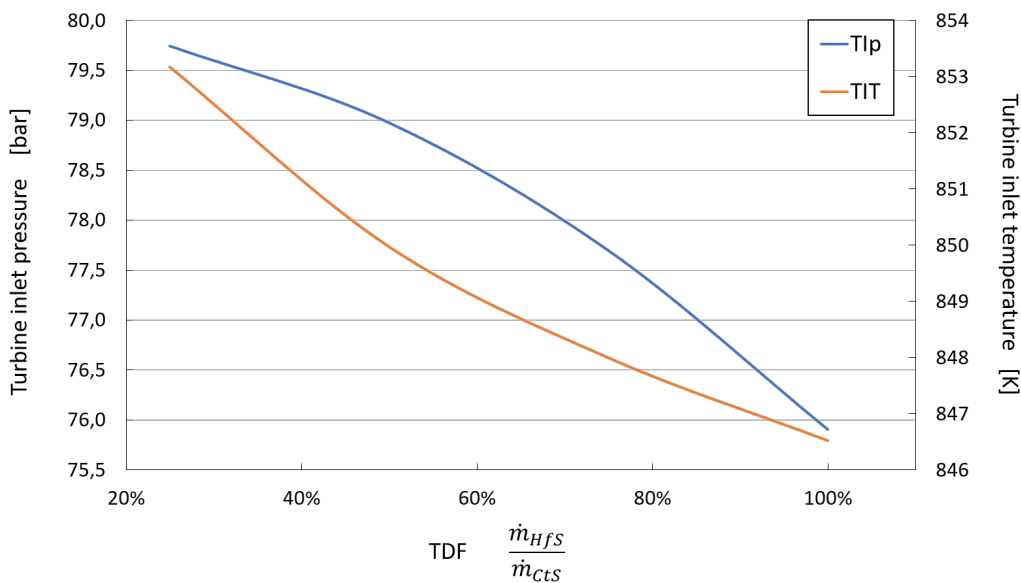
Figure 4.13. Turbine inlet pressure and turbine inlet temperature against TDF. Considering a compression section composed by four parallel trains of type B.2 and shafts connected by gearbox.

5. For this reason the turbine inlet is provided of a lamination valve. The $P_{expansion}$ decrease is obtained acting on the closure of the valve, increase the pressure drop at the inlet of the turbine, so that the pressure at the inlet is reduced. A proportional reduction is reflected on the $\dot{m}_{expansion}$ since the reduced flow rate, defined as

$$\dot{m}_{red} = \frac{\dot{m}_{expansion} * \sqrt{R_g * T_{in}}}{p_{in} * A} \qquad (4.11)$$

is considered constant.

Both the effects contribute in the power reduction. The polytropic efficiency is assumed constant and equal to the nominal value of 0.89 also during the part load condition. At off-design conditions of the turbine for a given TDF the T.E.S. behaves similarly to the case of nominal HfS with variable TDF: thermal power reduction due to the decrease for the mass air flow rate with small differences in the ΔT_{mln}.

4.8 Conclusions

In the end from the results of the preliminary analysis on the performances map found in literature, the most promising part load management strategy results in being the variable rotational speed. This trend is confirmed by the simulation on the compression section with the implemented model. Then considering the multishaft configuration two advantages are evinced: higher nominal performances and a more flexible behavior at part load. For this last case the performances difference between the usage of gearbox or electric motors dedicated to each shaft are nearly negligible, 1% increment of total relative mass flow and same power input ranges tolerated. The issue of a narrow operational range of the compressors, given by the required constant air tank pressure, could be solved using multiple parallel trains. A compression section designed with four parallel trains of type B.2 with one intercooler and two shafts presents a operational range wider of the 128% with respect to a single train of the same type. During a real part load management of the plant stresses on mechanical components could be an issue related to the exclusion of one or more parallel trains since during the switch the rotational speed appreciably change. Related to this aspect is interesting to observe that for four parallel trains overlapped operational curves are obtained. Finally it is important to underline that all the reported results are based on the assumption of compressors designed in similitude and neglecting scale effects, as reported in Chapter 3 this hypothesis need to be verified in a future work.

As a conclusion the T.E.S. system during the *CtS* phase at part load usage presents the issue of unequal relative levels of thermal power stored by each

unit. In this work as a solution an additional heat exchanger between the solar salts and diathermic oil has been introduced, together with the bypass of the sea water unit. Another interesting solution would be to consider the exchange units composed by smaller parallel heat exchangers. In this way the number of active heat exchangers could be switched depending on the mass flow rate values, trying to keep the working condition as much as possible close to the nominal one. Investigating over this configuration could be food for thought in a future work. Regarding the *HfS* phase the parameter affecting majorly the performances consists on the TDF. Which is the best TDF value can not be determined a priori but it depends on the UWCAES desired application and it is the results of a economical analysis. This aspect has been better discussed in Chapter 5 and Chapter 6.

Chapter 5

Case study

5.1 Introduction

In this chapter the UWCAES system is applied to a real case study. The plant configuration chosen as reference case consists on:

- · Compression section composed by four parallel trains of type B.2 with shafts connected by gearbox,

- · T.E.S. assumptions as reported in table 2.2 of chapter 2,

- · other assumptions as reported in table 2.1 of chapter 2.

The chosen location is off-shore the South West Sardinia in Italy, positioning the cement air tanks at about 820 m depth at which correspond an hydrostatic pressure of 80 bar. This kind of storage could be coupled with different RES but this work has been mainly focused on wind power energy. The need of deep-water location fits the possibility of exploiting an off-shore wind farm. Although the deep-water offshore wind technology is still under development, it is widely considered in long-term projections for its huge energy potential [1]. The UWCAES system is then coupled with a combination of off-shore wind parks, composed by Siemens SWT 2.3 MW turbines, which characteristics are reported in table 5.1. Wind field measurements for the years 2015 and 2016 related to the chosen location have been provided by the Spanish harbour weather forecast company Puertos [27]. Those datasets have been used to evaluate the the wind farm annual energy production of the wind farms through the use of the SAM tool [1].

---

[1]System Advisor Model, Version 2017 9.5, Release Date 2/12/2018, Author: National Renewable Energy Laboratory (NREL)

Table 5.1. Siemens SWT 2.3 MW characteristics and turbine power curve.

Cut-in speed	m/s	3.0
Rated speed	m/s	11.0
Rated power	MW	2.3
Rotor diameter	m	108
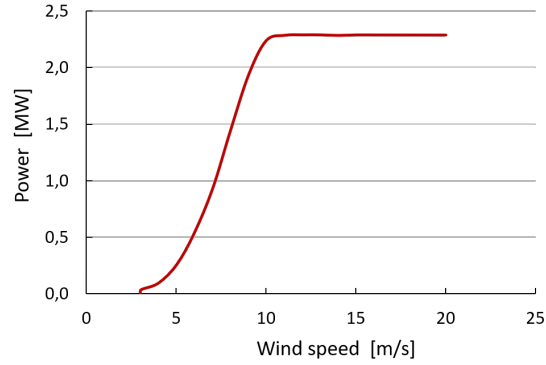
Storage systems could be employed following different logics, depending on the desired purpose:

· Peak shaving logic aims at improving the dispatchability of the wind energy. Fluctuations in the energy sent to the grid are mitigated by the use of a storage system. When the energy produced by the wind farm is too high part of it is stored, on the other hand when it is too low additional energy is extracted from the storage.

· Arbitrage logic decouples the wind availability from the price policy. The aim is to maximize the incomes of the wind park. The storage system then acts as a producer, storing energy when the electricity price is low and selling energy when it is more convenient. The dependence between prices and available energy implicitly makes the plant to operate as a grid stabilizer.

· Ancillary services logic aims at compensating the unbalances between the actual and predicted production or load profiles. The plant is asked to send energy to the grid compensating those variations, then the storage presence becomes necessary since the required energy could differ from the wind availability.

In the proposed case study the plant is simulated by an heuristic approach for both the management stategies: peak shaving and arbitrage.

5.2   Peak Shaving logic

The peak shaving management strategy aims to control the grid power injection, flattering the energy sent to the grid to a desired value. Thresholds need to be defined in order to establish the activation strategy of the UWCAES

compressors and turbine. In a real application they would be defined hour by hour on the basis of an economic optimization but in this chapter just a preliminary analysis is conducted and those limits are considered constant along the year. In particular an upper and a lower bounds are defined as fraction of the nominal power produced by the wind farm, see figure 5.1. When the power produced by the wind farm overcomes $P_{ub} = \text{ub}*P_{nom,w}$ then the difference between the exceeding power corresponds to the compression input to the compressor on the other hand when the P_{actual} is lower than the P_{lb} the turbine starts to expand the stored air.
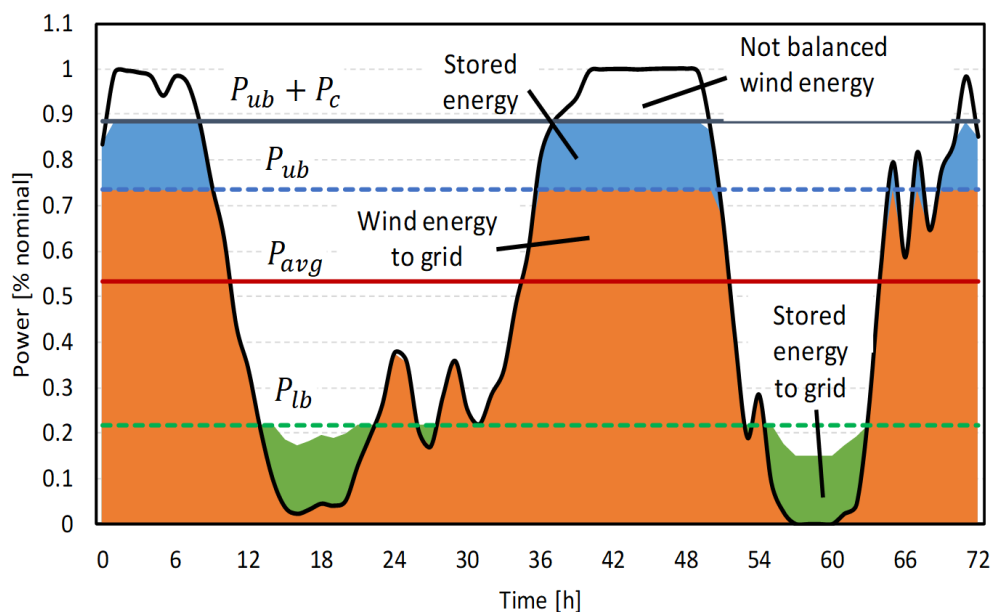
Figure 5.1. Example of operation strategy of the peak shaving energy storage coupled with the wind park production profile. [1]

As already introduced the compression section operational range affects the yearly performances of the storage system implying higher or lower amount of dissipated energy, depending on its size. As it can be visualized in figure 5.2 there is a power gap for which the compressor can not operate since the power coming from the wind that the storage should absorb does not reach the minimum tolerated load. If that power can not be injected on the grid it is dissipated. The lower is the power input tolerated by the compressor the smaller this gap is. This issue is intrinsic of the adopted management strategy and it can not be avoided, unless it is accepted to inject in the grid

an energy input with peaks. Another interest aspect is the advantage of having a turbine able to work at off design conditions. During the year it could happen that for some hours the power from the wind is lower the P_{lb} but the summation of the nominal turbine power and the power generated by the wind turbines is higher than P_{ub}. This is an undesired effect, since the aim of the storage integration is to have a flat injection to the grid and for this reason if the turbine is not able to reduce its output, it could not operate, see figure 5.3.
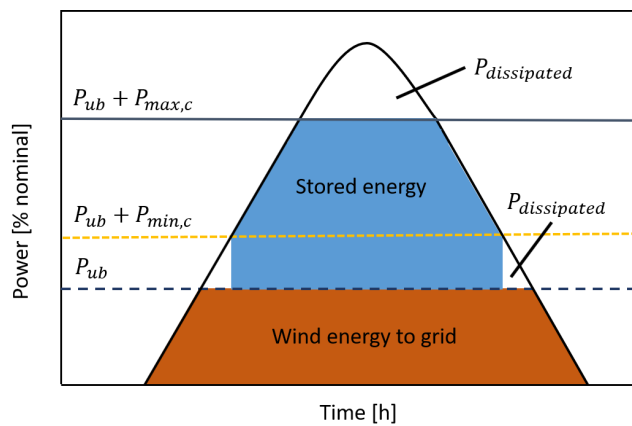
Figure 5.2. Example of compression section sizing for the peak shaving energy storage coupled with the wind park production profile.
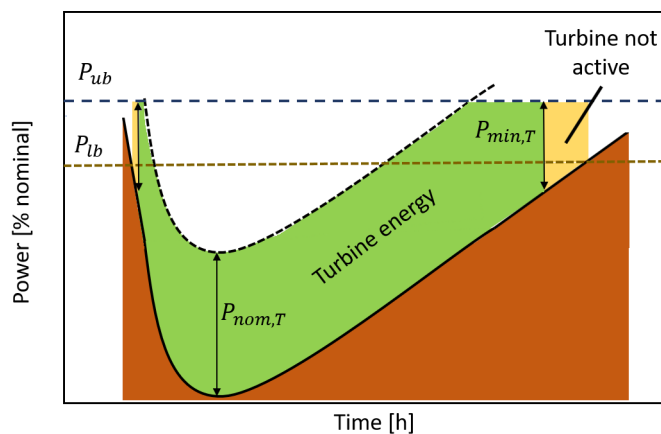
Figure 5.3. Example of turbine behavior for the peak shaving energy storage coupled with the wind park production profile.

The performance paramenters are different on the basis of the desired effect. Focusing on the effectiveness of shaving energy peaks the main indicator is the variance of the hourly energy send to the grid, defined as:

$$\sigma_P^2 = \frac{1}{T} * \int_T \left[P_{grid}(t) - P_{ref}(t) \right]^2 dt \qquad (5.1)$$

Where T is the considered time period and as reference case is kept a fully dispatchable plant ($\sigma_P = 0$), with a constant flat energy output along the whole year. Differently if the UWCAES usage is investigated the main parameter is the round trip effciency, which indicates how effciently the storage operates and it depends on the wind conditions combined with the design power of the plant, upper and lower bounds setting. Other indicators are the annual energy send to the grid and the annual energy produced by the turbine, which are related to the economics of the plant, considered in Chapter 6. This analysis becomes relevant if performed comparing to the cases of the wind park with and without the storage integration, to better understand which are the improvements of the UWCAES employment.

5.2.1 Wind farm without storage

The considered off-shore wind farm has a nominal power of 135 MW. Its integration with the wind measurements data give the annual performances reported in table 5.2.

Table 5.2. Wind field and wind farm of 135 MW characteristics for year 2015 and 2016.

		2015	2016
Maximum power	MW_e	135	135
Average power	MW_e	55	56
Average wind speed	m/s	6.47	6.56
Annual energy production	GWh	481	491
Capacity factor	%	40.2	40.6

Since a comparative analysis is desired in this chapter the wind park is supposed to be regulated avoiding energy output peaks. Then a threshold is

defined and the energy produced above this bound is dissipated, trying to keep the injection to grid as constant as possible. Varying this threshold the behavior reported in figure 5.4 is individuated for the annual energy produced and the standard deviation, which is defined as: $\sqrt{\sigma_P^2}$. The more ub is reduced the flatter is the power output of the plant but on the other hand the energy produced results lower and lower.
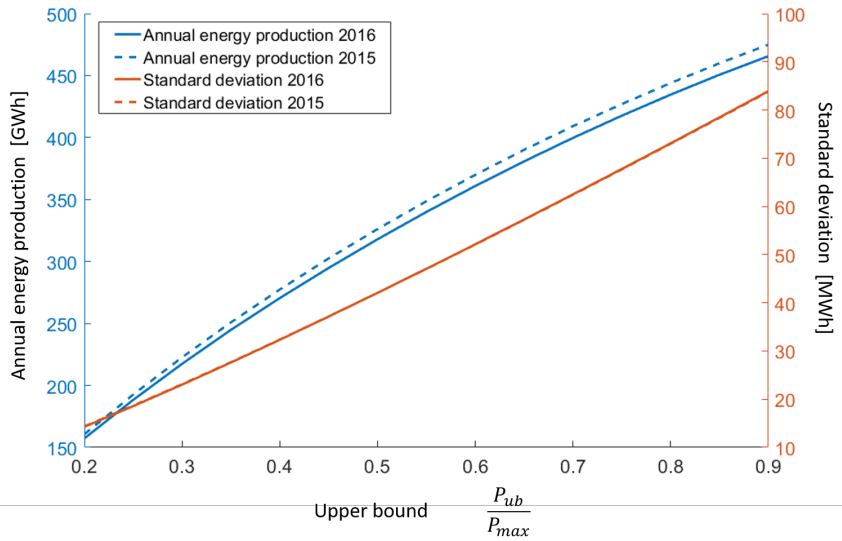
Figure 5.4. Wind farm without storage annual production and standard deviation as function of upper bound values.

5.2.2 UWCAES integration

The UWCAES is coupled with the considered wind farm, referring to the 2016 year. The simulations are performed by an heuristic approach for different values of compression design power and different upper bounds. Each time the design power of the compression section is changed the entire plant is re-sized on its basis, e.g. the turbine will vary its nominal power as well. The assumption of coinciding thresholds is made: $ub = lb$. In this way the turbine could expand the stored air as soon as the power of the wind park is lower than P_{ub}. This means that the plant is managed as close as possible to the reference case: fully dispatchable plant with constant energy injection to the grid. As first step the thermal and air tanks are assumed of infinite capacity and they are considered empty at the first hour of the year. In figure 5.5 the main results of the annual simulation for the year 2016 are mapped. First of all, many combinations of design power of the compressor and upper bound

(a) Round trip efficiency

(b) Standard deviation

(c) Annual energy to grid

(d) Annual energy produced by the turbine
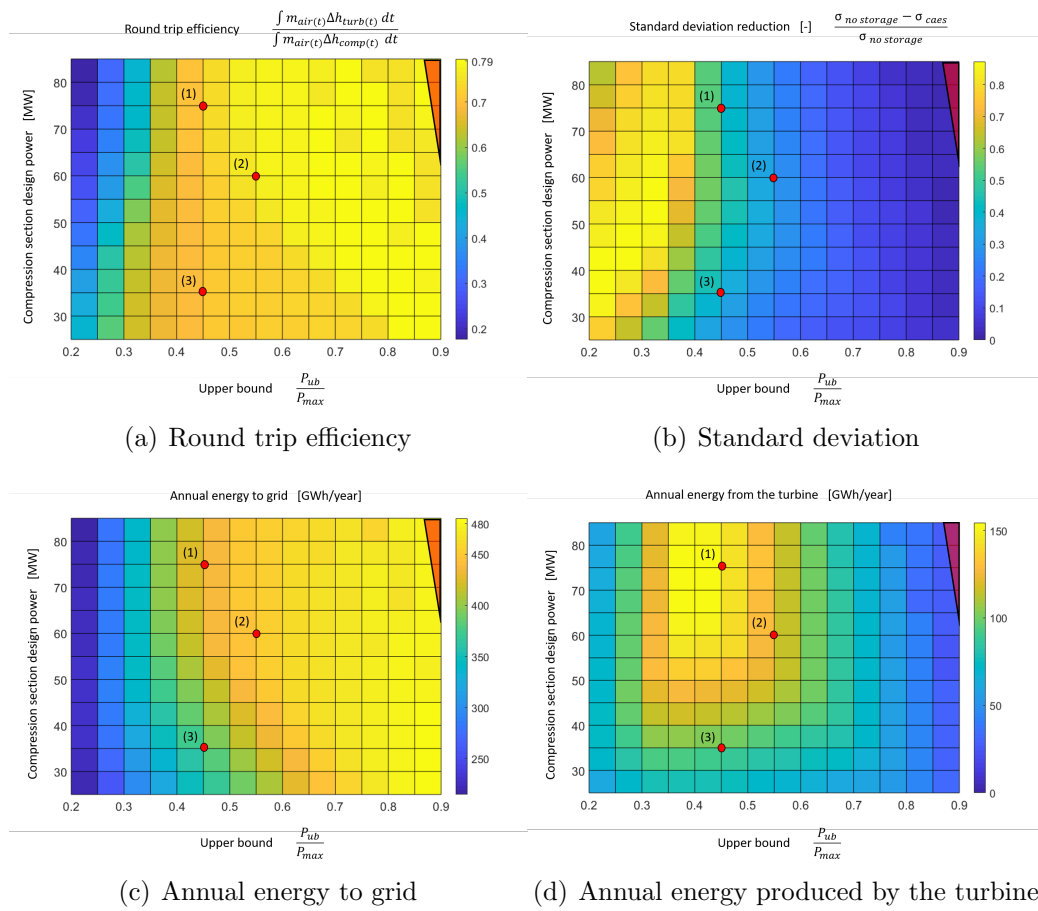
Figure 5.5. Annual simulations results for year 2016 of the wind farm coupled with UWCAES of infinite storage capacitiy.

are tried, but the up right area of the maps, highlighted in red, is meaningless since it corresponds to an activation threshold of the compressors higher than the power available to the storage system. The maximum power available to storage is determined by the rated power of the wind farm minus the upper bound.

The RTE efficiencies prensent an optimum trend along the diagonal line, from the down right corner to the up left direction at which correspod $P_{nom,c}$ about equal to the maximum power available to the storage, given by $P_{nom,wind}$-P_{ub}. At left side of the maps a steep decay of RTE can be individuated and it can be explained by the very low upper bound. The energy from the wind is majorly stored and very rarely the turbine is called to convert energy implying very high levels of stored energy at the end of the simulated year, see figure 5.6.
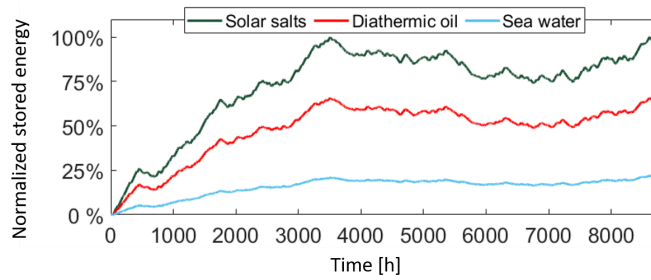
(a) Hourly thermal energy stored by each T.E.S. unit normalized with respect to the solar salts tank maximum level.
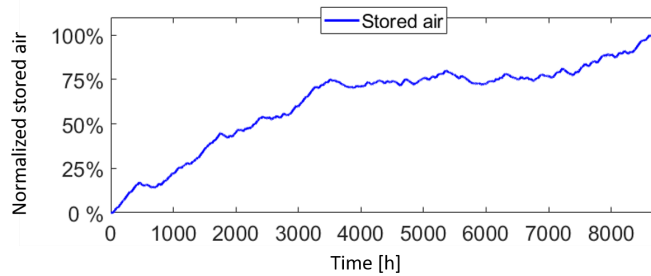
(b) Hourly air volume stored normalized with respect to its maximum.

Figure 5.6. Annual T.E.S. state for upper bound 0.20 and nominal power of the compression section of 45 MW.
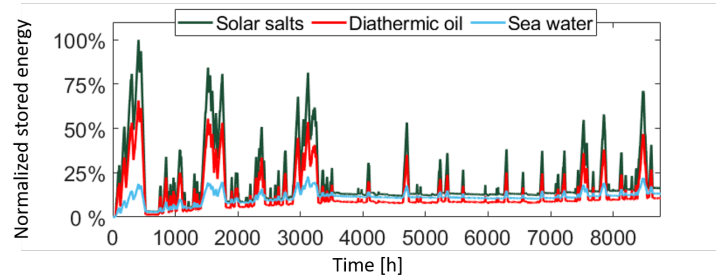
(a) Hourly thermal energy stored by each T.E.S. unit normalized with respect to the solar salts tank maximum level.
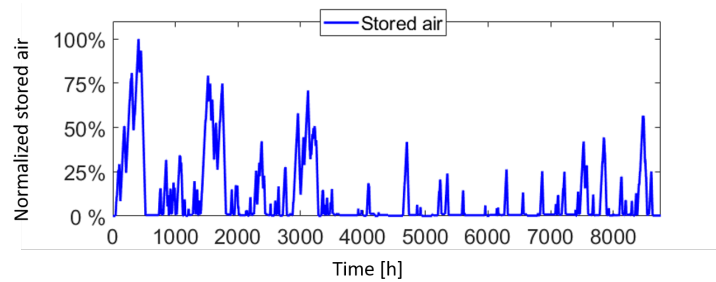
(b) Hourly air volume stored normalized with respect to its maximum.

Figure 5.7. Annual T.E.S. state for upper bound 0.80 and nominal power of the compression section of 45 MW.

Moving in up right direction from the center of the maps the opposite trend is presented: the compressors are over sized with respect to the P_{up} and they work most of the time at off-design conditions, implying less stored energy and then higher number of hours at which the tanks are empty, for this reason the annual energy produced by the turbine decreases, see Figure 5.7. The $\Delta\sigma_P$ has an inverse trend with respect to the annual energy send to the grid, so there is a trade off between the ammount and the quality of energy injected to the grid. Very consistent reductions of the stardard deviation are obtained decresing the upper bound and increasing the machine size, but these conditions imply reduction of the energy sent to the grid of about the 50% and RTEs lower down to 40-30 %. Finally interesting is to observe how the UWCAES system of infinite capacity works as a seasonal storage, reflecting the yealy wind availability. It stores energy mainly during winter/spring and it empties majorly during summer/fall seasons, see figure 5.6.

In table 5.3 more detailed performances of the cases highlighted in figure 5.5 are reported. The points 1) and 2) are taken along the RTE optimal

diagonal while the third point corresponds to a case with a down-sized compressor with respect to the wind farm power available for storage, in this case about the 70% of the wind park capacity can be exploited.

1) $ub = 45\%$ and $P_{des,compressor} = 75$ MW;

2) $ub = 55\%$ and $P_{des,compressor} = 60$ MW;

3) $ub = 45\%$ and $P_{des,compressor} = 35$ MW;

Table 5.3. Results of the annual simulation for the reference cases. The wind farm is coupled with UWCAES of infinite capacity and managed following a peak shaving strategy.

Case	ub	P_C	P_T	Storage size				η_{RT}	E_{grid}	$E_{unbalance}$	EOH_C	EOH_T	h_C	h_T	σ_P reduction
				Air	Solar salts	Oil	Water								
	[% P_{nomw}]	[MW]	[MW]	[10^3 m³]	[kton]	[kton]	[kton]	[%]	[GWh]	[GWh]	[hours]	[hours]	[hours]	[hours]	[%] of case without storage
	45			No storage					294.8	196.1	No storage				ref
	55								340	150.9					ref
1)	45	75	60	1694	109	76	36	74.5	474.1	3.7	2566	2401	3160	2934	39.1
2)	55	60	48	827	58	40	19	77.6	455.4	2.2	2479	2419	2924	2657	26.4
3)	45	35	28	1365	101	69	59	71.5	395.2	55.7	4011	3605	3359	3818	35.7

The storage dimensions are unfeasible, i.e. for case 2), which is the one requiring the lower mass of HTF, 6, 8 and 4 hot tanks are needed to store solar salts, diathermic oil and sea water respectively. The considered tanks are cylindrical concrete structures of 20 meters of diameter and 20 meters height. Therefore the same analysis has been repeated limiting the storage size to let the plant work for 48 hours at nominal charge conditions.

Table 5.4. Results of the annual simulation for the reference cases. The wind farm is coupled with UWCAES of capacity limited to 48 hours of nominal charge operation and managed following a peak shaving strategy.

Case	ub	P_C	P_T	Storage size				η_{RT}	E_{grid}	$E_{unbalance}$	EOH_C	EOH_T	h_C	h_T	σ_P reduction
				Air	Solar salts	Oil	Water								
	[% P_{nomw}]	[MW]	[MW]	[10^3 m³]	[kton]	[kton]	[kton]	[%]	[GWh]	[GWh]	[hours]	[hours]	[hours]	[hours]	[%] of case without storage
	45			No storage					294.8	196.1	No storage				ref
	55								340	150.9					ref
1)	45	75	60	174	13	9	5	77.6	390.4	72.9	1643	1602	2133	1913	23.5
2)	55	60	48	139	10	7	4	78.4	419.9	49.1	1698	1674	2088	1779	16.8
3)	45	35	28	76	6	4	2	73.6	328.1	150.9	1292	1195	1245	1350	8.9

In table 5.4 a slight RTE improvement is evinced due to a better exploitation of the stored energy being the charge and discharge cycles more frequent

and having empty air tank at the end of the year. Although the annual value of energy stored decreases if compared to the simulation with storages of infinite capacity, due to the presence of hours during which the T.E.S. and air tanks are saturated. For the same reason also the annual energy injection into the grid results in being lower. The standard deviation presents higher values since the limited storage implies also an increase of the time at which the tanks are empty, lowering the power send to the grid farer from the P_{ub} threshold. The number of required hot tanks is successfully reduced to at a maximum of 2, for example to store the solar salts in case 1).

Focusing on case 3) which is the one with smaller storage dimensions we can observe that the equivalent hours of the compressor are higher than the actual time during which the compressor is working. This behavior is due to the ability of the compressor to work at overload condition, up to 135% of its nominal power and due to the fact that in case 3) the compressor is down-sized with respect to the storable power coming from the wind farm. With the storage limited to 48 hours indeed the 35 MW compressor works during the year at an average power of about 106% of its nominal power. This issue could cause mechanical stresses to the machine along the plant life operation. The compressor is then limited to work at maximum its nominal power, obtaining the performances tabled in 5.5.

Table 5.5. Results for case (3) of the annual simulation of the wind farm coupled with UWCAES of limited capacity at 48 hours of nominal charge operation. The plant is managed following a peak shaving strategy and avoiding overload of the compression section.

Case	ub	P_C	P_T	Air	Storage size Solar salts	Oil	Water	η_{RT}	E_{grid}	$E_{unbalance}$	EOH_C	EOH_T	h_C	h_T	σ_P reduction
	[% P_{nomw}]	[MW]	[MW]	[10^3 m^3]	[kton]	[kton]	[kton]	[%]	[GWh]	[GWh]	[hours]	[hours]	[hours]	[hours]	[%] of case without storage
	45				No storage				294.8	196.1		No storage			ref
	55								340	150.9					ref
3)	45	35	28	81	6	4	2	78.7	350.6	124.9	2036	2013	2269	2147	17.1

In this last case a reduction in the standard deviation and an increment of the round trip are evinced. This means avoiding overload conditions helps in maintaining the T.E.S. and the air tank level better balanced. For the configurations 1) and 2) instead limiting the overload does not produce relevant effects since the upper bound and compressors are already sized in order to have storable power equal to the compression nominal power:

$$P_{nom,w} - P_{ub} = P_{max,storable} = P_{nom,c}$$

5.2.3 Sensitivity analysis based on lower bound and TDF variation

Considering the three analized cases:

1) $ub = 45\%$ and $P_{des,compressor} = 75$ MW;

2) $ub = 55\%$ and $P_{des,compressor} = 60$ MW;

3) $ub = 45\%$ and $P_{des,compressor} = 35$ MW;

Sensitivity analysis on the TDF and the lower bound variations is performed. All the three cases present similar trends if the storages capacity is assumed to be infinite:

· The annual energy stored does not vary;

· Reducing the lower bound or the turbine dimension factor, the round trip efficiency results in being lower and lower since the turbine is not able to exploit all the stored energy, which remain stored also at the end of the year. This effect is more marked for TDF reductions. At extreme case the RTE result in being reduced down to 20-30%. The RTE trend is directly reflected on the annual energy send to the grid and on the annual energy converted by the turbine, since the the annual energy stored is constant.

· Increasing the TDF more than 100% has the effect of empying faster the thermal tanks but since the RTE is almost constant as well as the annual energy produced by the turbine, it does not lead to more stored energy. This fact is confirmed by the standard deviation increase at higher TDF.

· The standard deviation has a minimum for lower bounds and/or TDF values sligthly lower than one and this happens because of the avoided hours during which the storage is empty,see figure 5.9 and the wind actual power is lower than P_{lb}. But in any case a reduction the standard deviation faces also a reduction in the annual power sent to the grid.

The same analysis has been reapeted limiting the storage size at 48 hours and the results can be observed in figure 5.10. There are optimal combination of TDF and lb that help in better exploiting the stored energy and then in having higher RTE and lower σ_P. Although the power injected to the grid reduces for lower TDF or smaller lb. This behavior is due the fact that smaller turbine convert less power as consequence the tanks empty slower during the year less energy could be stored as well. Increments in RTE are of about 1% and in the standard deviation reduction of about the 3%.
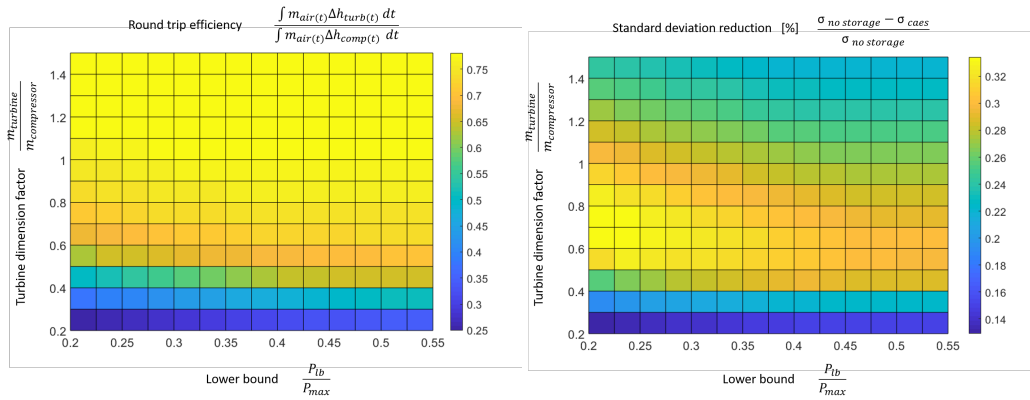
(a) RTE for case 2)

(b) σ_P reduction for case 2)
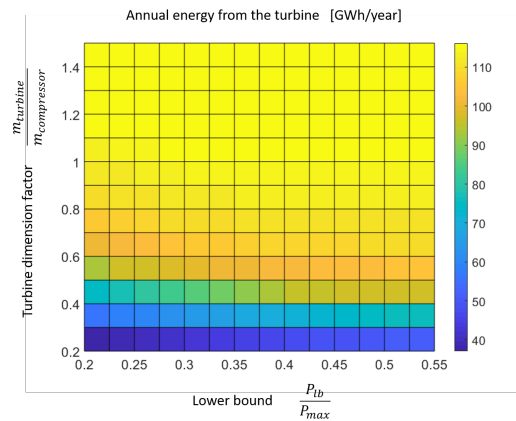
(c) Annual energy produced by the turbine
for case 2)

Figure 5.8. Annual simulation results for year 2016 of the wind farm coupled with
UWCAES of infinite storage capacity with variable lower bound and TDF.
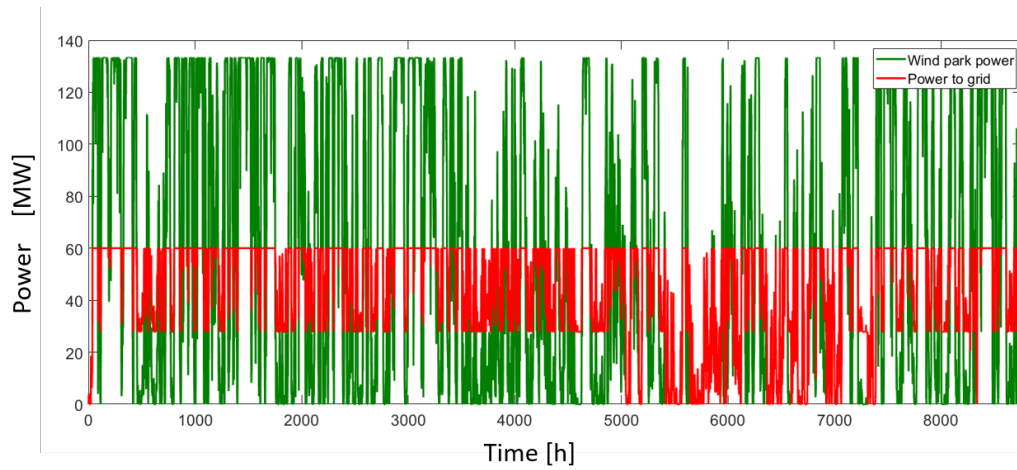
(a) P$_{des,c}$ =35MW, ub=0.45 , lb=0.45 and TDF=1
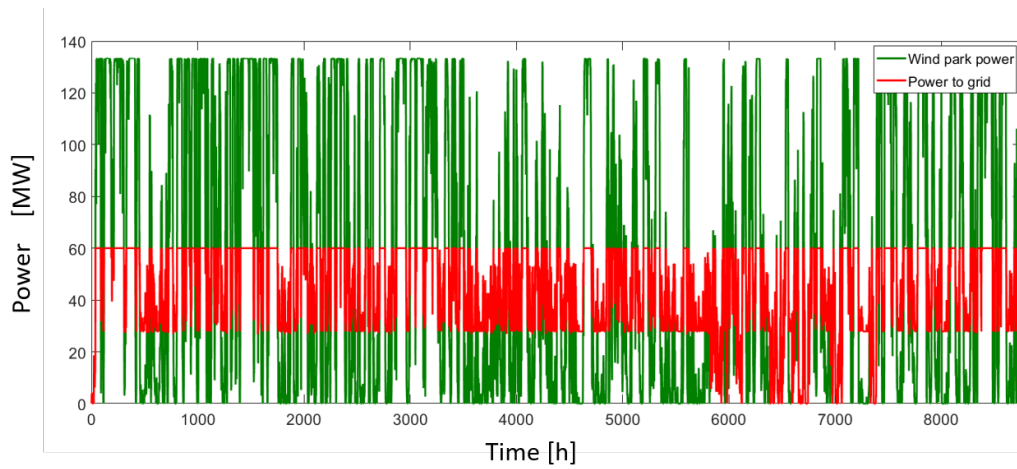
(b) P$_{des,c}$ =35MW, ub=0.45 , lb=0.20 and TDF=1

Figure 5.9. Annual simulations results for year 2016 of the wind farm coupled with UWCAES of infinite storage capacity with P$_{des,c}$ =35MW, ub=0.45 for different lower bounds.

(a) RTE for case 1) (b) σ_P reduction for case 1)

(c) RTE for case 2) (d) σ_P reduction for case 2)

(e) RTE for case 3) (f) σ_P reduction for case 3)
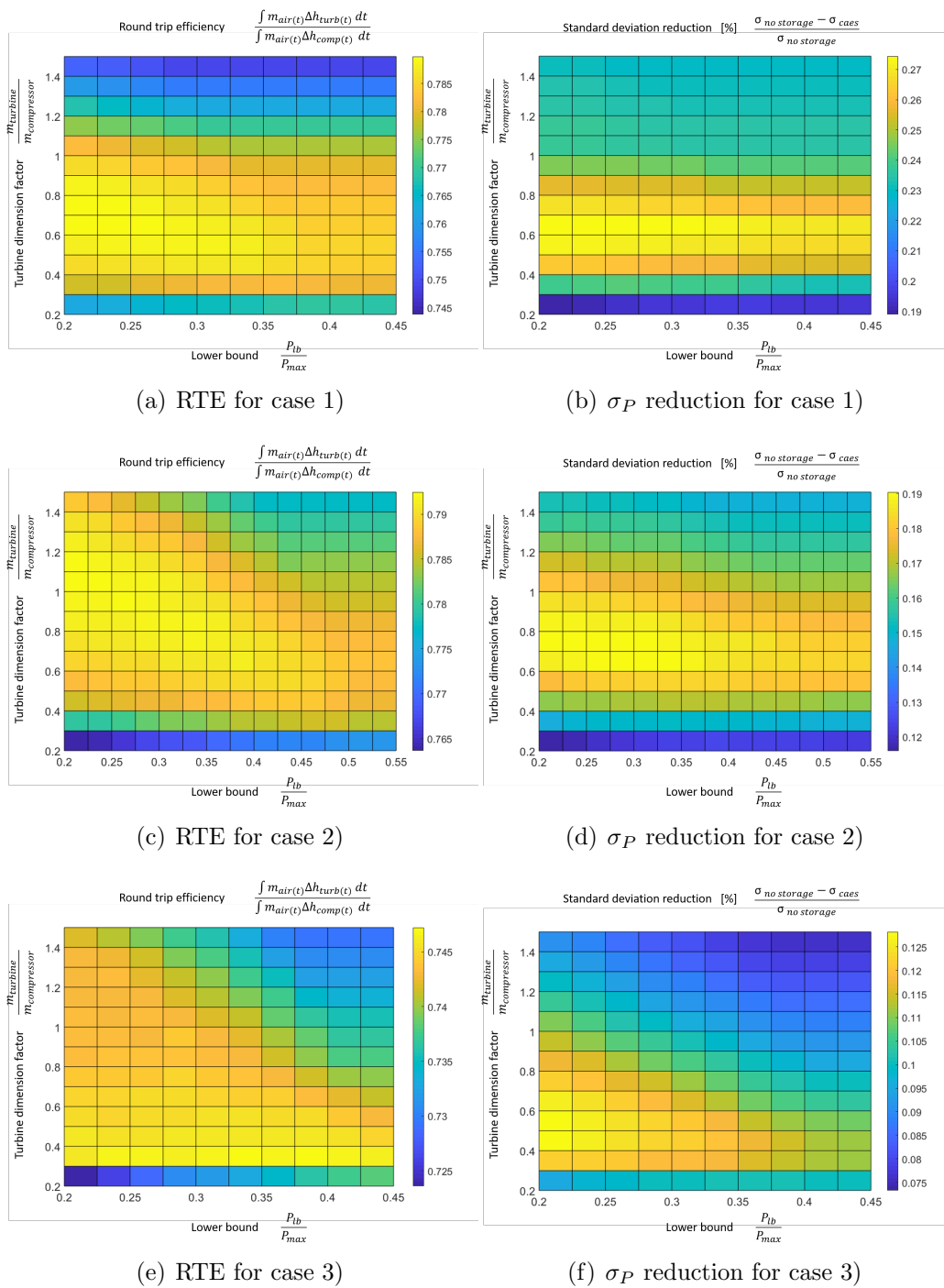
Figure 5.10. Annual simulations results for year 2016 of the wind farm coupled with UWCAES of 48 hours of charging phase storage capacity with variable lower bound and TDF.

5.3   Arbitrage logic

The arbitrage logic as introduced aims at maximizing the economics of the plant. The UWCAES system integrated to a wind farm is then regulated on the basis of the electricity price profiles: if the price is lower than the chosen threshold the plant stores the energy produced by the wind farm, otherwise in case of higher prices it expands the stored energy selling the energy coming from both the wind park and the turbine. Following this kind of management strategy the main performance parameter consists on the incomes increase at the end of the year, obtained comparing the incomes of the wind park operated with and without storage. The wind measurements related to this analysis are the same used in the previous section while the profile prices related to the chosen location, Sardinia, for the years 2015, 2016 are provided by [28]. The UWCAES is coupled to a wind farm of 68 MW still composed by Siemens SWT 2.3 MW turbines.

Table 5.6. Wind field and wind farm of 68 MW characteristics for year 2015 and 2016.

		2015	2016
Maximum power	MW$_e$	68	68
Average power	MW$_e$	27	28
Average wind speed	m/s	6.47	6.56
Annual energy production	GWh	240.3	245.4
Capacity factor	%	40.2	40.6

The nominal size of the plant in this case is related to the wind farm rated power, since the compression section ,if active, would be supposed to store all the energy available from the wind. As consequence the compression section nominal power is set to 60MW and it is composed by four parallel trains with one intercooler and two shafts. The two thresholds are defined again as percentage increment or decrement of the average price, calculated as the integral mean of the hourly zonal price along the whole year.:

· charging: zonal price $<$ average price $*(1-\mathrm{lb})$

· discharging: zonal price > average price ∗(1+ub)

At first simulations are performed considering storage of infinite capacity for different upper and lower threshold combinations and then to obtain more feasible tanks capacity the storage has been limited to 48 hours of nominal charge condition. The cases that maximize the incomes, calculated as:

$$income = income(windpark + UWCAES) - income(windpark)$$

are reported in Table 5.7 as case a) for infinite storage capacity and case b) for limited storage size.
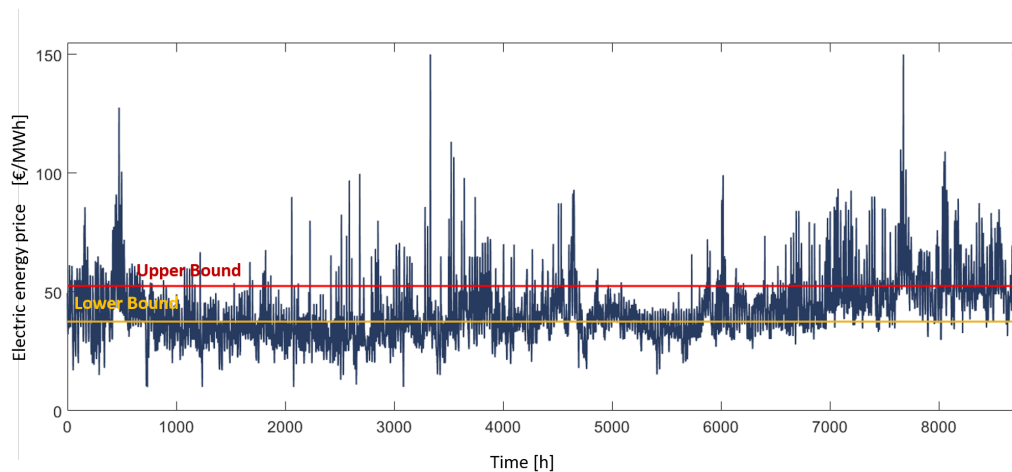
Figure 5.11. Electric energy price for the year 2016 with thresholds representation. Upper and lower bounds are set on the basis of the integral mean of the hourly zonal price along the whole year

Case a) present a low RTE value 58% and huge storage size, as can be seen in Figure 5.13 this fact is due to the air tank which is not empty at the end of the year and the stored energy is not completely exploited. Moreover unbalances are evinced between the quantities of thermal energy and of air stored, given the high amount of time during which the compressor is working at off-design conditions. Looking at case b) in Table 5.7 it can be noticed that the storage system is active for few hours along the year, indicating a not optimal thresholds definition. Than with the aim to enhance the UWCAES usage the bounds are set on the basis of the average price evaluated as a moving mean with monthly time span (Figure 5.12). The obtained best case, in terms of maximum income is reported in Table 5.7 as case c). The moving bounds have a positive effect to all the parameters of the plant and as can

be seen in figure 5.14 it helps in maintaing balanced storage levels and avoid many saturation hours.
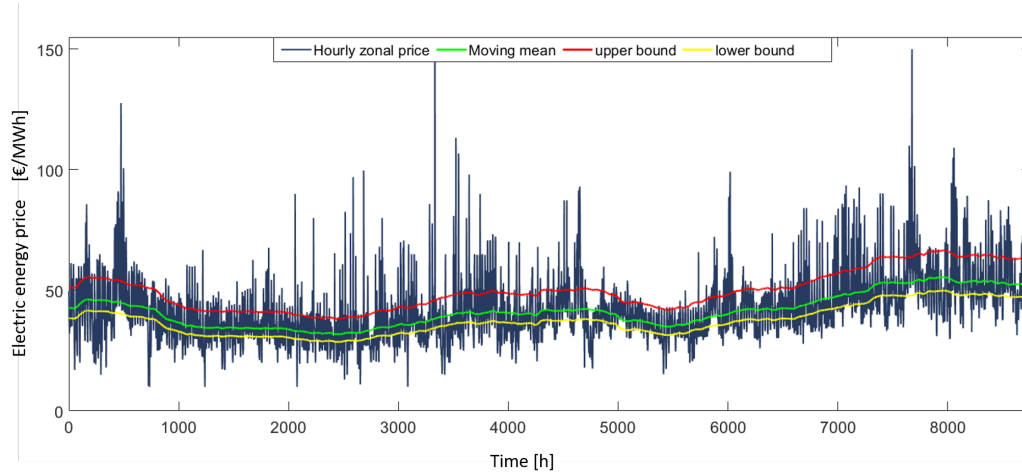
Figure 5.12. Electric energy price for the year 2016 with thresholds representation. Upper and lower bounds are set on the basis of the moving mean of the hourly zonal price evaluated for a monthly time span.

Table 5.7. Reference cases results of annual simulation of the plant managed by arbitrage strategy. Case a) refers to storage of infinite capacity and bounds defined on the basis of the integral mean of the hourly zonal price along the whole year. Case b) refers to storage sized to 48 hours at nominal charge operation and bounds defined on the basis of the integral mean of the hourly zonal price along the whole year. Case c) refers to storage sized to 48 hours at nominal charge operation and bounds defined on the basis of the moving mean of the hourly zonal price evaluated for a monthly time span.

Case	ub	lb	P_c	P_T	Storage size				η_{RT}	EOH_C	EOH_T	h_C	h_T	Income
					Air	Salt	Oil	Water						
	[%]	[%]	[MW]	[MW]	$10^3\,[m^3]$	[kton]	[kton]	[kton]	[%]	[hours]	[hours]	[hours]	[hours]	[M€]
a)	30	20	60	48	2099	140	97	53	58.0	1113	810	1329	810	0.66
b)	30	-10	60	48	139	10	7	4	77.2	848	663	1063	663	0.52
c)	20	10	60	48	139	10	7	4	78.3	1199	1020	1362	1020	0.88
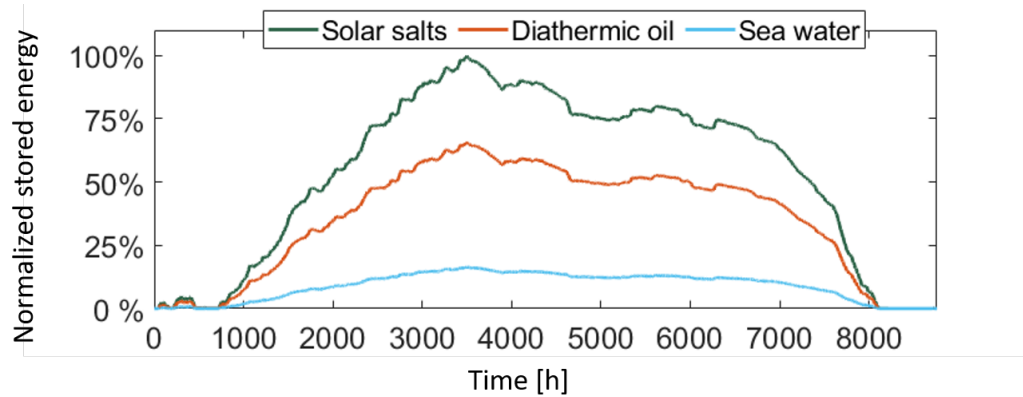
(a) Hourly thermal energy stored by each T.E.S. unit, normalized on the solar salts maximum capacity.
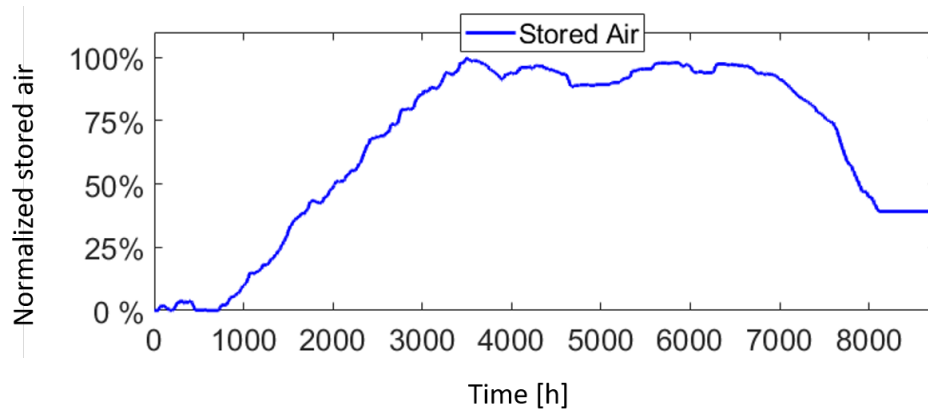
(b) Hourly air volume stored, normalized on its maximum capacity.

Figure 5.13. Annual storages state for UWCAES system of infinite capacity. The plant is managed following arbitrage logic. Referred to case a) of Table 5.7
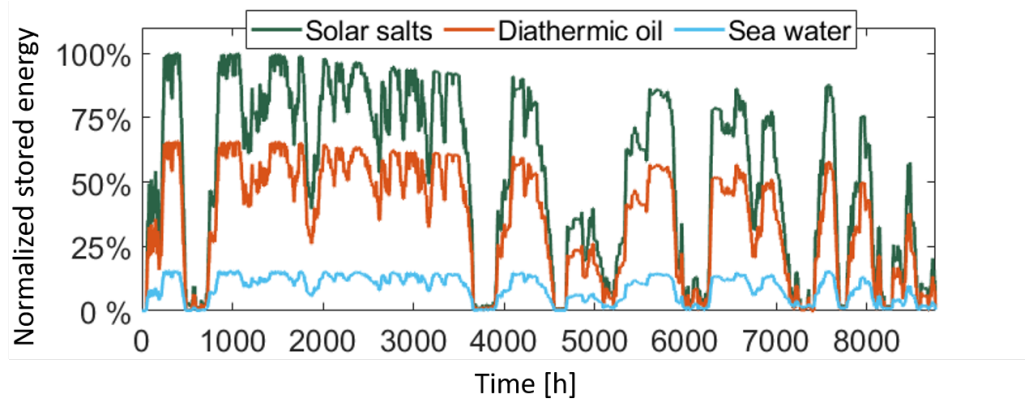
(a) Hourly thermal energy stored by each T.E.S. unit, normalized on the solar salts maximum capacity.
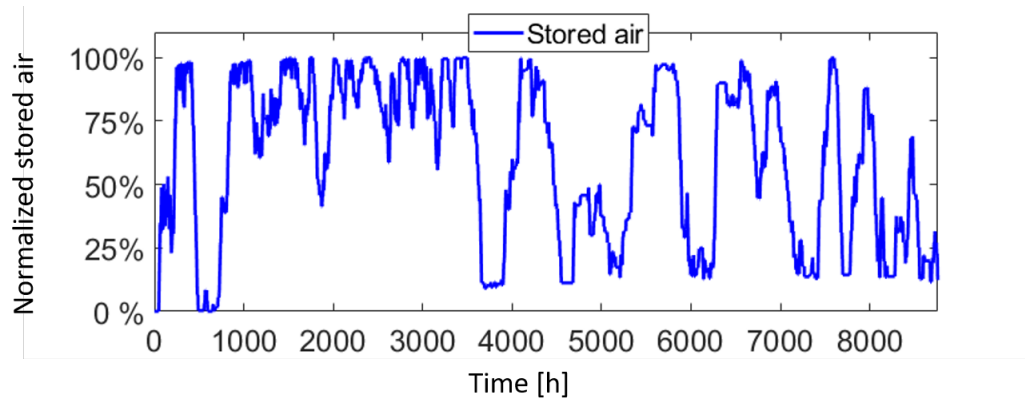
(b) Hourly air volume stored, normalized on its maximum capacity.

Figure 5.14. Annual storages state for UWCAES system sized for 48 hours of nominal charge operation. The plant is managed following arbitrage logic. Referred to case c) of Table 5.7

5.3.1 Sensitivity analysis based on TDF variation

Considering case c) of Table 5.7 the TDF is made varying and the obtained incomes and RTE variations are reported in Figure 5.15. For bigger turbines a better exploitation of the storage charge and discharge cycles leads to higher incomes and higher RTE efficiency. Anyway this analysis needs to be better investigated in light of the investment cost evaluation, in order to take into account also of the turbine cost increase, see Chapter 6.
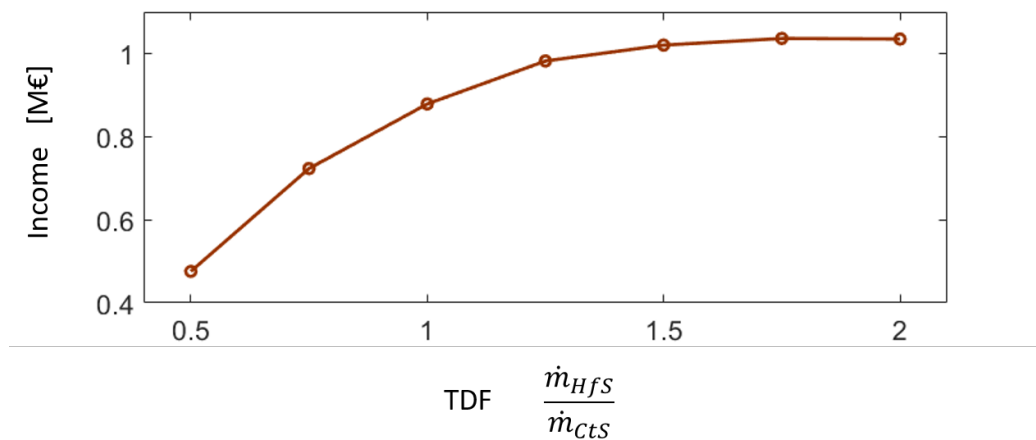
(a) Income against turbine dimension factor.
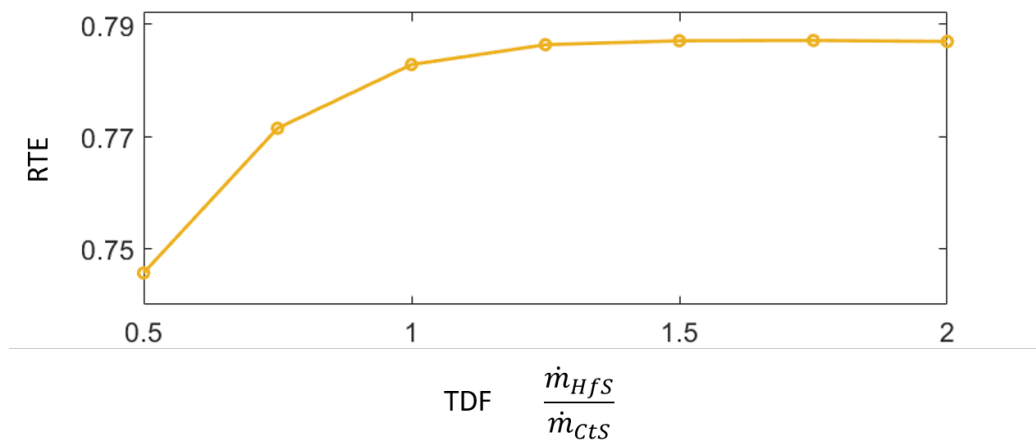
(b) Round trip efficiency against turbine dimension factor

Figure 5.15. Result of annual simulations for UWCAES system sized for 48 hours of nominal charge operation with variable TDF. The plant is managed following arbitrage logic. Referred to case c) of Table 5.7

5.4 Conclusion

From the considered case study the UWCAES system presents promising results. Following peak shaving logic it maintains high RTE values during yearly simulations and depending on the combination of plant size and upper/lower bounds it could also reach good performance in the peak shaving function, meant as σ_P reduction. E.g. for a plant sized on a nominal power of 60 MW and for an upper bound equal to the 55% of the wind park nominal power a round trip efficiency of 78.4% and a standard deviation reduction of 16.8% are obtained with storage tanks able to store energy for 48 hours at nominal charge operation. Variations on the TDF and lower bounds affect performances in a deeper way if infinite capacity of the storage is assumed. Considering storage capacity limited to 48 hours of nominal charge operation increments in RTE of about 1% and in the standard deviation reduction of about the 3% could be obtained with a proper combination of TDF and lower bound. The high RTE values obtained indicate that the stored energy can be completely exploited and the storage is empty at the end of the simulated year. This fact is relevant considering a long period simulation, during which the final state of one year coincides with the initial state of the next. Following an arbitrage management strategy good value of RTE are obtained and an income increment is registered if compared to the wind park without storage. RTE value of 78.3% and an income of 0.88 M€ correspond to the best case obtained with threshold defined on the moving mean of the hourly zonal price and storage capacity of 48h at nominal charge operation. Moreover referring to this last case an increase of both RTE and incomes has been observed for higher TDF values, due to a faster and more effective emptying of the storage. Anyway the proper size of the turbine could be determined only in light of an economic analysis, see chapter 6.

Chapter 6

Economic analysis

To confirm the already spoken hypothesis on the cost an economic analysis has been made. The methodology comes from [22] and [11]. Different aspects have been considered and the cost analysis aims at being an estimation of the economics of the problem and at highlighting the main critical aspects. In the end it will be possible to discuss the influence of some design choices and to compare different solutions.

It is important to highlight that the considered size of the plant is remarkable. As already explained in Chapter 1 the UWCAES is able to provide a wide range of services and one of the main applications is to control the grid. Therefore the earnings regarding the sale of electricity are not the unique scope of the plant and also the quality of the power introduced into the grid could be considered.

The plant is then assumed managed following a peak shaving logic in order to take into account of this useful effect on the grid. Additionally it has been simulated also for arbitraging investigating on the plant behavior and economics.

6.1   Investment cost

The fixed costs related to the plant represent the higher expenditure. No fossil fuel needs be burned and as for what concerns typically renewables, the initial investment requires lots of years to be paid back.

6.1.1   Turbomachinery
It is possible to have an estimation of the overall cost considering some empirical correlations provided by GECOS group. The costs depend on the size of the compressors and of the turbine and on the chosen compression section configuration (e.g. number of parallel trains adopted).

For the axial compressor design the equation from [56] is considered:

$$C_{compressor} = 450\frac{P_{comp}}{\dot{m}^{0.31}} \tag{6.1}$$

It is possible to see that there is a linear correlation between the compressor power P_{comp} expressed in kW and the overall cost $C_{compressor}$ in €. Than it is possible to see that the air mass flow rate ($\dot{m}$ in kg/s) decreases the cost. This is a scale effect. The higher is the power, and the lower will be the relative cost (€/kW): this is due to the fact that exists a fixed cost in the engineering of a new machine that do not depend on the size.

For radial machines another correlation taken from [57] is used:

$$C_{compressor} = 6490 * P_{comp}^{0.62} \tag{6.2}$$

Since they are characterized by lower dimension it is worth to use another function to evaluate the cost. The power will be expressed in British horse power. The scale effect is always present, and it is related to the used exponent.

Finally for the Turbine a relation similar to the one related to axial compressors can be adopted [11]

$$C_{turbine} = 500\frac{P_{turb}}{\dot{m}^{0.363}} \tag{6.3}$$

where P_{turb} are expressed in kW while $\dot{m}$ in kg/s and the cost is found in Euro.

6.1.2   Heat exchanger

Before doing any estimation a brief study on the heat exchangers type and material is necessary. From data provided by GECOS group :

· **air-salt HX**: from data provided by GECOS group specif cost will be near 100 €/kW - shell and tube-inox

· **air-oil HX**: from data provided by GECOS group specif cost will be near 40 €/kW - shell and tube-carboon steel

· **air-water HX**: from data provided [58] specif cost will be near 5 €/kW - shell and tube inox

6.1.3   TES

As already introduced the T.E.S. represents one of the major fraction of the total investment cost. To consider the related expenditures, the case reported in Table 6.1 is considered as reference.

Table 6.1. Main economic features of the T.E.S. [11]

		Molten salt	Thermal oil
Tank cost	€/m^3	350	168
Insulator cost	€/m^3	134	72
Foundation cost	€/m^3	449	250
Fluid costs	€/kg	0.7	2

Tank, insulation and foundation costs are scaled according to:

$$C_{TES} = C_0 \left(\frac{V_{TES}*}{V_0} \right)^{scale\,factor}$$

(6.4)

where scale factor is considered to be equal to 0.7 [59] [60]. The volume of the storage depends on the mass flow rate of heat transfer fluid and on the storage plant sizing expressed as hours of nominal charge operation. The HTF cost instead is considered without any scale factor.

Regarding the water tanks, [61] provides a cost of 500 €/m^3, while the water cost is considered to be negligible.

The extra costs related to pumping systems and electric equipment are assumed to be the 10 % of the total investment [62] [63] [64].

6.1.4 Under water air tank

Due to the novelty of the proposed storage concept, the air tank costs have been guessed starting from the chosen material: considering a submersed concrete structure data for an employable material have been searched in literature [65] [66] [67] The solution which fits more the considered case is the MARINE CONCRETE of [66] which provides a cost of 152 €/ton. The mass of concrete has been already calculated and then the material cost can be evaluated. Engineering, manufacturing and building phases are taken into account assuming them to the 25% of the material cost, reaching a final specific cost of 40 €/m^3.

6.1.5 Piping

From the Chapter 2 the size of the pipeline have been obtained. Considering the diameter and assuming that for marine application stainless steel tubes are typically adopted, it is possible to have an estimation on the cost of about 3 €/m [68]. In the end considering its length, the total cost is found. The material accounts for 15% to 35 % of the overall pipeline expenditure [69]:

therefore it is possible to calculate the overall amount considering the labour, administrative and engineering costs.

6.1.6 Connection to the grid

The cost related to grid connection includes the cable, installation and transportation to the land. Since the distance from the grid is considerable, HVDC cables are used, which adopt continuous current instead of alternate. This is done to avoid the effect of capacitance made by sea bed, causing a shift between current and voltage phases. From data provided by [58], [70], [71] it is possible to estimate that material cost is near 250 €/m, plus 350 €/m for installation and transportation. However given the hypothesis is to couple the UWCAES plant to a wind farm this cost is not differential and it is not considered, it is indeed in charge of the wind farm. Anyway it is necessary to evaluate the alternator and transformer costs connected to the turbine shaft. Starting from the reference value reported in Table 6.2 the cost for the case studied is found as:

$$C = C_0 \left(\frac{P}{P_0} \right)^{scale\,factor} \tag{6.5}$$

with a scale factor of 0.9 [11].

Table 6.2. Reference case quantity for alternator and tranformer [11]

		Alternator	Transformer
Power	MW	80	80
Cost	k€	3000	800

6.1.7 Gearbox

An estimation of the Gearbox cost is provided by[11] which assumes it to be proportional to the transmitted power: 5 M€/MW.

6.1.8 Off shore costs

All the expenditures considered till here are related to on-shore applications. Therefore considering that the pipeline and the concrete vessel are placed at deep water off-shore location, extra costs must be considered. Anchoring system, engineering phase and transportation are assumed to cover the half of the total cost of the structure to be placed off-shore [58] [72].

6.2 Variable costs

Variable costs are related to the management of the plant. The main expenditure is related to insurance, since no fuels are employed and since the value to be paid is proportional (0.5%) to the initial investment which is very high. Staff is assumed to be of 5 people for a total of 100 k€ per year. Operation and maintenance costs are considered equal to 0.5 €/MWh in both charge and discharge phases. Finally the electric energy service cost is considered to be equal to 0.256 €/MWh.

6.3 DCF analysis

For the discount cash flow analysis the following hypothesis have been considered [22]:

· life time of 30 years

· inflation rate at 2%

· Real interest rate 2.357% [73]

· Increase of electricity price during years 0.0%

Referring to year y: the cash flow is calculated as

$$CF_y = incomes_y - investment_y - expenditure_y \qquad (6.6)$$

where *investment* refers to the fixed costs to be sustained only in the first year, while *expenditure* represents the variable costs. The incomes are related to the sale of electricity and calculated as difference between the incomes of the wind park with and without storage integration. Inflation rate (i) modifies the value of the expenditures while the increase of electricity price ($EE_{increment}$) modifies the incomes.

$$expenditures = (O\&M + insurance + EEservice) * (1 - i)^{y-1} \qquad (6.7)$$

$$incomes = EE * (1 + EE_{increment})^{y-1} \qquad (6.8)$$

The actualization factor is provided by [73] and it used to consider the net value of a future economic quantity:

$$DCF_y = \frac{CF_y}{(1+d)^y} \qquad (6.9)$$

where d is the real interest rate; Finally the quantity which it is used to quantify the remuneration of the investment is NPV calculated as:

$$NPV = \sum_{y=0}^{LT} DCF_y \qquad (6.10)$$

Since the plant is characterized by high investment cost and the balance between energy stored and sold is negative(due to the RTE off the plant) it is obvious that some incentives are required to make it profitable. The wind farm alone is then advantaged with respect to the wind farm integrated with the UWCAES, since all what is produced is sold. However this is based on the assumption that the grid is able to manage all the injected energy. In a market characterized by deeper penetration or renewables, sooner or later these type of plant (wind farm) will be charged with penalties related to the fluctuating energy production or obliged to introduce a buffer to control the power supplied to the grid. It is reasonable therefore to think that storage systems would be supported in economical terms. In this analysis the incentives required for having a pay-back-time (PBT) equal to the life time (LT) of the plant have been estimated: this incentives represent the minimum required to make the plant at least profitable. NPV represent the absolute value that is added to the investment at the end of the life time. As can be shown, more sophisticated plant , with higher costs can have higher net present value with respect to easier layouts. However considering the risk of economic loans and the consistent investment required, it is reasonable for the investors to require an adequate internal rate of interest (IRR). This represent the actualization rate that makes the NPV null: the rate of discount that guarantees that the sum discounted cash flow, actualized will be equal to the initial investment. This index penalize the layout that increase costs without appreciable return in profits. also the incentives needed to reach an IRR of 15% have then been calculated.

6.4 Sensitivity Analysis - economic

It is interesting to highlight the effect on the overall costs of the plant design choices. The storage capacity is fixed at of 48 hours of nominal charge phase for both TES and air tank. These costs do not depend on the adopted plant management strategy (peak shaving or arbitrage). The comparison is made fixing the working equivalent hours and not energy stored. Indeed two cases characterized by different compression section configurations will be characterized by two different amount of air stocked, depending on the air rate flowing in the compressors. After that it is interesting to estimate in a

preliminary way the NPV, IRR and incentives required to make the plant sustainable in economical terms. A simplified simulation is then considered: from the case study (Chapter 5) compressors (75MW and 4 parallel trains) are found to work for about 1630 equivalent hours and the same can be said also for turbine. Considering fixed these two quantities it is possible to determine the power produced and the variable costs. A constant electricity price of 41.61 €/MWh is considered, being the average value of the hourly zonal prices along one year.

6.4.1 Tank pressure effect

In Chapter 3 the plant has been designed according the the hypothesis of 80 bar pressure tank. This is a choice, which depends on water depth availability (almost 815 meter are required to generate such pressure) and it has a significant impact on the cost. The major cost voices have been reported in Figure 6.1, as function of the air vessel pressure for the configuration B.2 (one intercooler, two shafts). To reach higher pressures, grater specific work is required by the compressors. Since the air mass flow rate is determined by the absorbed power over the specific work, the higher is the pressure the lower is the air flow rate. Turbo-machines are the only components which increase their cost, given a scale effect of the mass flow rate less relevant on the total cost. Compressors and turbine result in being smaller (lower section) but have to provide higher work. Air tank costs decrease strongly: having sized the storage for 48h of continuous charge at nominal load, the lower is the nominal air mass flow rate the lower is the mass of stored air. It is possible to verify that T.E.S. costs, which represent more than 50 % of the overall investment, decrease together with the tank pressure: this is due to the lower mass flow rate to be cooled, which implies a lower required mass flow rate of heat transfer fluids. Also the transferred thermal power decreases, reducing the cost of the T.E.S. HXs: however to maintain same the COT, intercoolers have to dissipate higher amount of thermal power. In the end the sum of HXs cost remains more or less the same. Piping costs increase: the angle of the seabed is kept constant and therefore increasing the depth, the length of the piping increases as well. However the incidence of this costs is less than 1 % and thus they are not particularly relevant on the total. Round trip efficiency, overall investment and economic parameter are reported in Table 6.3 for different tank pressures: the investment are valid under the hypothesis of sizing time equal to 48 hours , which means different level of energy stored. Incentives and RTE are reported normalized to the case at 80 bar.

Higher pressure solutions require a smaller invested capital since T.E.S and air tank are cheaper. Looking to low pressure cases, (discarding the case at 40 bar, for which configuration without intercooler is preferable, since

Figure 6.1. Trend of the the major cost as function of the air tank pressure for configuration B.2, 75MW, 4 parallel trains of compression:
C turbo represent turbomachinery costs; C off shore the cost related to air tank and piping installation; C air the cost of air tank; C HX the cost of heat exchanger; C TES the cost of thermal storage; C salt,oil, and water the single cost of the element which compose T.E.S.

Table 6.3. Economic parameter as function of tank pressure: NPV , incentives required to have PBT=LT ($incentives\,PBT_i$) and incentives for having an IRR = 15% ($incentives\,IRR_i$) are referred to case at 80 bar

p_{tank}	RTE	TIT	I_0	$\frac{NPV_i}{NPV_{80bar}}$	$\frac{incentives\,PBT_i}{incentives\,PBT_{80bar}}$	$\frac{incentives\,IRR_i}{incentives\,IRR_{80bar}}$
[bar]	[-]	[°C]	[M€]	[-]	[-]	[-]
40	0.797	547	98.3	1.63	1.63	1.31
60	0.811	575	82.6	1.11	1.09	1.04
80	0.798	575	77.9	1.00	1.00	1.00
100	0.798	575	73.9	0.88	0.88	0.94
120	0.758	575	71.2	0.86	0.88	0.93
140	0.759	575	69.7	0.85	0.90	0.93

COT is not enough to maximize TIT) the NPV is higher with respect to 80 bar case: however any case presents a negative NPV, meaning that low depth solutions are penalized. The same can be seen looking at the required incentives to reach the target of null NPV at the end of the lifetime and incentives required to reach IRR of 0.15. In the end the lower investment for deep UW solutions wins against the reduction in RTE, mostly due the truncation of the expansion phase at a TOT of $ang5C$, considered to avoid freezing phenomena on the turbine blades. Indeed the reduction of investment cost is higher than the incomes reduction related to lower efficiency.

6.4.2 Configuration of the plant (#shaft #intercooler) effect

The following analysis is focused on the economic impact of the adopted compression section layout. In particular the influence of the number of intercoolers and of shafts have been investigated. The calculations referred to the case at 80 bar denote interesting results, reported in Figure 6.2, where the notation which identifies the different configurations is the same used in Figure 3.8. As can be easily predicted, higher complexity requires higher investment. A solution without intercooling results in being the cheaper while the more intercooles or shafts are adopted the higher is the initial cost. It is possible to see that the investment and RTE trends coincide. The costs change in the following way:

- Turbomachinery costs depend on the size (in terms of MW) and on the mass flow rate: intercooling decreases the work required by the compression, causing an increase in air flow rate but the machine cost results in being reduced, given the scale effect on the air flow rate. On the other hand, higher round trip efficiency means bigger turbine characterized by higher costs. In the end overall turbo machines costs do not vary significantly.

- Air tank costs are directly linked to air mass flow, because the storage has a capacity of 48 hours at nominal charge operation. They are higher for intercooled solution due to lower compression work, as explained in the previous point.

- Thermal fluids required to recover the compression heat are demonstrated to be proportional to air mass flow rate (Equation 3.10). Not intercooled solutions require less fluids and in addition the sea water aftercooler is not present since pinch point is higher than 80 °C, having then a T.E.S. composed just of salts and oil units. This is the main cause in the huge difference between cooled (B,C) and not cooled (A) solution.
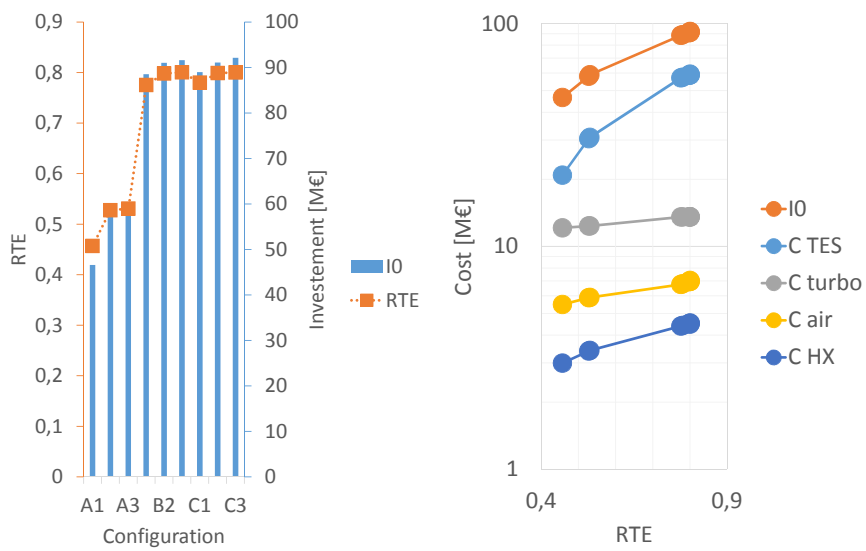
Figure 6.2. Analysis on case with 80 bar tank, 75 MW power, 4 parallel trains of compression. On the left the relationship between investment cost and round trip efficiency is reported. On the right an overview of the major costs for any configuration.

· Temperature differences between inlet and outlet of thermal fluid are fixed. Therefore the heat transferred (which determines the cost) is proportional to mass flow of each thermal fluid: HX costs follows T.E.S and Air storage costs. The only difference is the addition of the costs of the intercoolers, which is in any case much lower with respect to the cost of salt and oil HX.

· Other costs take into account piping, which does not vary, connection to grid, which depends on turbine power (both alternator and transformers are proportional to electrical power produced), gearbox, which depends only on the number of adopted shafts and off shore related costs, which depend on piping and air storage costs.

In the end the incidence of the turbomachines on the total decreases as the complexity increases and the reduction of its fraction on overall investment is related to the big increase of storage costs (air+T.E.S+HX).

The share of overall costs can be seen in Figure 6.3. T.E.S costs is predominant, almost half of total investment. This is due to the high quantity of thermal fluid required and the high cost of the storage in terms of foundation, fabrication and insulation. Oil is predominant because of its low density (require big volumes) and its higher costs. Round trip efficiency, overall

(a) TES cost share (b) Overall costs share
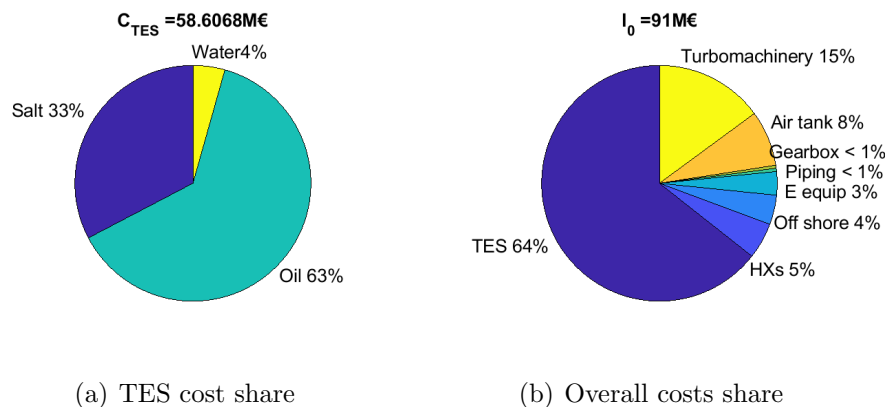
Figure 6.3. Share of total investment cost for configuration B2, 75MW, 4 parallel trains of compression, 80 bar air vessel pressure

investment and economic parameter are reported in Table 6.4: the investment are valid under the hypothesis of storage sized for 48 hours at nominal charge operation, which means different level of energy stored. Incentives and RTE are reported normalized to case B2. It is interesting to see that

Table 6.4. Economic parameter for different configuration of the plant: NPV , incentives required to have PBT=LT (*incentives PBT_i*) and incentives for having an IRR = 15% (*incentives IRR_i*) are referred to case B.2

Configuration	RTE	TIT	I_0	$\frac{NPV_i}{NPV_{B2}}$	$\frac{incentives\,PBT_i}{incentives\,PBT_{B2}}$	$\frac{incentives\,IRR_i}{incentives\,IRR_{B2}}$
[−]	[-]	°C	M€	[-]	[-]	[-]
A.1	0.457	409	45.5	0.94	1.61	1.09
A.2	0.528	443	53.2	0.97	1.46	1.08
A.3	0.531	446	53.9	0.98	1.48	1.09
B.1	0.775	575	76.0	1.00	1.03	1.01
B.2	0.798	575	77.9	1.00	1.00	1.00
B.3	0.801	575	78.5	1.01	1.01	1.00
C.1	0.780	575	76.3	1.00	1.02	1.00
C.2	0.799	575	78.0	1.00	1.00	1.00
C.3	0.800	575	78.9	1.02	1.02	1.01

simpler schemes (A configurations) characterized by much lower investment are not penalized by the low efficiency. NPV (negative for all configuration) is smaller compared to case B.2. However looking to incentives required, these solution are penalized by very low RTE. Intercooled solution instead are almost comparable in terms of costs, NPV and incentives required. B.2 solution has been demonstrated to be effective and not penalized with respect to other, more complex layout.

6.4.3 Maximum molten salt temperature effect
Aiming at decreasing the costs and maximizing the profit, the T.E.S. maximum temperature effects have been examined. For a compression section B.2 with 75 MW nominal power, the study of maximum temperature of the storage on total cost is reported in Figure 6.4 In order to maximize the TIT and to keep charge and discharge phases balanced, the COT is considered equal to the maximum HTF temperature plus the nominal pinch point. Lower COT solutions imply higher duty of the intercooler and then the overall compression work decreases. As already seen this causes higher mass flow rate of air and leads to higher storage cost (air+T.E.S.). Compressor cost benefits of the higher mass flow rate, exploiting their scale effect; expansion in turbine
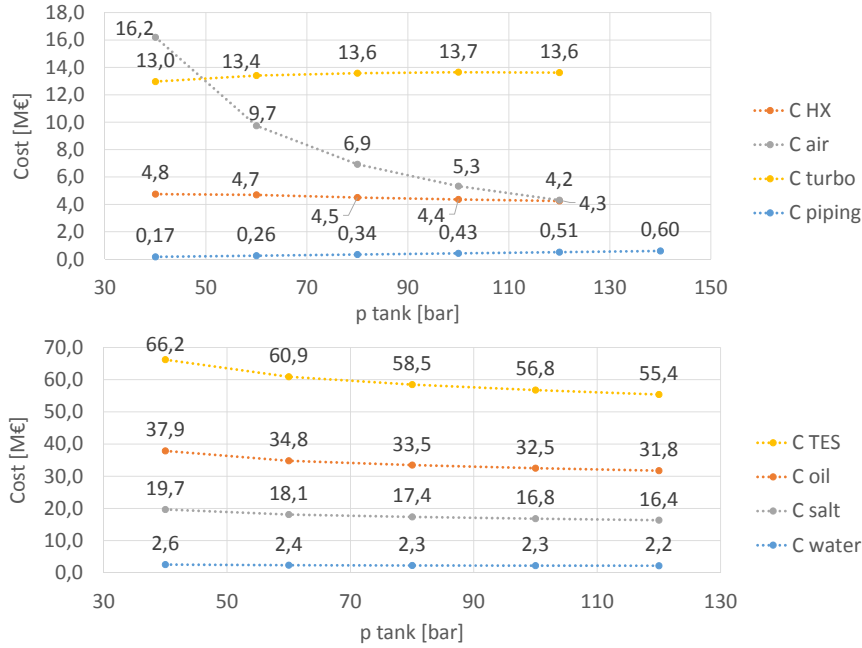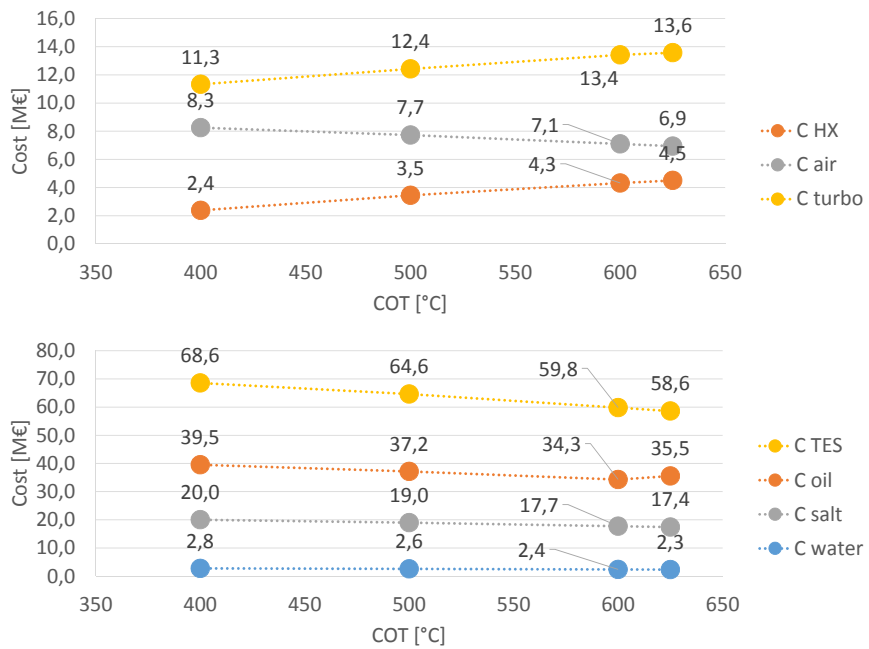
Figure 6.4. Trend of the the major cost as function of maximum storage temperature for configuration B.2, 75MW, 4 parallel trains of compression.

starts from a lower TIT. The exergy content of the air is then lower and the power converted by the turbine decreases, as well as its cost. Molten salt heat exchanger costs decreases because in this case maximum temperature is changing. The lower is the COT, the lower is the heat exchanged with salt and so is the HX cost. Duty of the intercooler is higher but since water HX have lower cost, the sum of all heat exchanger costs makes lower temperature solution cheaper. Economic parameter and overall investment are reported in Table 6.5). Efficiency decreases because expansion starts from

Table 6.5. Economic parameter as function of COT:NPV , incentives required to have PBT=LT (*incentives PBT_i*) and incentives for having an IRR = 15% (*incentives IRR_i*) are referred to case at 625°C

COT	RTE	TIT	I_0	$\frac{NPV_i}{NPV_{625}}$	$\frac{incentives\,PBT_i}{incentives\,PBT_{625}}$	$\frac{incentives\,IRR_i}{incentives\,IRR_{625}}$
°C]	[-]	[°C]	[M€]	[-]	[-]	[-]
625	0.798	575	77.9	1.00	1.00	1.00
550	0.750	550	79.8	1.18	1.27	1.11
475	0.669	450.25	81.3	1.45	1.73	1.31
400	0.570	350.4	81.6	1.73	2.43	1.60

lower temperature and it has to be truncated to avoid icing. The sum of higher cost and lower RTE highlight the strong influence of thermal storage limit. The higher is the temperature achievable and the lower will be the cost of the plant and incentives required.

6.4.4 Oil temperature limited solution (with and without reheating)

Looking for future developments of the plant devoted to a decrease in the investment, a new configuration is investigated. Since the major cost is related to T.E.S., it is interesting to asses if removing salt storage the plant results in being more profitable. This solution aims at increasing the compressor efficiency, adding a more consistent intercooling phase to decrease the COT. This have strong implications in RTE which decreases a lot, since TIT drops to 300 °C and therefore expansion must be stopped for limitation in minimum TOT. Solutions without reheating follow the traditional scheme, the only difference is the absence of salt TES. To obtain high efficiency number of intercooler has been increased from 2 to 4 and differences in costs are

calculated. Instead solution with re-heater (RH) is assumed to use the heat removed by the intercooler to heat up air spilled from intermediate stage of turbine (Figure 6.5) . Energy is assumed to be stored into into the sea water unit of the TES (which is the least expensive). The main differences of
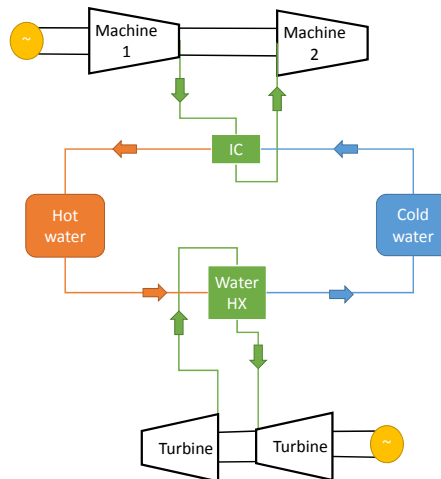
Figure 6.5. layout of extra TES required in re heated configuration: heat is removed from intercooling phase to heat up spilled air from turbine.

costs are reported in Figure 6.6 with the case B.2 reported as reference. The solutions without solar salt recovery unit are characterized by much lower temperature and thus by stronger intercooling duty. The main cause is the decrease in the required compression work and higher mass flow of air, if fixed absorbed power is considered. Air tank costs increase, since the nominal air flow rate is higher and the storage is sized for 48 hours at nominal charge operation. Turbomachinery costs decreases thanks to higher mass flow rate, which is accounted as scale effect on the cost. Lower round trip efficiency (related to start the expansion from lower temperature, and the truncation for icing) lead to lower power of the turbine and thus lower cost. To cool down air stream higher flow rate of thermal fluid in *CtS* phase are required as well as the water needed for intercooling. Compared to case B.2 the cost of oil and water T.E.S increases, however avoiding solar salt usage the overall cost of the apparatus is lower. Reheated solutions instead require to store water used for intercooling and therefore the amount of water that has to be stored is massive. This effect nullify the benefit of the salt storage removal.
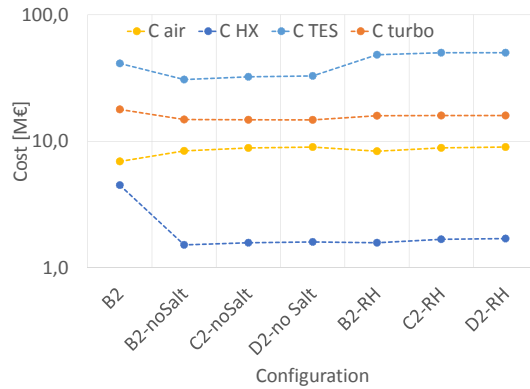
Figure 6.6. Main voice of investment costs for the case without salt configuration, with and without RH, compared to the case B.2 (80 bar, 75MW, 4 parallel trains of compression). Configuration C is made by 3 intercoolers while configuration D is made by 4 intercoolers.

Heat exchanger cost drops even if the thermal power exchanged in the oil, water, and intercooling units. This happens because of the high specific cost of solar salts HX, which is not adopted.

Overall results are shown in Table 6.6: it is possible to see that a clear advantage on the overall costs is not achieved. For non reheated solution the effect of the reduction in round trip efficiency wins against the advantage in lower cost. This can be seen by higher investment needed to reach same target of configuration B.2. Reheated solution instead requires almost the same investment of configuration B.2 without any advantage in RTE. This is due to the high cost of thermal oil and the need of having very big storage of water for the intercooling phase.

6.5 Results

To complete the analysis considered in chapter 5 the same cases have been investigated under an economical point of view. The considered cost and incomes are differential to the reference case of wind farm operated without the UWCAES integration. The UWCAES and wind farm have been located off-shore the South-West Sardinia. The cement air tanks are positioned on the sea bed at 815 m depth, reaching a storage pressure of 80 bar. The wind data of the considered location have been provided by the Spanish harbour weather forecast company Puertos [27]. The used electric energy zonal prices instead have been found in [28].

Table 6.6. Economic parameter for different configuration of the plant: NPV , incentives required to have PBT=LT (*incentives PBT$_i$*) and incentives for having an IRR = 15% (*incentives IRR$_i$*) are referred to case B.2

Configuration [−]	RTE [-]	I$_0$ M€	$\frac{NPV_i}{NPV_{B2}}$ [-]	$\frac{incentives\,PBT_i}{incentives\,PBT_{B2}}$ [-]	$\frac{incentives\,IRR_i}{incentives\,IRR_{B2}}$ [-]
B.2	0.80	77.92	1.00	1.00	1.00
B.2-noSalt	0.50	62.74	1.33	2.11	1.38
C.2-noSalt	0.53	65.08	1.33	1.99	1.35
D.2-noSalt	0.54	65.87	1.33	1.96	1.34
B.2-RH	0.67	81.92	1.48	1.78	1.33
C.2-RH	0.72	84.83	1.42	1.58	1.26
D.2-RH	0.73	85.13	1.40	1.53	1.24

6.5.1 Peak shaving

The case study related to UWCAES coupled to a 135 MW off-shore wind farm is considered in this section. The plant is operated by a peak shaving strategy with the aim of flattering the energy grid injections to a desired value, imposed by the definition of an upper threshold. This bound ,ub, is defined as a percentage value of the nominal power of the wind park. The reference case is the wind park without storage integration and it is considered to have a power outcome curtailed by the upper thresholds, considering then a grid which do not receive energy peaks and they would be dissipated. This is done in order to take into account of the positive effect that the storage has on the grid injections.

The UWCAES performance parameters are sensitive to the activation thresholds and nominal compression power choices. Those aspect is also reflected on the economics of the plant. In Figure 6.7 it can be individuated the total investment cost plotted against the nominal power of the compression section for UWCAES sized for 48 hours of nominal charge operation. The total investment increases together with the compressor size to which the size of the other plant components is related, e.g. higher compressor nominal power means higher nominal power of the turbine. An example of investment cost composition is reported in Figure 6.8, but in any case the T.E.S. covers the higher fraction of it, given the consistent quantities of HTF required. This preliminary analysis is conduced for a time span correspondent to the
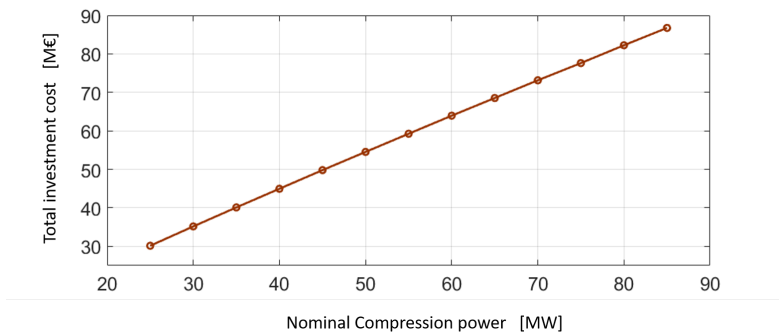
Figure 6.7. Total investment cost as function of the compression nominal power, of UWCAES sized on 48 hour for nominal charge operation.

(a) Investement cost fractions

(b) T.E.S. investement costs
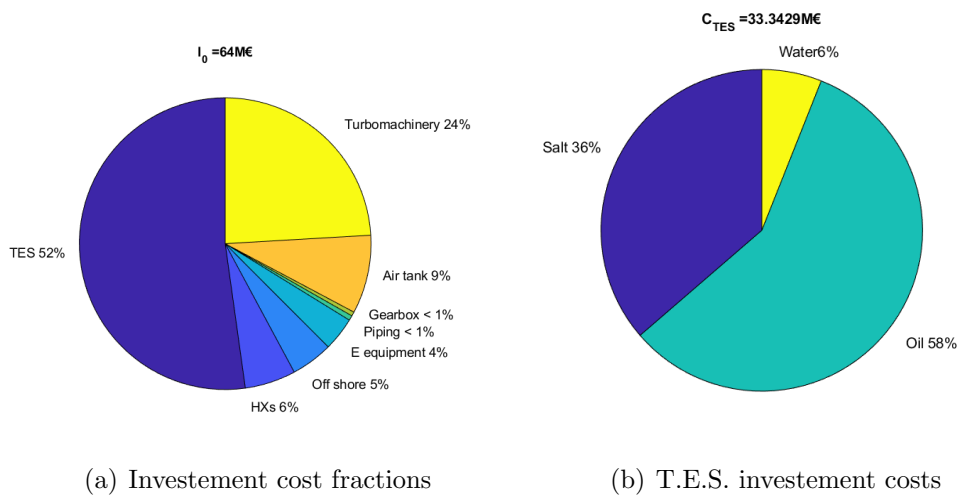
Figure 6.8. Investement cost fraction rapresentation for UWCAES with $P_{nom,c}$ =60MW, TDF=1 and storages sized for 48 hours of nominal charge operation.

life time of the plant assumed to be of 30 years. It is referred to plant with storage tanks sized for 48 hours of nominal charge operation and for a turbine activation threshold, lb, equal to the compression one,ub. The resulting NPV values are plotted in Figure 6.9 as function of the upper threshold and P_C, nom combinations and the highlighted points correspond to:

a) $P_{nom,c} = 75$ MW, ub= 45%;

b) $P_{nom,c} = 60$ MW, ub= 55%;

c) $P_{nom,c} = 35$ MW, ub= 45%;
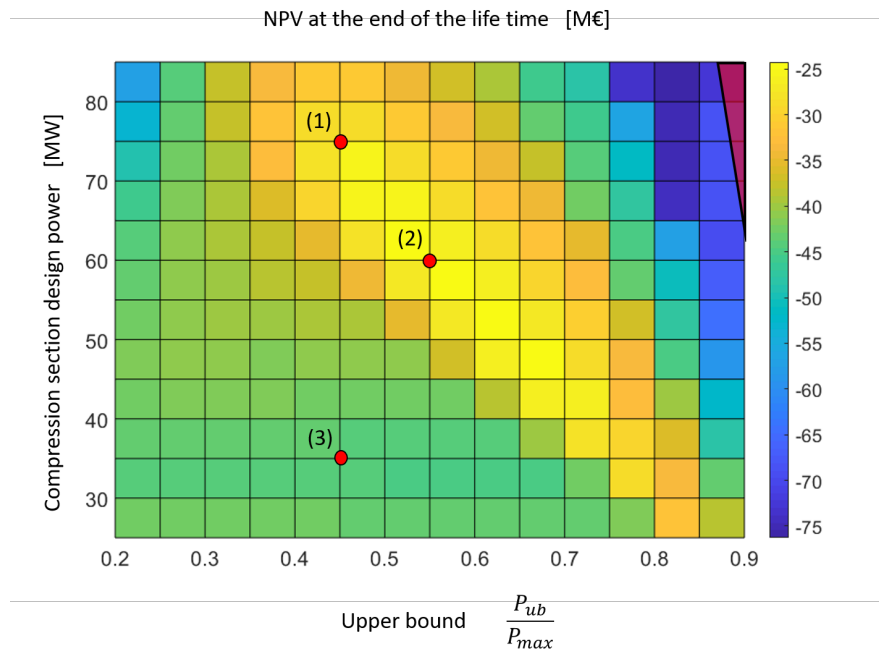
Figure 6.9. NPV as function of nominal power of the compression section and upper bound. The considered plant is coupled to 135MW wind farm and operated following peak shaving logic. The storage is sized for 48 hours at nominal charge operation. The red triangle on top right side represents not possible solutions for which the power that the compressors should absorb is always lower than the minimum activation power.

Similarly to the RTE, the NPV results to have an optimum trend for combinations of $P_{nom,c}$ and ub corresponding to compression sections sized to exploit the 100% of the wind farm capacity. RTE efficiency is indeed an indicator of how efficiently the plant is operated and it can be directly related

to the incomes. Although in any case the NPV results to be negative having incomes not sufficient to beak even neither at the end of the LT. A chance to solve this issue is to consider incentives on the sold energy. These incentives have been expressed as an extra-price of the electric energy price paid to each MWh produced by the turbine of the UWCAES system:

$$EEprice = zonalprice + incentive[€/MWh]$$

They have been evaluated at first as the minimum incentive required to reach null NPV at the end of the LT and secondly to reach an IRR of 15%. In Table 6.7 the economic results are listed for the cases a), b) and c).+

Finally it is interesting to consider the same cases but confronted to a reference wind park able to sell all the produced energy. The resulting NPV and incentives are tabled in 6.8.

Table 6.7. Economic results obtained for UWCAES operated for 30 years following a peak shaving management strategy. The plant is sized for 48 hours of nominal charge operation. Case a) refers to $P_{nom,c}$ = 75 MW, ub= 45%; case b) refers to $P_{nom,c}$ = 60 MW, ub= 55%; case c) refers to $P_{nom,c}$ = 35 MW, ub= 45%. The reported results are related to a reference wind park without storage and with output power curtailed if above the upper threshold.

Case	NPV without incentives [M€]	Incentive $(NPV = 0)$ [€/MWh]	Incentive $(IRR = 15\%)$ [€/MWh]
a)	-28.65	20.65	144.0
b)	-25.95	22.39	143.3
c)	-44.26	68.85	248.5

6.5.2 Arbitrage

Referring to Chapter 5 the UWCAES is now supposed to be coupled with a 68 MW wind farm and operated by an arbitrage strategy. The compression and expansion activation thresholds of the storage plant are here defined as function of the electric energy zonal price profile:

· charging: zonal price < average price *(1−lb)

· discharging: zonal price > average price *(1+ub)

Table 6.8. Economic results obtained for UWCAES operated for 30 years following a peak shaving management strategy. The plant is sized for 48 hours of nominal charge operation. Case a) refers to $P_{nom,c}$ = 75 MW, ub= 45%; case b) refers to $P_{nom,c}$ = 60 MW, ub= 55%; case c) refers to $P_{nom,c}$ = 35 MW, ub= 45%. The reported results are related to a reference wind park without storage which sells all the produced energy.

Case	NPV without incentives [M€]	Incentive ($NPV = 0$) [€/MWh]	Incentive ($IRR = 15\%$) [€/MWh]
a)	-207.6	104.4	227.7
b)	-164.9	99.31	220.2
c)	-217	309.5	489.1

The incomes are in this case considered as the difference between the incomes of the wind park with and without storage integration. The wind park alone is supposed to inject to the grid and then to sell all the produced energy. The UWCAES with a compression section nominal power of 60MW and sized to work at nominal charging condition for 48 hours is considered. The correspondent investment cost composition can be seen in Figure 6.8. The optimal upper and lower bounds, in terms of maximum income, are already defined in Chapter 5 and they do not affect the investment cost but just the annual energy produced and then the annual revenues. In Table 6.9 the economic results are reported for reference cases elected in Chapter 5:

b) $P_{C,nom} = 60MW$, $P_{T,nom} = 48MW$ and $ub = 30$, $lb = -10$ defined on average EEprice evaluated by integral mean along the year.

c) $P_{C,nom} = 60MW$, $P_{T,nom} = 48MW$ and $ub = 20$, $lb = 10$ defined on average EEprice evaluated by moving mean with a monthly time span.

The resulting NPV is negative in both the considered cases and then the chance of receiving incentives is taken into account. These incentive have been expressed as an extra-price of the electric energy price paid to each MWh produced by the turbine of the UWCAES system:

$$EEprice = zonalprice + incentive[€/MWh]$$

And they have been evaluated at first has the minimum extra-price required to reach null NPV at the end of the LT and secondly to reach an IRR of

Table 6.9. Economic results obtained for UWCAES operated for 30 years following arbitrage management strategy. The plant is sized for 48 hours of nominal charge operation. Case b) refers to $P_{C,nom} = 60MW$, $P_{T,nom} = 48MW$ and $ub = 30$, $lb = -10$ defined on average EEprice evaluated by integral mean along the year. case c) refers to $P_{C,nom} = 60MW$, $P_{T,nom} = 48MW$ and $ub = 30$, $lb = -10$ defined on average EEprice evaluated by moving mean with a monthly time span. . The reported results are related to a reference wind park without storage which sells all the produced energy.

Case	NPV without incentives [M€]	Incentive $(NPV = 0)$ [€/MWh]	Incentive $(IRR = 15\%)$ [€/MWh]
b)	-90.92	141.1	447.7
c)	-83.93	84.99	283.9

15%. The turbine size is then varied analyzing how it affects the economics of the plant. The considered case is:

c) $P_{C,nom} = 60MW$, $P_{T,nom} = 48MW$ and $ub = 20$, $lb = 10$ defined on average EEprice evaluated by moving mean with a monthly time span.

In Figure 6.10 the TDF effect on the total investment cost and on the annual incomes of the plant can be visualized. The combination of these two trends gives the resulting required incentives reported in the same figure.

6.5.3   Number of parallel trains - Economics relations
In Chapter 4 the effects of compression sections composed by different number of parallel trains have been studied. At this point it possible to verify how these different configurations affect not only the technical parameters, but also the behavior of the plant during a life time simulation and then the economic performances. Choosing to integrate to the 135 MW wind farm an UWCAES with the characteristics reported in Table 6.10. The number of parallel trains is made vary obtaining the results reported in figure 6.11. The total investment cost increases together with the number of trains but at the same time also performances are higher in terms of RTE. Confronting the related required incentives it could be distinguished a clear advantage in adopting 3 or 4 trains instead of 2 or 1. The choice between 3 or 4 instead is a technical economic trade-off. Increasing the number of trains to more than 4 would lead to investment cost higher and higher with not relevant performances increase.
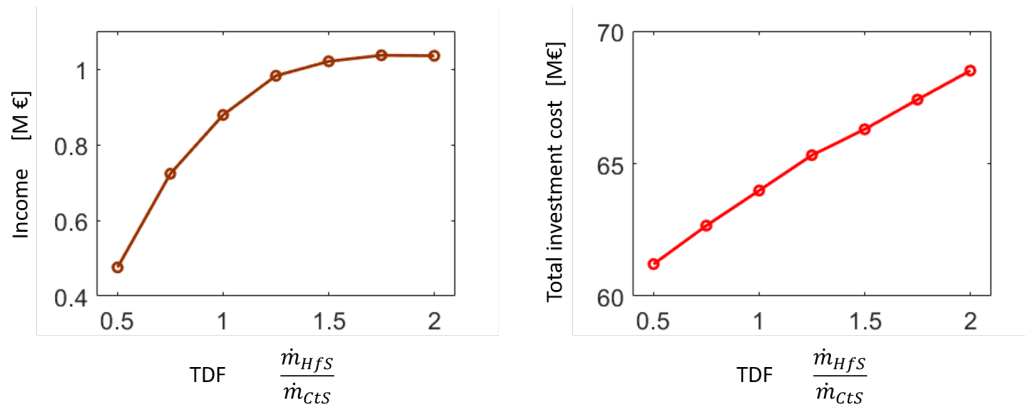
(a) On the left: Annual income against TDF. On the right: total investment cost agains TDF.
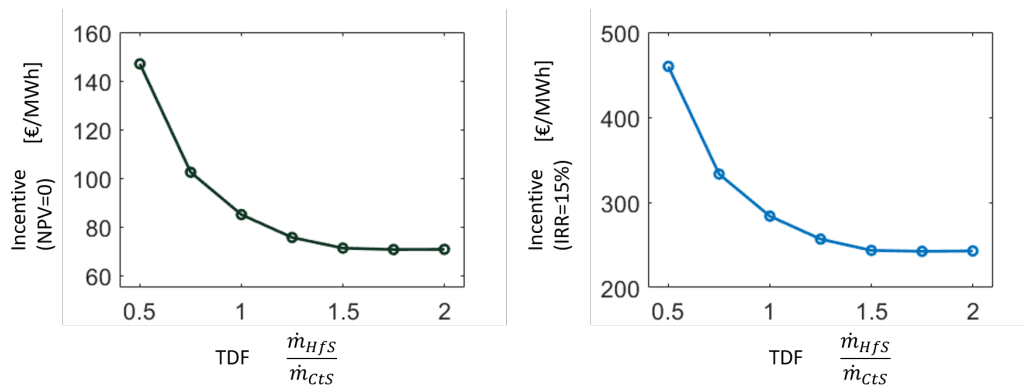
(b) On the left: incentives required to break even at the end of the plant life time against TDF. On the right: Incentive required to have IRR of 15% against TDF.

Figure 6.10. TDF effects on incomes, investment cost and required incentives for UWCAES operated by arbitrage strategy and with $P_{nom,c}$ =60MW and storages sized for 48 hours of nominal charge operation.

Table 6.10. UWCAES characteristics when coupled to a 135 MW wind farm for peak shaving.

Compression nominal power	MW	60
TDF	[-]	1
Storage sizing	hours	48h of nominal charge operation
Management strategy		Peak shaving
upper bound	%	55% of wind farm nominal power
lower bound	%	55% of wind farm nominal power

131

Afterwards the arbitrage logic is considered, the plant is then coupled to a 68MW wind farm and it is characterized by parameters reported in Table 6.11. The obtained economic results are reported in Figure 6.12. In this case the

Table 6.11. UWCAES characteristics when coupled to a 68MW wind farm for arbitraging.

Compression nominal power	MW	60
TDF	[-]	1
Storage sizing	hours	48h of nominal charge operation
Management strategy		Arbitrage
upper bound	%	$(1 + 20\%)*$ moving mean of EEprice
lower bound	%	$(1 - 10\%)$ moving mean of EEprice

increasing the number of trains up to four is economically convenient. This is due to the fact that operating the plant for arbitraging the compression section is most of the time at part load conditions. Referring to Chapter 5, Tables 5.4 and 5.7 it can be seen that the difference between actual and equivalent compression hours is lower for the peak shaving case.

6.6   Conclusion

A brief summary on all the voices which affect investment for the realization of the plant has been made. The main expenditure is related to the cost of thermal storage, which account more than 50 % in the selected cases B.2.

Starting from a reference case which adopt 4 parallel trains, 75MW power, and 1630 equivalent hours for both compressor and turbine, sensitivity analysis were made on the design choices. Storage are assumed to be sized for 48h of continuos chargin phase at nominal power of the compressor.

Investment costs are found to be strictly connected to the choice of air vessel pressure: deeper UW-storage guarantee lower investment, but plant efficiency. In the end they result to be more attractive since requires lower incentives to reach break even point and to reach an IRR = 0.15.

Then the initial choice of the use of B.2 configuration is analysed and investment and economic parameter are calculated for each case from zero to two intercooler and from one to three shaft. Simplier solution (A) enable to reduce the investment, but the lower RTE penalize the plant incomes, and in
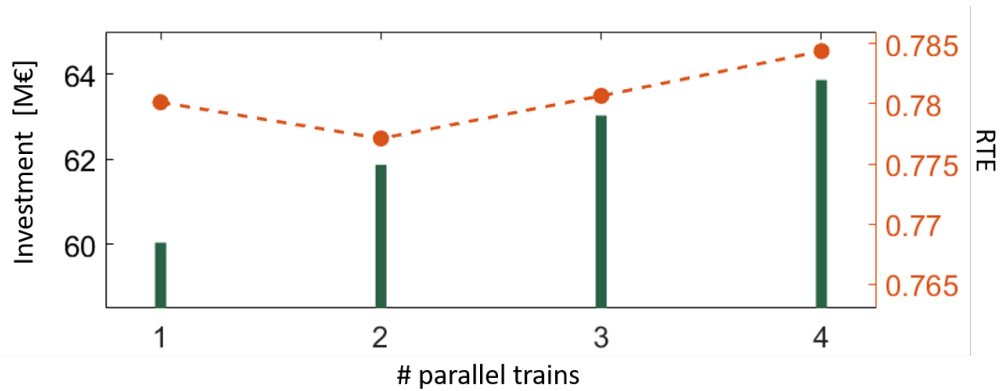
(a) Left y-axis represents the total investment cost, the right y-axis instead represents the Round trip efficiency. Both the y-axis are plotted as function of the number of parallel trains adopted in the compression section.
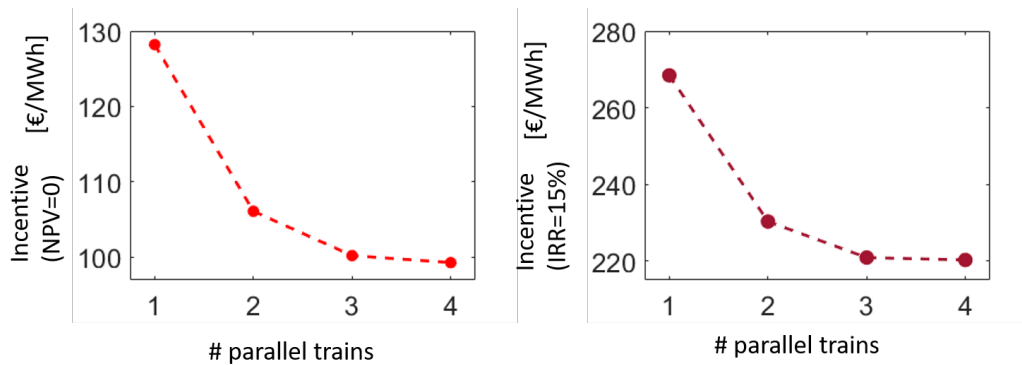
(b) On the left the required incentives to break even at the end of the LT against the number of parallel trains adopted in the compression section. On the right the required incentives to reach IRR equal to 15% against the number of parallel trains adopted in the compression section.

Figure 6.11. Life time economic simulation results for compression section composed by different number of parallel trains. The storage plant is coupled to 135MW wind farm and sized for 48h of nominal charge operation and managed by peak shaving strategy.
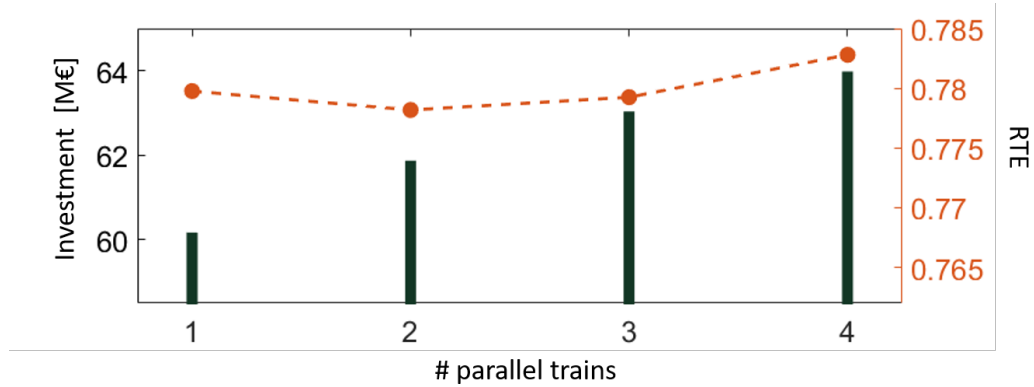
(a) Left y-axis represents the total investment cost, the right y-axis instead represents the Round trip efficiency. Both the y-axis are plotted as function of the number of parallel trains adopted in the compression section.
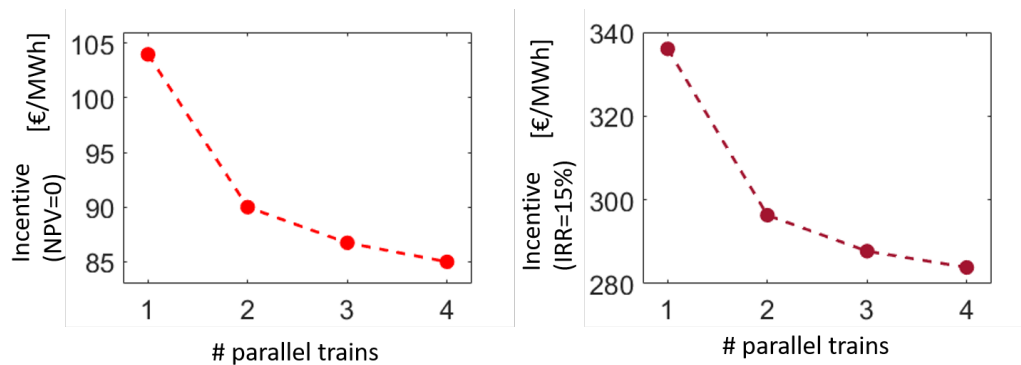
(b) On the left the required incentives to break even at the end of the LT against the number of parallel trains adopted in the compression section. On the right the required incentives to reach IRR equal to 15% against the number of parallel trains adopted in the compression section.

Figure 6.12. Life time economic simulation results for compression section composed by different number of parallel trains. The storage plant is coupled to 68MW wind farm and sized for 48h of nominal charge operation and managed by arbitrage strategy.

the end requires higher incentives to reach target of payback time and IRR. Instead multiple shaft configuration with one or two intercooler show similar results, justifying the adoption of configuration B.2 as a good compromise between easiness of layout and economic impact on the plant.

Analysis on maximum thermal storage temperature shows the need of reaching high temperature to decrease the cost and increase incomes. Higher temperature increase the work required for compression and reduces the air that have to be cooled and stocked. This result into lower dimension of storage apparatus (thermal+air+HX). Therefore future development in high temperature thermal fluid will enhance the performance of the plant as well as its economic feasibility.

Afterwards the plant economics have been investigated following two different management strategies: *peak shaving* and *arbitraging*. The first logic resulted in being more effective under an economical point view, if the positive effect of controlling the grid energy injection is considered. This means that the reference case of wind park without storage is considered with an energy output curtailed above the upper threshold assuming that the grid is not able to manage energy fluctuations related to the wind availability. The net present value has been evaluated, assuming a plant life of 30 years. Although not even the best configuration provided incomes sufficient to reach the break-even point at any time of the examined period. Regarding the arbitraging strategy the incomes are still not sufficient to pay the fixed and variable cost, resulting in negative NPV. This fact is related to the high investment costs, which major fraction is given by the T.E.S.. The chance of receiving incentives becomes fundamental to make the plant sustainable or competitive under an economical point of view. These incentives have been calculated as the minimum extra price paid for each MWh produced by the UWCAES turbine to reach null NPV at the end of the LT and then to reach IRR equal to 15%. Comparing the two management strategies it can be seen the arbitraging logic is more remunerative if compared to peak shaving without considering the positive effect on the grid injection, meaning that the incomes are calculated as the difference between the wind park with storage and wind park without storage which could sell all the produced energy. Otherwise if the quality of the grid injections is taken into account the peak shaving logic implies lower needed incentives. In a market characterized by a deeper penetration of renewables, sooner or later R.E.S power plants (e.g. wind farm) will be charged with penalties related to the fluctuating energy production or obliged to introduce a buffer to control the power supplied to the grid. It is therefore reasonable to think that storage systems would be supported in economical terms.

Finally the effects of compression sections composed by different number

of parallel trains have been examined for both the management strategies. An increase in the technical economic performances has been found passing from one up to four parallel trains. This positive effects are more marked if the plant is operated for arbitraging since this kind of management implies compressors working at part load condition for more hours per year if compared to the peak shaving case.

Chapter 7

Conclusion

With the penetration of renewable energy in electricity market, energy storage
system becomes attractive for providing grid support. Unpredictable pro-
duction up to now is balance by traditional plant, obliged to work at partial
load, to be prone to accomplish lack or over production. In this scenario
the UW-CAES system is able to provide a high density storage, comparable
with pumped hydro technology. Preliminary design of all the plant has been
provided in this work. The influence of the use of the intercoolers is carefully
investigated highlighting its fundamental role for obtaining high value of
round trip efficiency (RTE) (from 75 to 80 %). This result is obtained by
means of the control the compressor outlet temperature (COT), to reach
maximum allowed temperature before turbine inlet. The use of multiple shaft
lead to small increase of efficiency, and therefore for sophistication-economical-
efficiency trade off the solution with just two shaft and one intercooler has
been chosen for off design and economic evaluation. Thermal energy storage
(T.E.S.) and heat exchanger (HX) are designed according to charging phase
(CtS), keeping fixed temperature difference between air and heat transfer
fluid (equal to 25°C for the intercooled solution). Maximum molten salt
temperature is kept at 600°C demonstrating to be the more efficient and
more economic solution. Considering large scale of the problem (compressor
of tens MW nominal power) scale effect are assumed to be negligible, with
the result that the compressors design can be simply scaled, in similitude,
maintaining same performace for different number of parallel trains or dif-
ferent power of the plant. Pressure of the air tank is a key strategic design
choice since it influences costs, storable power and efficiency. The deeper is
positioned the air storage the lower would be the investment cost as well
as the RTE. A technical-economical trade-off must be considered, together
with the deep-water location availability. In this thesis a focus on 80 bar
air vessel has been considered. The design of the plant has the aim to be
just a preliminary assessment, and therefore some issues on feasibility of

machine are highlighted at the end of the work. Type of stage and their configuration have been obtained through the use of Baljé map, modified to be consistent with modern performance of compressors. A specific design once that type of machine, compression ratio and mass flow rate, obtained throw the methodology adopted, should be done to have more reliable performance of compressors.

After the compression section has been designed the part load behavior of the plant has been investigated. The main issue in the off design operation is found to be related to the compressor operational range. Indeed the peculiar conditions at which the compressors are subjected hinder their flexibility: the outlet pressure is kept nearly constant for all the power inputs and it is imposed by the hydro-static load since the air tank is positioned under water. The proposed solution consists in the adoption of multiple parallel trains composed by parallel machines. Different management strategies and configurations have been tested obtaining promising results for variable speed control and multishaft configuration, e.g. increasing the number of parallel trains from one to four allows to lower the minimum part load tolerated from 85% down to about 20% of the nominal power. Focusing on the T.E.S. at off-design usage concerns arose about unequal relative levels of thermal power stored by each unit. Those unbalances during a long time span of plant application would lead to undesired shutdowns, due to the saturation of one tank, e.g. solar salts unit and the emptying of another, e.g. the diathermic oil unit. To keep the stored energy level balanced an additional heat exchanger has been added, letting solar salts and oil transfer heat. Moreover the sea water aftercooler is provided by a bypass valve for both the *CtS* and *HfS* phases. Another interesting solution would be to consider the exchange units composed by smaller parallel heat exchangers. In this way the number of active heat exchangers could be switched depending on the mass flow rate values, trying to keep the working condition as much as possible close to the nominal one. This configuration could be investigated in a future work.

Afterwards the UW-CAES has been contextualized in a real case study. Given the need of a deep water off-shore location the choice of coupling the storage with an off shore wind farm was taken. Annual simulations have been performed for two different management strategies: peak shaving and arbitraging. With the right combination of the storage activation thresholds and plant sizing, high value of RTE efficiency, around the nominal 79%, are obtained. This value compared to land based CAES with RTE which span from 40-55% [24] [15] and the value achived by most recent adiabatic-CAES projects of 70% [16] highlight the advantage of the adoption of the Adiabatic-UW layout. Moreover this technology could be competitive with the state of the art of pumped hydro storage system which achieve efficiency

nearly 70% [23]. In the first case the plant affected positively the grid energy injections, reducing the standard deviation of the sold energy between the 30 and 10%. The economic aspect has been taken into account through a preliminary economic analysis. No one of the tested solutions succeeded in break even, neither at the end of the life time. This kind of technology would then require incentive policy in order to be economically sustainable. In a market characterized by a deeper penetration of renewables, sooner or later R.E.S power plants (e.g. wind farm) will be charged with penalties related to the fluctuating energy production or obliged to introduce a buffer to control the power supplied to the grid. It is therefore reasonable to think that storage systems would be supported in economical terms. The required incentives have been calculated to beak even at the end of the LT and to reach IRR of 15% and they are of the order of 100 and 200 €/MWh respectively. In addition the proposed UW-CAES technology could be employed to provide ancillary services. This market aims at compansating grid unbalances between production and consumption profiles and it results in being the more remunerative. Nowadays energy provided is paid by the Transmission System Operator (TSO) [74] around 120 €/MWh. The additional contribute gained by the dispatchability of the energy and the possibility to provide grid balancing services can be the key for the future spread of this technology.

Chapter 8

Nomenclature and acronyms

Acronyms	
CAES	Compressed Air Energy Storage
UW CAES	Underwater Compressed Air Energy Storage
TES	Thermal Energy Storage
PV	Photovoltaic
COT	Compressor Outlet Temperature
COp	Compressors Outlet Pressure
HFT	Heat Transfer Fluid
CtS	Cooling To Storage
HfS	Heat From Storage
TIT	Turbine Inlet Temperature
TIp	Turbine Inlet Pressure
TOT	Turbine Outlet Temperature
TOp	Turbine Outlet Pressure
HX	Heat eXchanger
RES	Renewable Energy Sources
GDP	Gross Domestic Product
LCOE	Levelized Cost Of Electricity
ES	Energy Storage

Continue in the next page

Acronyms

UW	Under Water
RTE	Round Trip Efficiency
IC	InterCooler
TDF	Turbine dimension factor ($\dot{m}_{turbine}/\dot{m}_{compressor}$)
NPV	Net Present Value
IRR	Internal Rate of Return
PBT	Pay Back Time
VIGV	Variable Inlet Guide Vanes

Nomenclature

ω	rad/s	Rotational speed
D	m	Diameter
dh_{is}	J/kg	specific iso entropic work
Ns	-	Specific speed
$l_{turbine}$	J/kg	turbine work
$l_{compressor}$	J/kg	compressor work
η_{CAES}	-	CAES efficiency = RTE
c_p	J/kgK	specific heat at constant pressure
T	K	Temperature
p	Pa	pressure
ρ	kg/m^3	Density
h	J/kg	Enthalpy
s	J/kgK	Entropy
β	-	compression ratio
γ	-	c_p/c_v ratio

Nomenclature		
$\dot{V}$	m³/s	volumetric flow rate
$Vris$	-	isoentropic volume ratio
SP	m*s$^{0.25}$	Size Parameter
P_{nom}	W	Nominal power of the compressor
$\eta_{totCompression}$	-	whole compression train adiabatic effiency
$\eta_{organic-electric}$	-	organic electric efficiency
$\dot{m}$	kg/s	mass flow rate
β_{exp}	-	expansion ratio (p_{in}/p_{out}
U	m/s	peripheral speed
θ	-	$(\gamma - 1)/\gamma$
$\eta_{politropic}$	-	polytropic efficiency
Q	W	Theramal power
U	W/m²K	global heat transfer coefficient
A	m²	Area
UA	W/K	U*A product
K	W/mK	conductivity
μ	Pa*s	viscosity
Pr	-	Prandtl number
Nu	-	Nusselt number
v	m/s	stream speed
λ	-	resistance index
Re	-	Reynolds number
ϵ	-	surface roughness
h	W/m²K	convective heat transfer coefficient
R	J/kgK	universal gas constant
I_0	M€	Investment costs

Conclusion from the previous page

Bibliography

[1] Marco Astolfi, Giulio Guandalini, Marco Belloli, Adriano Hirn, Paolo Silva, and Stefano Campanari. Preliminary design and perfomance assessment of an underwater CAES system (UW-CAES) for wind power balancing. In *ASME Turbo Expo 2019: Turbomachinery Technical Conference and Exposition*, Phoenix, Arizona, USA, 2019.

[2] IRENA Renewable Energy Cost Database. Levelised Cost of Electricity. `http://resourceirena.irena.org/gateway/dashboard/`. [Online; accessed June-2018].

[3] Angus McCrone, Ulf Moslener, Francoise D'Estais, and Christine Grünig. Global Trends in Renewable Energy Investment 2017. *FS-UNEP Collaborating Centre*, page 2016, 2017.

[4] IRENA. Renewable Energy Balances: Afghanistan, Albania, Algeria and 111 more Primary Renewable Energy Supply. `http://resourceirena.irena.org/gateway/dashboard/?topic=18{&}subTopic=45`. [Online; accessed June-2018].

[5] RSE SpA. L ' accumulo di energia elettrica. `http://www.nuova-energia.com/files/Monografia{_}2011{_}Accumulo{_}prime{_}pagine.pdf`. [Online; accessed October-2018].

[6] H. Benoit, L. Spreafico, D. Gauthier, and G. Flamant. Review of heat transfer fluids in tube-receivers used in concentrating solar thermal systems: Properties and heat transfer coefficients. *Renewable and Sustainable Energy Reviews*, 55:298–315, 2016.

[7] Therminol. Therminol 66. `http://twt.mpei.ac.ru/TTHB/HEDH/HTF-66.PDF`. [Online; accessed April-2018].

[8] Meherwan P. Boyce. Axial Flow Compressors, 2012.

[9] Terry Wright. *Fluid machinery: performance, analysis, and design*. CRC Press LLC No, 1999.

[10] S.L Dixon and C.A. Hall. *Fluid Mechanics and Thermodynamics of Turbomachinery.* 2005.

[11] Giulio Federico Carbone. Simulazione di funzionamento e dimensionamento preliminare di sistemi CAES sottomarini (UW-CAES) connessi a centrali eoliche offshore, 2016.

[12] Zhiwen Wang, David S.K. Ting, Rupp Carriveau, Wei Xiong, and Zuwen Wang. Design and thermodynamic analysis of a multi-level underwater compressed air energy storage system. *Journal of Energy Storage*, 5:203–211, 2016.

[13] Alfred J. Cavallo. Energy Storage Technologies for Utility Scale Intermittent Renewable Energy Systems. *Journal of Solar Energy Engineering*, 123(4):387, 2001.

[14] Binghui Li and Joseph F. DeCarolis. A techno-economic assessment of offshore wind coupled to offshore compressed air energy storage. *Applied Energy*, 155:315–322, 2015.

[15] Samir Succar and Robert Williams. Compressed Air Energy Storage : Theory , Resources , And Applications For Wind Power Acknowledgments. *Princeton Environmental Institute Report*, 8(April):81, 2008.

[16] Pio Lombardi, Christian Röhrig, Krzysztof Rudion, Roland Marquardt, Matthias Müler-Mienack, André S. Estermann, Zbigniew A. Styczynski, and Nikolai I. Voropai. An A-CAES pilot installation in the distribution system: A technical study for RES integration. *Energy Science and Engineering*, 2(3):116–127, 2014.

[17] Xing Luo, Jihong Wang, Mark Dooner, Jonathan Clarke, and Christopher Krupke. Overview of current development in compressed air energy storage technology. *Energy Procedia*, 62:603–611, 2014.

[18] B. Cheung, N. Cao, R. Carriveau, and D.S.-K. Ting. Distensible air accumulators as a means of adiabatic underwater compressed air energy storage. *International Journal of Environmental Studies*, 69(4):566–577, 2012.

[19] A. J. Pimm, S. D. Garvey, and R. J. Drew. Shape and cost analysis of pressurized fabric structures for subsea compressed air energy storage. *Proceedings of the Institution of Mechanical Engineers, Part C: Journal of Mechanical Engineering Science*, 225(5):1027–1043, 2011.

[20] Tonio Sant, Daniel Buhagiar, and Robert N. Farrugia. Evaluating a new concept to integrate compressed air energy storage in spar-type floating offshore wind turbine structures. *Ocean Engineering*, 166(August):232–241, 2018.

[21] E Keneth and P. E. Nichols. How to Select Turbomachinery For Your Application How to Select Turbomachinery For Your Application. *Barber-Nichols Inc.*, page 10, 2010.

[22] Silvia Di Michele and Nicola Frascella. Numerical Simulation and Economic Analysis of Adiabatic Underwater CAES for the Enhancement of an Offshore Wind Farm, 2017.

[23] Terna SpA. Statistical data. `http://www.terna.it/`. [Online; accessed October-2018].

[24] A. B. Gallo, J. R. Simões-Moreira, H. K.M. Costa, M. M. Santos, and E. Moutinho dos Santos. Energy storage in the energy transition context: A technology review. *Renewable and Sustainable Energy Reviews*, 65:800–822, 2016.

[25] Atlas Copco. Driving Centrifugal Compressor Technology. `http://www.atlascopco.us/published{_}content/Images/DrivingCentrifugalCompressorTechnology{_}tcm795-1714387.pdf`. [Online; accessed October-2018].

[26] MAN Energy Solution. Axial-Flow Compressors (Type AG/AGM). `https://turbomachinery.man-es.com`. [Online; accessed April-2018].

[27] Puertos del Estado. South west Sardinia oceanography map. `http://www.puertos.es/en-us/oceanografia/Pages/portus.aspx`. [Online; accessed August-2018].

[28] Gestore dei Mercati Energetici S.p.A. profile prices, Sardinia, 2015, 2016. `http://www.mercatoelettrico.org/It/default.aspx`. [Online; accessed October-2018].

[29] BP. Statistical Review of World Energy 2018. pages 1–53, 2018.

[30] Paolo Silva. Energy solution, 2017.

[31] BBC Brown Boveri. BBC Huntorf Broshure. `http://www.solarplan.org/Research/BBC{_}Huntorf{_}engl.pdf`. [Online; accessed October-2018].

[32] PowerSouth Energy Cooperative. Compressed Air Energy Storage - McIntosh power plant, McIntosh, Alabama. `http://www.powersouth.com/files/McIntoshBrochure[FINAL].pdf`. [Online; accessed April-2018].

[33] JEFF ST. JOHN. Texas to Host 317 MW of Compressed Air Energy Storage. `https://www.greentechmedia.com/articles/read/texas-calls-for-317mw-of-compressed-air-energy-storage2{#}gs.sr0cwd0`. [Online; accessed June-2018].

[34] RWE Power : Rheinisch Westfälisches Elektrizitätswerk AG. ADELE Adiabatic Compressed Air Energy Storage for Electricity Supply. `https://www.rwe.com/web/cms/mediablob/en/391748/data/364260/1/rwe-power-ag/innovations/Brochure-ADELE.pdf`. [Online; accessed April-2018].

[35] Dresser-rand SmartCaes. SMART CAES Compressed.

[36] Javier Mas and Jokin Mendia Rezola. Tubular design for underwater compressed air energy storage. *Journal of Energy Storage*, 8:27–34, 2016.

[37] Jalal Moradi, Hossein Shahinzadeh, Amirsalar Khandan, and Majid Moazzami. A profitability investigation into the collaborative operation of wind and underwater compressed air energy storage units in the spot market. *Energy*, 141:1779–1794, 2017.

[38] Sammy Houssainy, Mohammad Janbozorgi, Peggy Ip, and Pirouz Kavehpour. Thermodynamic analysis of a high temperature hybrid compressed air energy storage (HTH-CAES) system. *Renewable Energy*, 115:1043–1054, 2018.

[39] A.J. Pimm, S.D. Garvey, and M. de Jong. Design and testing of Energy Bags for underwater compressed air energy storage. *Energy*, 66:496–508, 2014.

[40] (T.U. ambientale). decreto legislativo 3 aprile 2006 n. 152. `https://www.legambiente.it/sites/default/files/docs/d.lgs{_}.{_}n.{_}152{_}2006{_}t.u.{_}ambientale-1.pdf`. [Online; accessed October-2018].

[41] Saniel D. Lim, Andre P. Mazzoleni, Joong Kyoo Park, Paul I. Ro, and Brendan Quinlan. Conceptual design of ocean compressed air energy storage system. *OCEANS 2012 MTS/IEEE: Harnessing the Power of the Ocean*, 2012.

[42] Google Earth. South West Sardinia map. `https://earth.app.goo.gl/?apn=com.google.earth{&}ibi=com.google.b612{&}isi=293622097{&}ius=googleearth{&}link=https{%}3A{%}2F{%}2Fearth.google.com{%}2Fweb{%}2F{%}4039.18642627,8.64380766,586.52082207a,622722.13416204d,35y,0h,0t,0r`. [Online; accessed April-2018].

[43] Yong Bai and Qiang Bai. *Subsea Engineering Handbook.* 2010.

[44] Det Norske Veritas. DNV GL-ST-F101 Submarine pipeline systems. [Online; accessed October-2018].

[45] ENI. ENI Gela-Malta project cost estimation. (April), 2009.

[46] Didier Clamond. Efficient resolution of the colebrook equation. *Industrial and Engineering Chemistry Research*, 48(7):3665–3671, 2009.

[47] E Torselletti, L Vitali, and R Bruschi. Design Criteria Vs. Line Pipe Requirements for Offshore Pipelines. *Super-High Strength Steels*, pages 1–18, 2005.

[48] Kevin Williams. Deepwater Pipeline Design Against Collapse Under External Pressure. (October), 2015.

[49] N. Autissier, F. Palazzi, F. Marechal, J. van Herle, and D. Favrat. Thermo-Economic Optimization of a Solid Oxide Fuel Cell, Gas Turbine Hybrid System. *Journal of Fuel Cell Science and Technology*, 4(2):123–129, 2007.

[50] Meherwan P Boyce. *GasTurbine Engineering Handbook.* 2002.

[51] Michael J D Powell. A FORTRAN subroutine for solving systems of nonlinear algebraic equations. Technical report, 1968.

[52] Frank P Incropera, David P DeWitt, Theodore L Bergman, and Adrienne S Lavine. Fundamentals of Heat and Mass Transfer, 2007.

[53] Matrix Arguments, Passing Extra Parameters, See Iterations, and Can Violate. Find minimum of constrained nonlinear multivariable function (fmincon). *Matlab Documentation*, (x):2014, 2016.

[54] Ian H. Bell, Jorrit Wronski, Sylvain Quoilin, and Vincent Lemort. Pure and pseudo-pure fluid thermophysical property evaluation and the open-source thermophysical property library coolprop. *Industrial and Engineering Chemistry Research*, 2014.

[55] John E Edwards. Design and Rating Shell and Tube Heat Exchangers. *Chemical Engineering*, 2008.

[56] P. Chiesa. Stato dell ' arte e prospettive dei sistemi di accumulo energetico basati sulla tecnologia CAES, 2014.

[57] R. Ja. Couper, W. P. Roy, R. F. James, and W. M. Stanley. Costs of individual equipment. *Chemical Process Equipment*, 11(8):663–669, 1988.

[58] GECOS. Stato dell'arte e prospettive dei sistemi di accumulo energetico basati sulla tecnologia CAES, 2014.

[59] G Glatzmaier. Developing a cost model and methodology to estimate capital costs for thermal energy storage. Technical Report December, National Renewable Energy Laboratory, National Renewable Energy Laboratory 1617 Cole Boulevard Golden, Colorado, 2011.

[60] K. Nithyanandam and R. Pitchumani. Cost and performance analysis of concentrating solar power systems with integrated latent thermal energy storage. *Energy*, 64:793–810, 2014.

[61] Alessia Gatto. Analisi dell'applicazione di impianti trigenerativi e riduzione delle emissioni di CO2 per i Campus di Bovisa del Politecnico di Milano, 2015.

[62] Daniele Cocco and Fabio Serra. Performance comparison of two-tank direct and thermocline thermal energy storage systems for 1MWe class concentrating solar power plants. *Energy*, 81:526–536, 2015.

[63] J.C.O. Santos, M.G.O. Santos, J.P. Dantas, M.M. Conceição, P.F. Athaide-Filho, and A.G. Souza. Comparative study of specific heat capacities of some vegetable oils obtained by DSC and microwave oven. *Journal of Thermal Analysis and Calorimetry*, 79(2):283–287, 2005.

[64] J Fradera, R. Serrano-López, and S. Cuesta-López. Chemical Engineering and Processing : Process Intensification Molten salts database for energy applications. *Chemical Engineering & Processing: Process Intensification*, 73:87–102, 2013.

[65] Italcementi. Listino Prezzi. `https://it.i-nova.net/documents/23505/0/Listino+Prezzi+Italcementi/20d08434-e030-481b-9a03-dc8aaf8ffac9`. [Online; accessed October-2018].

[66] I.nova. Listino Prezzi. `https://www.calcestruzzi.it/it/listinohttp://www.i-nova.net`. [Online; accessed October-2018].

[67] CIPRE. Listino prezzi. [Online; accessed October-2018].

[68] Marcegalia specialties. stainless steel tube price list. `www.marcegaglia.com`. [Online; accessed October-2018].

[69] Nathan Parker. Using Natural Gas Transmission Pipeline Costs to Estimate Hydrogen Pipeline Costs. Technical report, Institute of Transportation Studies University of California One Shields Avenue Davis CA 95616, Davis CA 95616, 2004.

[70] Lazaros P Lazaridis. Economic Comparison of HVAC and HVDC Solutions for Large Offshore Wind Farms under Special Consideration of Reliability. *Electrical Engineering*, 12(4):203–208, 2005.

[71] M. Dicorato, G. Forte, M. Pisani, and M. Trovato. Guidelines for assessment of investment cost for offshore wind generation. *Renewable Energy*, 36(8):2043–2051, 2011.

[72] Entec UK Ltd. Cost estimation methodology: The Marine Energy Challenge approach to estimating the cost of energy produced by marine energy systems. Technical Report May, Carbon Trust. [Online; accessed October-2018].

[73] The World Bank Group. Real interest rate (%). `https://data.worldbank.org/indicator/FR.INR.RINR?end=2015{&}start=2015{&}view=map{&}year=2017`. [Online; accessed October-2018].

[74] Gestore dei Mercati Energetici S.p.A. Rapporto mensile sul Sistema Elettrico. `https://www.terna.it/it-it/sistemaelettrico/dispacciamento/datiesercizio/rapportomensile.aspx`. [Online; accessed December-2018].